Master Thesis

POLITECNICO DI MILANO

ON CORRELATION EFFECTS IN HUMAN-INDUCED VERTICAL VIBRATIONS OF FOOTBRIDGES

Francesco Bonato

July 25, 2018

Contents

Introduction

Modern footbridges are increasingly slender and lighter than in past, mainly as a result of technical innovation and finer structural analyses. Due to these characteristics they are more likely to experience uncomfortable vibrations caused by pedestrians.

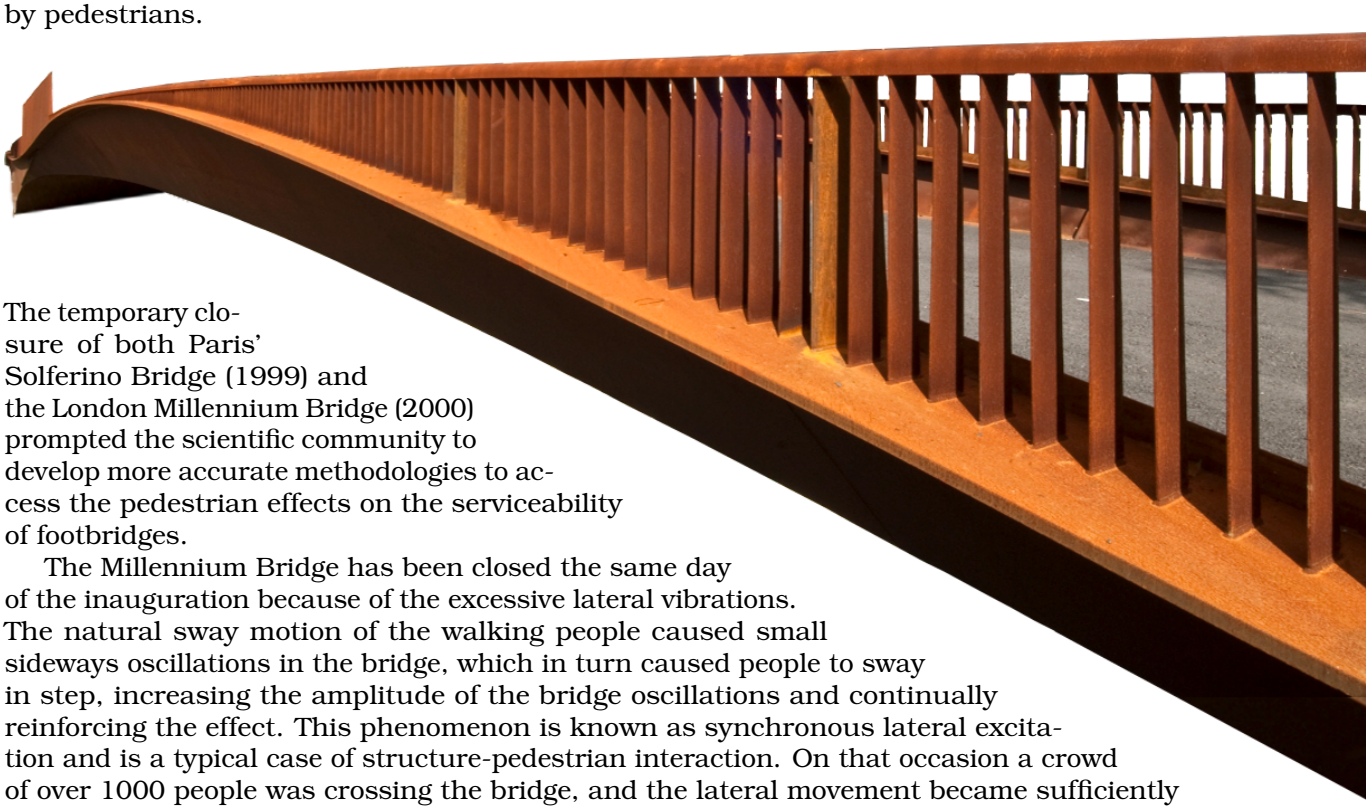

The temporary closure of both Paris' Solferino Bridge (1999) and the London Millennium Bridge (2000) prompted the scientific community to develop more accurate methodologies to access the pedestrian effects on the serviceability of footbridges.

The Millennium Bridge has been closed the same day of the inauguration because of the excessive lateral vibrations. The natural sway motion of the walking people caused small sideways oscillations in the bridge, which in turn caused people to sway in step, increasing the amplitude of the bridge oscillations and continually reinforcing the effect. This phenomenon is known as synchronous lateral excitation and is a typical case of structure-pedestrian interaction. On that occasion a crowd of over 1000 people was crossing the bridge, and the lateral movement became sufficiently large for people to stop walking to retain their balance. The detected amplitude of the oscillation was $7.5\,\mathrm{cm}$ at $1\,\mathrm{Hz}$. The natural frequency of the later mode was $0.9\,\mathrm{Hz}$. The problem was finally fixed by the retrofitting of 37 fluid-viscous dampers.

Despite these issues are concerning lateral human-induced excitation, the vertical excitation shall also be taken into account in the serviceability assessment. In dense crowds, interaction dynamics among the pedestrians themselves also occur. On these pedestrian-pedestrian interactions a relevant amount of research has been carried out (i.e. Wheeler 1980 [36]; Papadimitriou et al., 2009; Venuti and Bruno, 2009 [35]; Andersen, 2009).

This thesis aims to examine how the response of a simple supported footbridge, from the serviceability point of view, changes as a result of an interaction of this kind: the pedestrian-pedestrian interaction. As a representative response of the bridge the vertical displacements and accelerations at the midspan are considered. The vertical behaviour of this kind of structure is mainly affected by the first modes of vibrations, also, the vertical dynamic force exerted by humans has a greater order of magnitude with respect to the lateral one, so its effects are more immediate to investigate. The response is predicted on theoretical basis by means of the response spectrum approach, and then it is supported and validated by numerical simulations. The pedestrian load is simplified as a continuous string of equally

spaced pedestrians having variable phases and frequencies. A variation of the density results in a change of the total number of pedestrian present on the bridge at the same time. The pedestrian-pedestrian interaction is thus implemented in terms of the randomness of the pedestrian properties, and regulated by proper parameters. Finally, the results are compared with the current guidelines, in particular with Sétra (2009) [13].

Chapter 1

Beam dynamics

1.1 Equations of motion in discrete form

The equation of the dynamic equilibrium of a beam is:

$$\frac{\partial^2}{\partial x^2}\left[EI(x)\frac{\partial^2 v(x,t)}{\partial x^2}\right] + \gamma(x)\frac{\partial^2 v(x,t)}{\partial t^2} = f(x,t) \tag{1.1}$$

where $v(x,t)$ is the deformed shape, function of time t and x abscissa along the beam axis. $f(x,t)$ represents a generic load, which may vary in time and in space, being distributed in any way along the beam; E is the modulus of elasticity, while $\gamma(x)$ and $I(x)$ are the linear mass and the moment of inertia, both depending on x if the beam section is not constant. The equation is valid under the assumptions of:

- small oscillations
- linear elastic materialcomportamento lineare elastico
- symmetric section with respect to x, v plane
- rotational inertia, axial deformability and shear deformability negligible
- no internal dissipation

The direct integration of the equation, which is a partial differential equation, is possible just in few simple cases. The classical approach to reduce the problem in a more manageable form is discretize it, that is to say reduce it to a finite number of degrees of freedom. For this purpose the deformed shape is approximated by a linear combination:

$$v(x,t) = \sum_j \psi_j(x) y_j(t) \tag{1.2}$$

$\psi_j(x)$ are the shape functions, they are set a priori and chosen such that all the imposed constrains are respected. The $y_j(t)$ are the generalized coordinates, they module the shape functions in time giving rise to the system response and represent the unknown quantities. The greater the number of summed up terms, the more accurate is the method.

In order to derive the equations of motion the Lagrange equations are used. For them are required the kinetic energy, the total potential energy, and the generalized component of the excitation force.

It is necessary to compute the following derivatives of v with respect to the time and the space:

$$\dot{v}(x,t) = \sum_j \psi_j(x)\dot{y}_j(t) \qquad \dot{v}^2(x,t) = \sum_j \sum_k \psi_j(x)\psi_k(x)\ \dot{y}_j(t)\dot{y}_k(t)$$

$$v'(x,t) = \sum_j \psi_j'(x) y_j(t) \qquad v''(x,t) = \sum_j \psi_j''(x) y_j(t) \qquad v''^2(x,t) = \sum_j \sum_k \psi_j''(x)\psi_k''(x)\ y_j(t) y_k(t)$$

The kinetic energy of the beam is:

$$T = \frac{1}{2}\int_0^l \gamma(x)\dot{v}^2(x,t)\mathrm{d}x = \frac{1}{2}\sum_j\sum_k \dot{y}_j(t)\dot{y}_k(t)\int_0^l \gamma(x)\psi_j(x)\psi_k(x)\mathrm{d}x \tag{1.3}$$

it can be collected in the matrix format:

$$T = \frac{1}{2}\,\dot{\mathbf{y}}^T\mathbf{m}\dot{\mathbf{y}}$$

where $\mathbf{m}$ is the inertia matrix and his generic element is:

$$m_{ij} = \int_0^l \gamma(x)\psi_j\psi_k\mathrm{d}x$$

The total potential energy reads:

$$V = \frac{1}{2}\int_0^l EI(x)v''^2(x,t)\mathrm{d}x = \frac{1}{2}\sum_j\sum_k y_j(t)y_k(t)\int_0^l EI(x)\psi_j''(x)\psi_k''(x)\mathrm{d}x \tag{1.4}$$

in matrix notation:

$$V = \frac{1}{2}\,\mathbf{y}^T\mathbf{k}\mathbf{y}$$

the stiffness matrix $\mathbf{k}$ consists of the following elements:

$$k_{ij} = \int_0^l EI(x)\psi_j''\psi_k''\mathrm{d}x$$

The generalized component of the perturbing forces is the one generating work in the free coordinate, that is $Q_j(t)$ in:

$$\delta W = \sum_j Q_j(t)\delta y_j$$

The virtual work done by the perturbating forces is:

$$\delta W = \int_0^l f(x,t)\delta v\ \mathrm{d}x \qquad \delta v = \sum_j \psi_j(x)\delta y_j$$

$$\delta W = \sum_j \left(\int_0^l f(x,t)\psi_j(x)\mathrm{d}x\right)\delta y_j$$

so that:

$$Q_j(t) = \int_0^l f(x,t)\psi_j(x)\mathrm{d}x$$

The Lagrange equations represent a system of ordinary differential equations which are as many as there are degrees of freedom of the system:

$$\frac{\mathrm{d}}{\mathrm{d}t}\frac{\partial T}{\partial \dot{y}_j} + \frac{\partial D}{\partial \dot{y}_j} + \frac{\partial V}{\partial y_j} = Q_j(t) \qquad j = 1,2,3...n$$

The expression also includes the viscous damping by mean of the Rayleigh function D.

We obtain the well known system of motion equations in the n free coordinates:

$$\mathbf{m}\ddot{\mathbf{y}} + \mathbf{c}\dot{\mathbf{y}} + \mathbf{k}\mathbf{y} + \mathbf{Q} \tag{1.5}$$

It must be said that the function of dissipation D, as well as the terms of the matrix $mathbfc$ which derive from it, are difficult to interpret. In the practise, because the structure is homogeneous, it becomes possible to directly impose the value of the modal damping factors ξ_j as shown in the following.

1.2 Eigenfunctions

Shape functions must ensure the derivability and integrability in order to compute the integrals 1.3 and 1.4. If we substitute the deformed shape, separating the spatial and temporal variables $v(x,t) = \psi(x)g(t)$ in the equation of motion for free oscillations:

$$EIv^{IV}(x,t) + \gamma\ddot{v}(x,t) = 0$$

one finds:

$$\frac{EI}{\gamma}\frac{\psi^{IV}(x)}{\psi(x)} = -\frac{\ddot{g}(t)}{g(t)} = \omega^2 \tag{1.6}$$

the first and the second term must be equal for each time instant, so they can put equal to a constant ω^2. One side we obtain:

$$\ddot{g}(t) + \omega^2 g(t) = 0$$

which is the equation of the harmonic motion, with the simple solution:

$$g(t) = A\sin(\omega t) + B\cos(\omega t)$$

on the other:

$$\psi^{IV}(x) - \lambda^4\psi(x) = 0 \tag{1.7}$$

with

$$\lambda^4 = \omega^2\frac{\gamma}{EI}$$

that has the general integral:

$$\psi(x) = C_1\sin(\lambda x) + C_2\cos(\lambda x) + C_3\sinh(\lambda x) + C_4\cosh(\lambda x) \tag{1.8}$$

by imposing the geometric boundary conditions for the simple supported beam:

$$\psi(0) = 0 \qquad \psi(l) = 0 \qquad M(0) = EI\psi''(0) = 0 \qquad M(l) = EI\psi''(l) = 0$$

the nontrivial solutions of the system are the ones that makes null the determinant of the coefficient matrix:

$$\sin(\lambda l)\sinh(\lambda l) = 0 \iff \lambda = \frac{j\pi}{l} \qquad j = 1,2,3...\infty$$

and that provide, if substituted in 1.8:

$$\psi_j(x) = \sin\frac{j\pi x}{l} \tag{1.9}$$

Furthermore, inverting the 1.7, they make possible to understand the physical meaning of ω_j:

$$\omega_j = \sqrt{\frac{EI}{\gamma}}\left(\frac{j\pi}{l}\right)^2 \tag{1.10}$$

The problem exposed in 1.6 can be viewed as a eigenvalues problem, where ω_j^2 are the eigenvalues and $\psi_j(x)$ the associated eignefunctions. The ω_j are also called pulsatance, or circular frequency, and are linked to the frequency with the relation $\omega = 2\pi f$. The eigenfunctione, each one with its proper associated frequency, represent the vibrational modes of the structure. As one can see from 1.10, increasing the index j, the oscillation frequency increases. As a consequence the modes of vibration are a potentially infinite set, numerable, with increasing frequency.

Orthogonality of eigenfunctions implies that:

$$\int_0^l \gamma(x)\psi_j(x)\psi_k(x)\mathrm{d}x = 0 \qquad \int_0^l EI(x)\psi_j''(x)\psi_k''(x)\mathrm{d}x = 0$$

Modal mass	$m_j = \int_0^l \gamma(x)\psi_j^2 \mathrm{d}x$	$=$	$\gamma \int_0^l \sin^2 \frac{j\pi x}{l} \mathrm{d}x$	$=$	$\frac{\gamma l}{2}$	$\forall j$
Modal stiffness	$k_j = \int_0^l EI(x)\psi_j''^2 \mathrm{d}x$	$=$	$EI \int_0^l \left(\frac{j\pi}{l}\right)^2 \sin^2 \frac{j\pi x}{l} \mathrm{d}x$	$=$	$EI \left(\frac{j\pi}{l}\right)^2 \frac{l}{2}$	
Generalized modal force	$Q_j = \int_0^l f(x,t)\psi_j \mathrm{d}x$	$=$	$\int_0^l f(x,t) \sin \frac{j\pi x}{l} \mathrm{d}x$			

Table 1.1: Properties of the j^{th} mode.

as a consequence all the extra-diagonal terms of the matrices $\mathbf{m}$ and $\mathbf{k}$ are null:

$$\begin{aligned} m_{jk} &= 0 \\ k_{jk} &= 0 \end{aligned} \quad \text{if } j \neq k$$

what derives is that the $\mathbf{m}$ and $\mathbf{k}$ matrices are diagonal, and under the assumption that $\mathbf{c}$ is too, the system of equations of motion 1.5 uncouples to n ordinary equations:

$$m_j \ddot{y}_j + c_j \dot{y}_j + k_j y_j = Q_j(t) \tag{1.11}$$

each one for a mode of vibration j of the system. Thus the y_j coordinates play the role of principal coordinates. Since they describe the amplitude of the modal shape in time, they also have the meaning of modal coordinates. The other terms are: for simple supported beam istance.

The 1.11 is usually written dividing for m_j:

$$\ddot{y}_j + 2\xi_j \omega_j \dot{y}_j + \omega_j^2 y_j = \frac{1}{m_j} Q_j$$

where ξ_j is the damping factor related to the j^{th} mode. While

$$\omega_j^2 = \frac{k_j}{m_j} \tag{1.12}$$

is the usual way to define the pulsatance. Substituting the modal stiffness and the modal mass one finds the definition of 1.10 again.

1.3 Solution for arbitrary load

As we have seen, read the problem in terms of modal coordinates not only restrict it to a finite number of degrees of freedom, but also give us equations in a single degree of freedom, which are quite handy to solve. Each one of these equations is the motion of a simple oscillator $y_j(t)$, with viscous damper, subjected to a certain forcing function.

If we know the expression in time of the modal coordinates $y_j(t)$, the final deformed shape of the beam is also automatically defined. It is nothing but the superposition of every modal shape, multiplied by the corresponding modal coordinate varying in time.

When the forcing function is null (free oscillations), constant, or harmonic, the solution of the modal equations can be found analytically. Otherwise, if the forcing function has an arbitrary variation in time or space, the solution requires numerical methods.

The resolution approach here adopted is the Duhamel's integral. That is the easier and more reliable way to be implemented in the code, in order to solve any kind of load case.

The Duhamel's integral is in extended form:

$$y(t) = \int_0^t Q(\tau) h(t-\tau) \mathrm{d}\tau$$

where $h(t)$ is the response of the oscillator to a unit impulse ($Q = \delta(t-0)$) acting at time $t = 0$ and represents the Green's function for that dynamic system. It can be derived from the free oscillator response

$$y = e^{-\xi\omega t}\left[A\cos\omega_D t + B\cos\omega_D t\right]$$

by imposing zero initial displacement, and starting velocity equal to the ratio between impulse and mass:

$$y|_{t=0} = 0$$
$$\dot{y}|_{t=0} = \frac{I}{m}$$

we obtain:

$$y = \frac{I}{m\omega_D}e^{-\xi\omega t}\sin\omega_D t \qquad \omega_D = \omega\sqrt{1-\xi^2}$$

with unitary impulse:

$$h(t) = \frac{1}{m\omega}e^{-\xi\omega t}\sin\omega_D t$$

The Duhamel's integral in discrete form becomes:

$$y_j(t) = \sum_n Q_j(n\Delta t)h_j(t-n\Delta t)\Delta t$$

The Duhamel's integral coincides with the convolution of the forcing function and the Green's function of the system. Namely:

$$y = Q(t) * h(t) \tag{1.13}$$

The interesting property of the Green's function $h(t)$ is that its Fourier transform is the Frequency Response Function (FRF) of the system:

$$\mathscr{F}\{h(t)\} = H(f)$$

which is:

$$H(\beta) = \frac{1}{k}\frac{1}{1-\beta^2+2i\xi\beta} \qquad \beta = \frac{\Omega}{\omega}$$

and by mean of the convolution theorem, which states that the Fourier transform of the convolution of two functions is equal to the product of the Fourier transform of each function, in formula:

$$\mathscr{F}\big\{h(t) * g(t)\big\} = \mathscr{F}\{h(t)\}\cdot\mathscr{F}\{g(t)\}$$

one finds that the transform of the response is the product of the FRF for the transform of the forcing function:

$$\mathscr{F}\{y(t)\} = H(f)\cdot\mathscr{F}\{Q(t)\}$$

That is the basis of the frequency response study.

1.4 Generalized forces

From the perspective of the code compilation are now presented the generalized forces that one can deal with in the handling of pedestrian forces. Reference is made to the third equation of table 1.1.

	$f(x,t)$	$Q_j(t)$
Impulsive force applied in x_0 at the instant t_0	$P\delta(x-x_0)\delta(t-t_0)$	$P\sin\frac{j\pi x_0}{l}\delta(t-t_0)$
Force constant in time and space	$P\delta(x-x_0)$	$P\sin\frac{j\pi x_0}{l}$
Force constant in time, moving with velocity c	$P\delta(x-ct)$	$P\sin\frac{j\pi c}{l}t$
Harmonic concentrated force	$P\sin(\Omega t+\phi)\delta(x-x_0)$	$P\sin(\Omega t+\phi)\sin\frac{j\pi x_0}{l}$
Harmonic concentrated force, moving at velocity c	$P\sin(\Omega t+\phi)\delta(x-ct)$	$P\sin(\Omega t+\phi)\sin\frac{j\pi c}{l}t$
Force with constant component and harmonic component, moving at velocity c	$P_S\delta(x-ct)+$ $+P_D\sin(\Omega t+\phi)\delta(x-ct)$	$\sin\frac{j\pi ct}{l}\left[P_S+P_D\sin(\Omega t+\phi)\right]$
Distributed standing load constant in time	q	$q\frac{l}{j\pi}\left[1-\cos(j\pi)\right]$
Distributed standing load varying in time	$q(t)$	$q(t)\frac{l}{j\pi}\left[1-\cos(j\pi)\right]$

Table 1.2: Generalized forces related to different loadings conditions, for a simply supported beam. The j^{th} generalized force excites the j^{th} modal coordinate.

Chapter 2

Human forces: Literature review

2.1 Single person force modelling

What we nowadays know about pedestrian-induced forces started to be studied by Harper et al. as recently as 1961. They recorded the characteristic shape with two peaks of the vertical force time history. Many other researchers have confirmed and deepened the subject, among them: Galbraith and Barton 1970 [17], Andriacchi 1977 [2], Blanchard et al. 1977 [6], Ohlsson 1982 [30], Kerr 1998 [21], Bertram and Ruina 2001 [5], Wheeler 1982 [36].

Andriacchi for instance measured single step walking forces in all three directions by mean of a force plate, whose typical patterns are presented in figure 2.1.

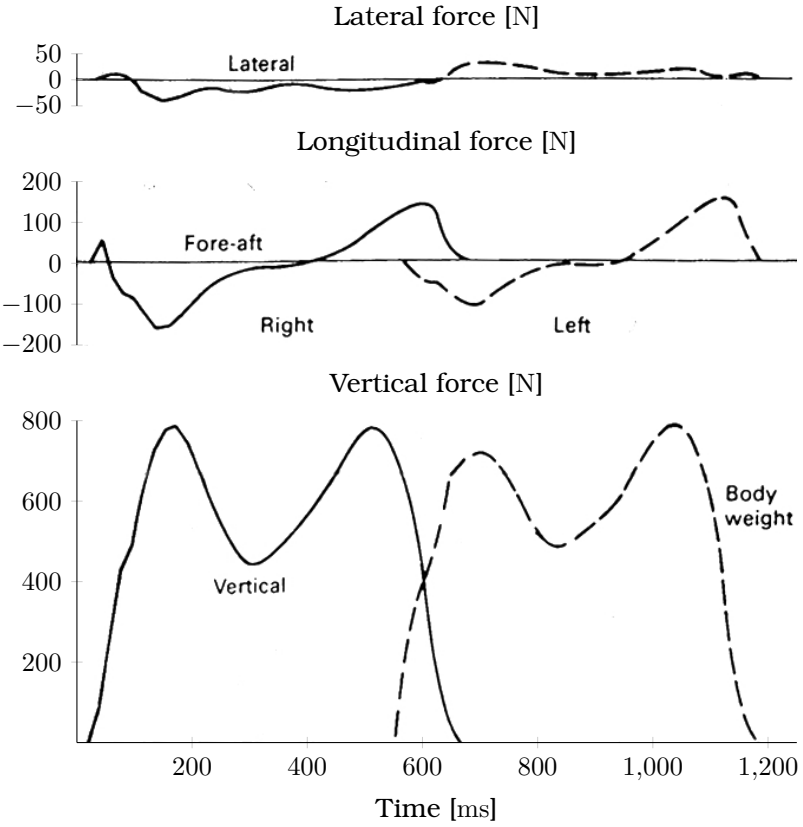

Figure 2.1: Tipical shapes of walking force in a) lateral, b) longitudinal and c) vertical direction (after Andriacchi et al. [2])

The walking force exhibits, besides the vertical one, two other components: the lateral and

the longitudinal one. Their presence is mainly due to the friction between the foot and the floor.

The vertical action is at least one order of magnitude greater with respect to the other two. Despite of this the minor components are not negligible in many cases. For instance, the lateral component is responsible for the lateral instability of footbridges.

If the footsteps are put consecutively in the time history, as they are recorded, one finds a continuous force. This force has not empty holes cause the feet of the pedestrian never find themselves simultaneously raised from the ground (this would be the case of running, which is not under discussion). We refer to this force as the Ground Reaction Force, GRF.

The natural next step is to decompose it in Fourier series, as the engineer's basic instinct requires. The formula first given by Bachmann [4] in 1955 is of the type:

$$F_{\text{ped}} = W + \sum_{i}^{n_{\text{arm}}} W\alpha_i \sin\left(2\pi i f_{\text{ped}} t + \phi_i\right) \tag{2.1}$$

where:

W person's weight, typically $700\,\text{N}$ (Bachmann & Ammann assumed $800\,\text{N}$);

α_i Fourier's coefficient of the i^{th} harmonic;

f_{ped} activity rate [Hz], that is to say pacing frequency;

ϕ_i phase lag of the i^{th} harmonic relative to the 1^{st} one;

i order number of the harmonic;

n_{arm} total number of contributing harmonics.

2.2 Dynamic Loading Factor

Since the α_i coefficient has the meaning of a *Dynamic Loading Factor* we are calling it DLF from now on. It is clear that the complete series includes an arbitrary number of DLFs, which are referred to the first n_{arm} harmonics. In order to identify them, the index i should be added: DLF_i.

Many researchers have tried to quantify the DLFs. What they found is that it depends on the pacing frequency, or analogously on the speed. An overview of the DLFs for single person force, provided by different authors, is given in table 2.1.

Authors	DLF_1	DLF_2	ϕ_2	DLF_3	ϕ_3	Notes
Blanchard et al. 1977	0.257					
Shultze 1987	0.37	0.10		0.12		at 2 Hz
Bachmann & Ammann 1995	$0.4 \div 0.5$	0.10	$\pi/2$	0.10	$\pi/2$	at $2 \div 2.4$ Hz

Table 2.1: DLF_i for i^{th} harmonic and corresponding phase lag. The data refer to the vertical components of the GRF due to walking.

Figure 2.2 gives an example of the decomposition by means of Fourier series of the Ground Reaction Force until the third harmonic. The used coefficient are by Bachmann & Ammann [3].

As figure 2.3 shows, the GRF changes with the type of activity: it generally increases its magnitude with the intensity of the motion. DLF analogous to those in table 2.1 have been derived for the *running* case and the *jumping* case, but these do not concern this study.

Young in 2001 introduced DLF as a function of the walking frequency, supposed to be in the range $1 \div 2.8\,\text{Hz}$. He examinated the DLFs from the 1^{st} to the 4^{th} harmonic:

$$\begin{aligned}
&\text{DLF}_1 \quad 0.37\,(f_{\text{ped}} - 0.95) \leq 0.56\\
&\text{DLF}_2 \quad 0.069 + 0.0056 f_{\text{ped}}\\
&\text{DLF}_3 \quad 0.033 + 0.0064 f_{\text{ped}}\\
&\text{DLF}_4 \quad 0.013 + 0.0065 f_{\text{ped}}
\end{aligned}$$

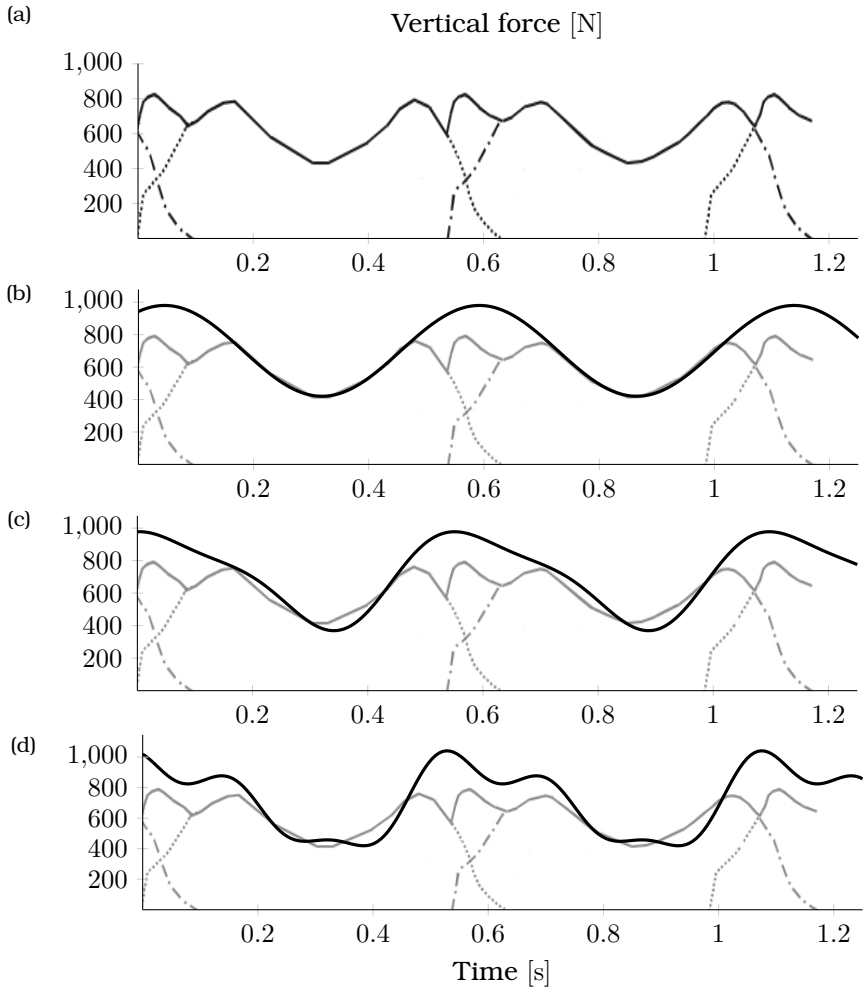

Figure 2.2: GRF decomposition by means of Fourier series. Original GRF time history (a), its first harmonic (b), first two harmonics (c), and first three harmonics (d). The DLF_i coefficients are taken from Bachmann & Ammann 1995.

Anyway, the data collections are very scattered and with the exception of the first, the other DLF appear quite unreliable.

A further contribute is provided by Kerr [21], who interpolated the experimental data by a cubic curve, for the first DLF:

DLF_1	upper bound	$-0.3497 f_{\text{ped}}^3 + 1.7432 f_{\text{ped}}^2 - 2.3228 f_{\text{ped}} + 1.0049$
	mean	$-0.2649 f_{\text{ped}}^3 + 1.3206 f_{\text{ped}}^2 - 1.7597 f_{\text{ped}} + 0.7613$
	lower bound	$-0.1801 f_{\text{ped}}^3 + 0.8980 f_{\text{ped}}^2 - 1.1966 f_{\text{ped}} + 0.5177$

Also, he computed the upper and lower bound of the DLF_1 range of variation. These curves are plotted in figure

2.3 Speed

The velocity of undisturbed pedestrian walking is generally reported as *free speed*. Several studies have been carried out to provide the statistical description of the pedestrian free speed as a random variable through its Probability Density Function (PDF). It is well estabilished that the Gaussian PDF better agrees with the measured data.

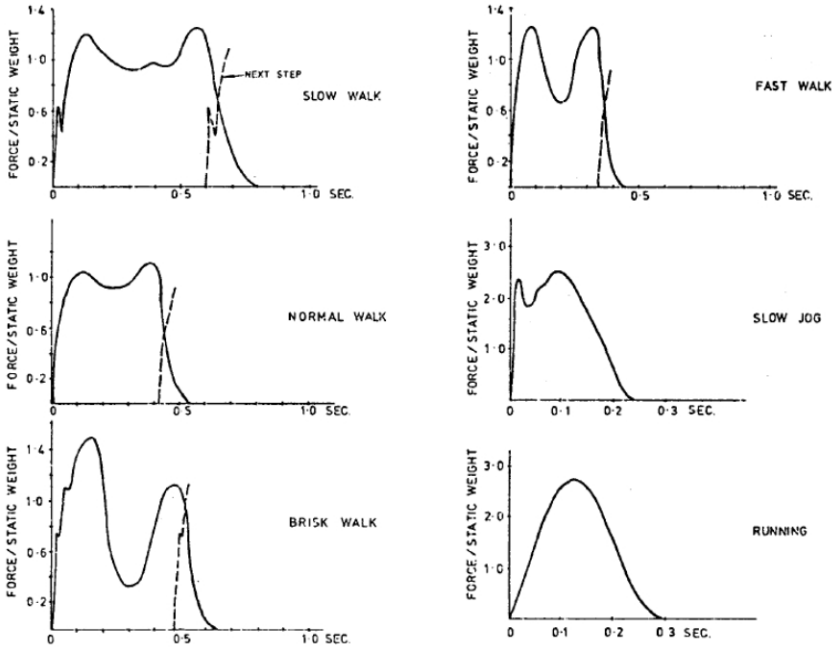

Figure 2.3: Typical vertical force patterns for different types of human activities (Wheeler 1982 [36])

Table 2.2 reports a selection of the PDF parameters obtained by different authors [10]. The differences among the mean values ($1.08 \div 1.6\,\mathrm{m/s}$) are due to the fact that they have been measured in different locations and traffic situations (subway stations, shopping streets, indoor walkways). Indeed, walking parameters are influenced by physiological and psychological factors, such as body weight, height, age, gender, travel purpose, type of walking facility.

2.4 Frequency

As far as the walking frequency is concerned, it has to be intended as a vertical walking frequency $f_{\mathrm{ped,v}}$, that is the number of times a foot touches the ground in a time unit, while the horizontal or lateral walking frequency $f_{\mathrm{ped,l}}$ is intended as the number of times the same foot touches the ground. The lateral step frequency is therefore half the vertical one.

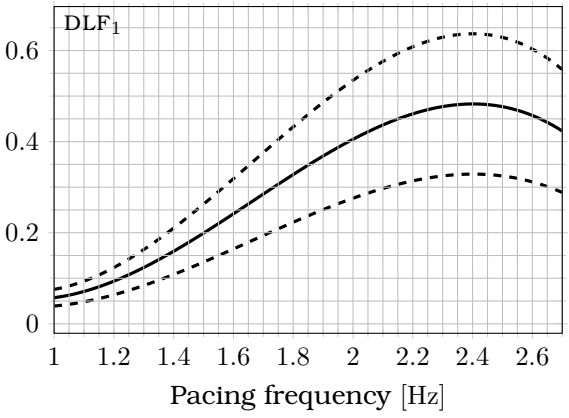

Figure 2.4: Kerr's expression for the Dynamic Loading Factor of the 1st harmonic as function of the pacing frequency.

Authors	Mean speed c_μ m/s	Standard deviation c_σ m/s	Geographic area
Fruin	1.40	0.15	US
Hankin and Wright	1.60	-	US
Koushki	1.08	-	Saudi Arabia
Lam et al.	1.19	0.26	Hong Kong
Older	1.30	0.30	UK
Pauls	1.25	-	US
Ricciardelli et al.	1.41	0.224	Italy
Sanhaci and Kasperski	1.37	0.15	Germany
Sarkar and Janardhan	1.46	0.63	India
Tanariboon et al.	1.23	-	Singapore
Virkler and Elayadath	1.22	-	US
Weidmann	1.34	-	-
Mean value	1.32	0.286	

Table 2.2: Mean value and standard deviation of pedestrian free speed from different authors.

Human motion		Forward speed m/s	Pacing frequency Hz	Stride length m
Walking	Slow	1.1	1.7	0.6
	Normal	1.5	2.0	0.75
	Fast	2.2	2.3	1.0

Table 2.3: Correlation of forward speed, pacing frequency and stride length for walking (Bachmann & Ammann, 1987 [4])

Table 2.4 summarises the mean values of the vertical frequency measured in unconstrained circumstances by different authors. One of the first reliable statistical description was given by Matsumoto et al. [25], who concluded that the vertical frequencies follow a Gaussian distribution, with a mean value $f_\mu = 2\,\mathrm{Hz}$ and a standard deviation $f_\sigma = 0.173\,\mathrm{Hz}$. The other authors found mostly lower mean values inside the interval $1.82\,\mathrm{Hz} \div 1.90\,\mathrm{Hz}$.

The complexity of the walking behaviour makes it difficult to find relationships between the three walking parameters (speed, frequency, step length), as pointed out by Bertram and Ruina [5], who obtained different $\mathrm{speed}(\mathrm{frequency})$ relations under different constrained circumstances.

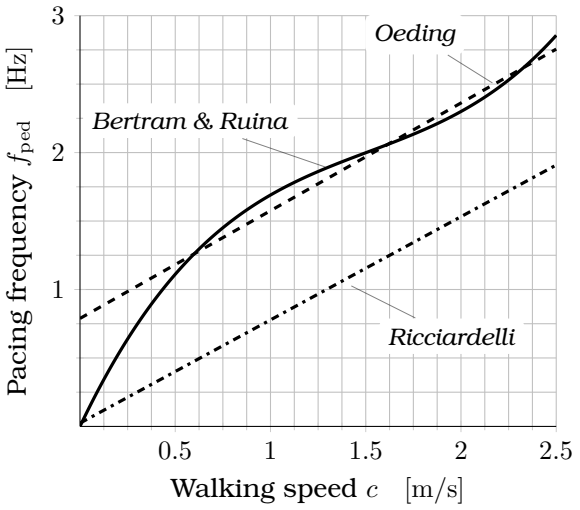

Figure 2.5: Examples of $f_{\mathrm{ped}}(c)$ relations.

The pacing frequency depends on the motion activity we are considering, which is to say the speed of the motion. Also, the walking speed is an individual property, and it is influenced by many factor like age, gender, height, and so on. Many studies have investigated how these aspects are correlated.

According to Ricciardelli et al. [32], linear relations can be found between the walking velocity and the step length or the walking frequency, while the latter two parameters can be considered as uncorrelated. Various $f_{\mathrm{ped}}(c)$ laws have been proposed as a fitting to empirical

Authors	Mean frequency f_μ Hz	Standard deviation f_σ Hz	Samples (people)
Leonard	1.7÷2.3	-	-
Matsumoto et al. 1972-78 [25]	2.0	0.173	505
Kerr and Bishop [21]	1.9	-	40
Bachmann et al. 1995 [4]	1.6÷2.4	-	-
Butz et al. [1]	1.84	0.126	-
Pachi and Ji	2.0÷1.83	0.135÷0.11	800
Ricciardelli et al.	1.835	0.172	116
Sanhaci and Kasperski	1.82	0.12	251
Živanović et al.	1.87	0.186	1976
Mean value	1.92	0.146	

Table 2.4: Probability distribution of the pacing frequency by different authors.

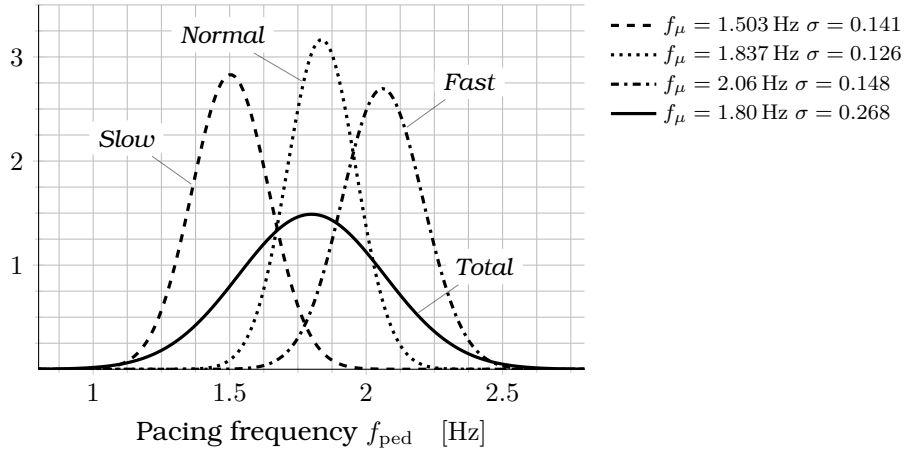

Figure 2.6: Probability density functions of the step frequencies regarding the walking intention taken from Butz [1].

measurements. Linear expressions have been proposed, for instance, by Oeding [29]:

$$f_{\text{ped}} = 0.7886 + 0.7868\ c$$

and by Ricciardelli et al. [32]:

$$f_{\text{ped}} = 0.024 + 0.754\ c$$

A non-linear relation based on a cubic fitting to the data has been formulated by Bertram and Ruina [5]:

$$f_{\text{ped}} = 2.93\ c - 1.59\ c^2 + 0.35\ c^3$$

These three $f_{\text{ped}}(c)$ relations are compared in figure 2.5.

The difference between the Bertram and Ruina and Ricciardelli et al. data, can be due to the different way in which the tests have been performed: in the first case, pedestrians walked on a treadmill with imposed constant speed, while, in the second, pedestrians were asked to walk naturally over a length of $72\,\text{m}$ on a sidewalk.

2.5 Density

The pedestrian density greatly influences the speed of the individual and is therefore important for the dynamic analysis. The relation between velocity and pedestrian density has been widely

researched. A physically-based formulation for the density estimation has been provided by Oeding:

$$n = \frac{N}{b_{\text{eff}} L} = \frac{\zeta}{c\ b_{\text{eff}}}$$

with the following meanings of the symbols:

n Pedestrian density

ζ Rate of pedestrian arrival

c Velocity of pase

N Number of pedestrian on bridge deck

b_{eff} Effective width of the bridge

L Length of bridge

In general the walking velocity reduces with increasing traffic density because of the reciprocal inhibition of the movement freedom. With high pedestrian densities, the mean velocity of the pedestrians decreases and the individual pedestrian attempts to adjust his frequency of pace to coincide with his neighbours.

Among the relations proposed it can be mentioned the linear law by Nelson:

$$c = 1.4(1 - 0.266n) \tag{2.2}$$

and the exponential law by Kladek [34]:

$$c_{\text{Kladek}} = 1.34\left(1 - e^{-1.913(1/n - 1/5.4)}\right) \tag{2.3}$$

The table 2.7 includes quite a number of relations and experimental data by different authors.

Together with the slowing down of the speed, that also means the frequency, what mostly affect the action exercised on the structure is the progressive concentration through a common speed, thus a common frequency. The evidence is given by the more narrow distribution of c for high density. This effect is shown, just qualitatively, in Fig. 2.8a and more or less corresponds to the initial description of human-human interaction as provided by Wheeler (1981).

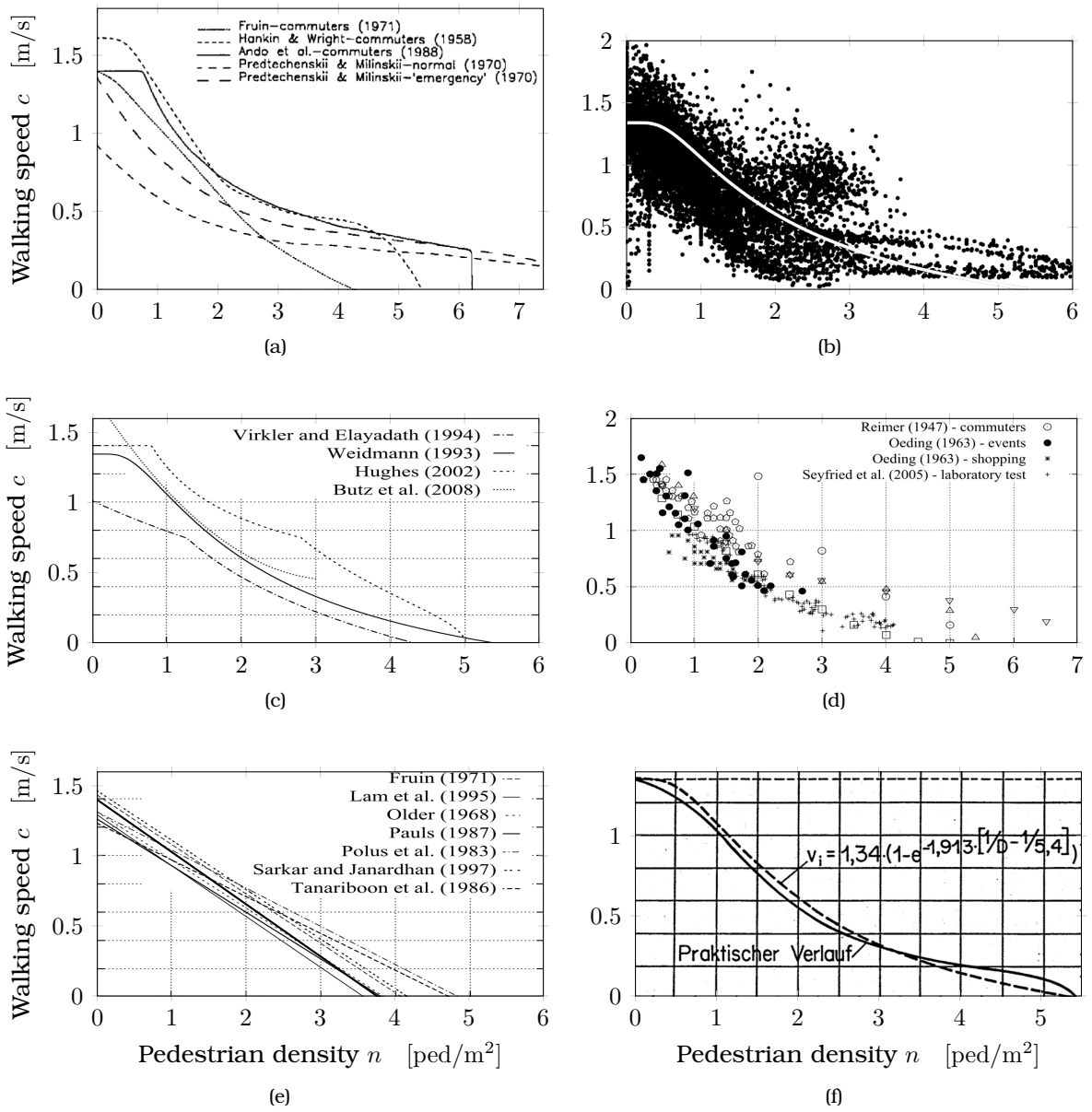

Figure 2.7: Speed(Density) relations and field measurements taken by different authors. a) Thompson and Marchant 1995 [33]; b) Bosina 2015: many literature data compared with Kladek's formula [7]; c) Non-linear relation proposed by different authors; d) Experimental measurements from Reimer et al.; e) Linear relations by different authors, and in addition Nelson's law (eq. 5.1) overlaid in black; f) Kladek's formula 1993 [34].

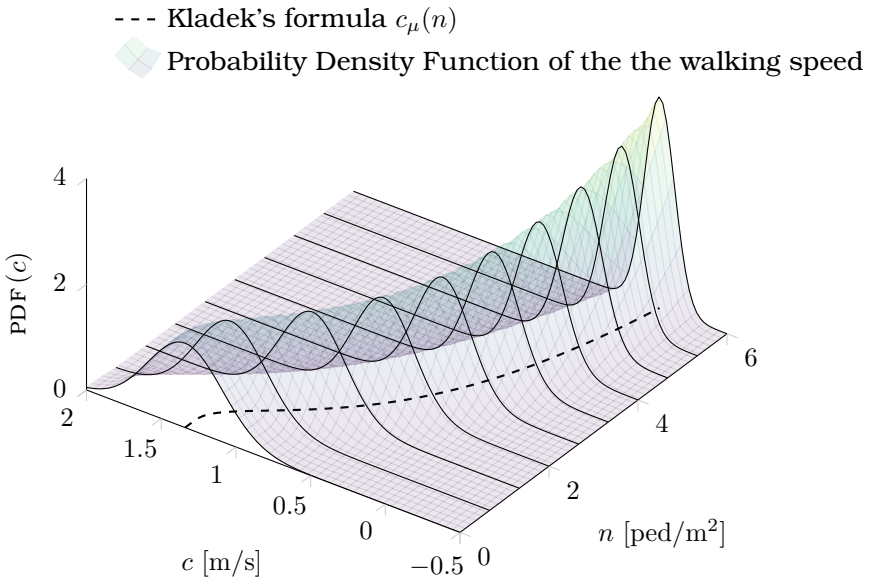

(a) Probability density function of the pacing velocity in three-dimensional view.

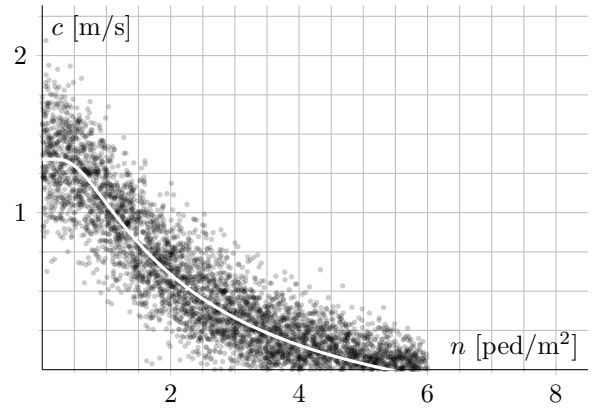

(b) Random sample points generated by means of the above distribution.

Figure 2.8

Chapter 3

MATLAB program validation

In this chapter some tests are performed in order to validate the performace of the MATLAB program. The code consists in a MATLAB script that aims to solve the dynamic equation of the beam under arbitrary loading conditions, in terms of modal coordinates. This is achieved by performing the convolution between the generalised load and the impulse response function (eq. 1.13) in vector form. The solution is constituted by the time history of the modal coordinate $y_j(t)$ in vector form. An arbitrary number of modal coordinates can be computed, based on the required accuracy, and finally the output in term of deformed shape in time $v(t)$ is reassembled by summing up all the modal contributions (eq. 1.2).

Unless otherwise stated, the data of the structure, intended as a beam-like, simply supported footbridge, are prescribed in table 3.1.

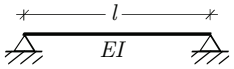

	Text notation	Code notation	Value
Length	l	`l`	$50\,\mathrm{m}$
Elastic modulus	E	`E`	$200\,000\,\mathrm{N/mm^2}$
Linear mass	γ	`gamma`	$3000\,\mathrm{kg/m}$
Sectional moment of inertia[a]	I	`I`	$1.5198 \times 10^{11}\,\mathrm{mm^4}$
Natural frequency of the structure (first mode)	f_{str}	`fstr`	$2\,\mathrm{Hz}$
Circular frequency (first mode)	ω_{str}	`omega_j(1)`	$12.56\,\mathrm{rad/s}$
Viscous damping factor	ξ	`csi`	0.2 (20%)
Number of modes	n_{arm}	`n_armoniche`	10

Table 3.1: Basic model for testing

[a]The moment of inertia is derived from 1.10 in order to have the natural frequency equal to $2\,\mathrm{Hz}$

Static concentrated load at the midspan

The load is applied at time $t = 0$. After a transition which is typical of the damped motion, the displacement stands at about $0.060\,\mathrm{mm}$. If static conditions are imposed in eq. 1.11 (acceleration and velocity null), the modal coordinates assume the following form:

$$y_j(t = \infty) = \frac{2Pl^3}{\pi^4 EI} \frac{\sin\left(\frac{j\pi}{2}\right)}{j^4}$$

The displacement value corresponds to that we obtain from the eigenfunction summation:

$$v_{l/2,t=\infty} = \frac{2Pl^3}{\pi^4 EI} \sum_{j=1}^{10} \frac{\sin^2 \frac{j\pi}{2}}{j^4} = \frac{2Pl^3}{\pi^4 EI} \left(1 + \frac{1}{3^4} + \frac{1}{5^4} + \frac{1}{7^4} + \frac{1}{9^4}\right) = 5.997 \times 10^{-2}\,\mathrm{mm} \tag{3.1}$$

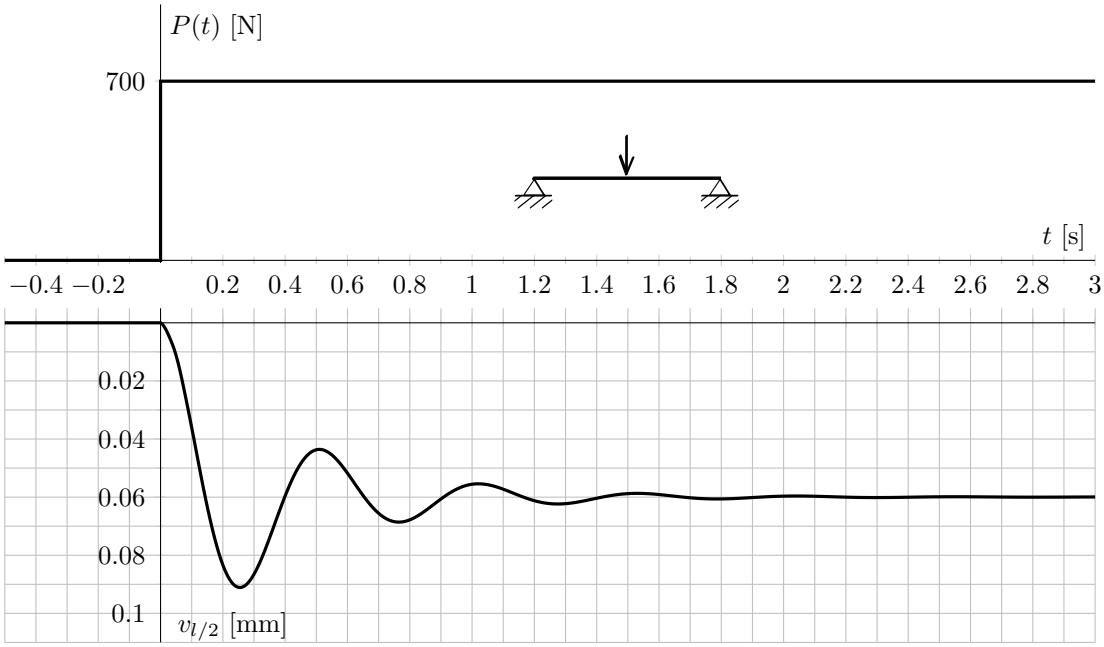

Figure 3.1: Displacement at the midspan due to concentrated constant load applied at starting time.

which in turn tends to the exact value by Euler-Bernoulli:

$$v_{l/2} = \frac{1}{48}\frac{Pl^3}{EI} = 5.997 \times 10^{-2}\,\mathrm{mm} \tag{3.2}$$

with an error equal to 9.6×10^{-6}. The diagram is plotted in figure 3.1, while in figure 3.2 it is shown that by removing the load the displacement tends back to zero after an analogous transition.

Concentrated moving load with constant amplitude

The motion of the load can magnify the dynamics displacements in the beam. Such a result occurs when the load moves in a period of time which has the same order of magnitude of the natural period of the structure. We might say that the load is in a sense *steering into* the beam.

The maximum effect is reached when the load crosses at a speed equal to the critical one, which is the speed required to cover the entire beam in a time corresponding to the period of the first mode of vibration.

As defined, it is:

$$c_{cr} = \frac{\pi}{l}\sqrt{\frac{EI}{\gamma}} \tag{3.3}$$

In this case it provides $c_{cr} = 200\,\mathrm{m/s}$, a speed which is pretty far from the usual pedestrian range.

In the diagram 3.3 are plotted the results of three runnings of the code with different load speeds. We can see how the displacement track for $c = 2\,\mathrm{m/s}$ and $c = 20\,\mathrm{m/s}$ correctly resembles the influence line of the beam. This means that the effect of such a moving load is approximately the same of a load statically placed point by point. Vice versa for $c = c_{cr}$ the displacement track is magnified and its maximum exceeds the static one.

In the diagram 3.4 the same plot set has been normalised with respect to the crossing period.($T = c/l$) The so obtained shapes coincides with those reported by Frýba [16]. We observe again that if the speed is in the walking range ($c \approx 1.8\,\mathrm{m/s}$) the dynamic effects are negligible.

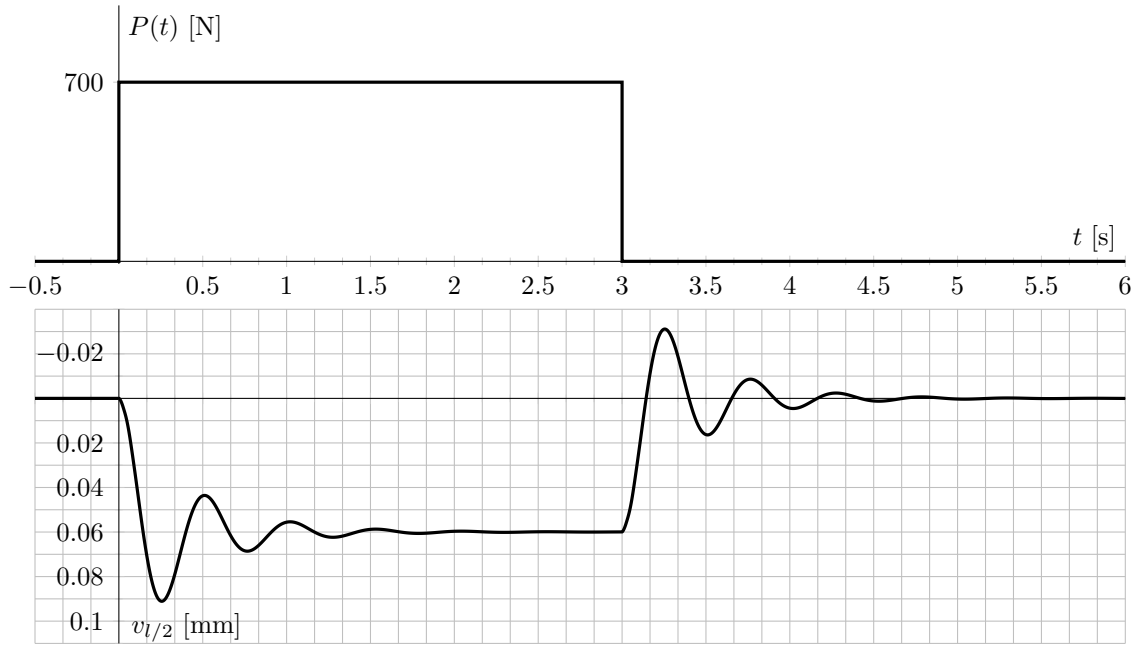

Figure 3.2: Displacement at the midspan due to concentrated constant load applied at starting time and then removed at time $t = 3\,\mathrm{s}$.

As a conclusion we can state that a static approach is equally representative of the problem. This means that if we model the pedestrians as a static harmonic force which is not effectively moving, we expect to obtain mainly the same results as they are moving.

That fact allows us not to take them into account in the developing of the next theoretical formulation.

Harmonic concentrated load in the midspan

The system is analogous to the damped oscillator subjected to harmonic force. The discriminant is here the load pulsatance, which can produce the amplification or the reduction of the beam displacements, as a function of the ratio with the natural frequency.

In figure 3.5 it is shown the curve for a load that could represent the single pedestrian. It is assumed as the amplitude of the force, the conventional value equal to the 40% of the weight force $P_S = 700\,\mathrm{N}$, that is to say $P_D = 280\,\mathrm{N}$. While the frequency is the representative value $1.8\,\mathrm{Hz}$.

We can state that the maximum displacement $v_{D,\max}$ under harmonic load is given by the one due to an equivalent static load v_S times the amplification factor $N(\beta)$, with $\beta = \dfrac{f_{\mathrm{ped}}}{f_{\mathrm{str}}}$:

$$v_{D,\max} = N(\beta) \cdot v_S \tag{3.4}$$

with the usual form for $N(\beta)$:

$$N(\beta) = \frac{1}{\sqrt{(1-\beta^2)^2 + 4\xi^2\beta^2}} \tag{3.5}$$

In the current case we get $\beta = 1.8\,\mathrm{Hz}/2.0\,\mathrm{Hz} = 0.9$, and then $N(0.9) = 2.456$. It follows:

$$v_{S,l/2} \simeq \frac{1}{48}\frac{P_D l^3}{EI} = 2.39 \times 10^{-2}\,\mathrm{mm}$$
$$v_{D,l/2} = 2.456 \times 2.39 \times 10^{-2}\,\mathrm{mm} = 5.89 \times 10^{-2}\,\mathrm{mm}$$

That validates the result of figure 3.5.

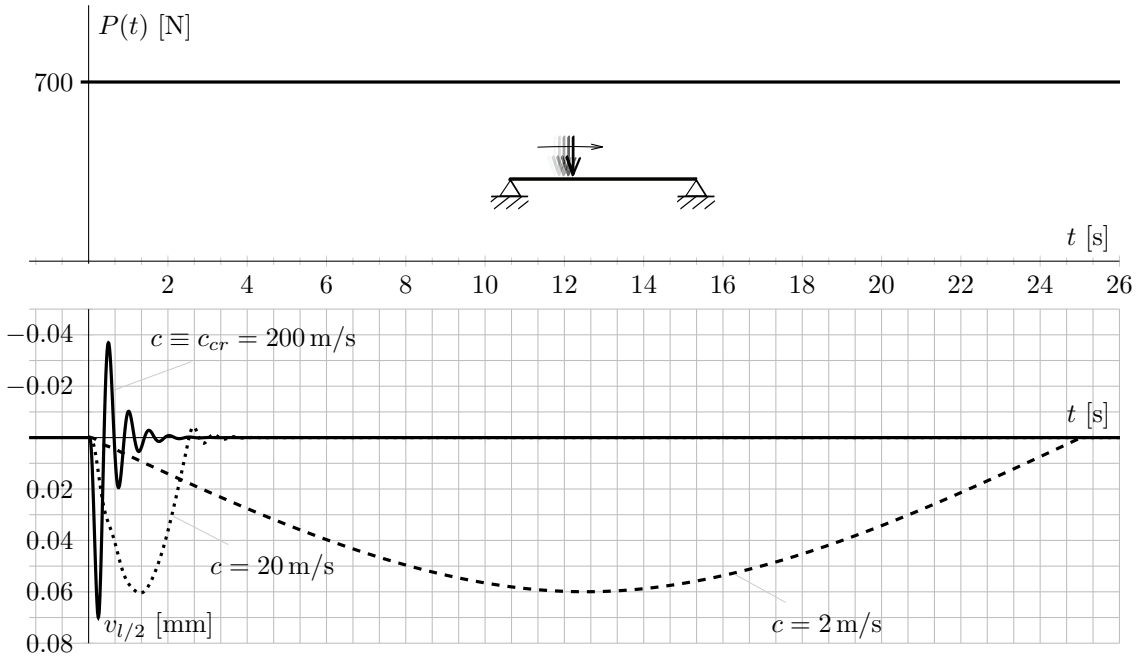

Figure 3.3: Midspan displacement due to concentrated load moving at three different speeds. The crossing begins at time $t = 0$.

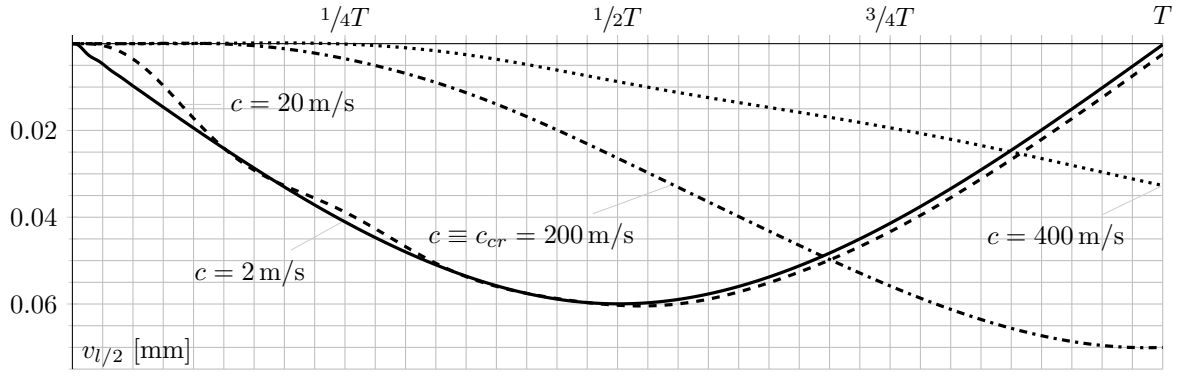

Figure 3.4: Midspan displacement due to concentrated load, moving with four different speeds, time axes normalised with respect to the crossing period ($T = c/l$).

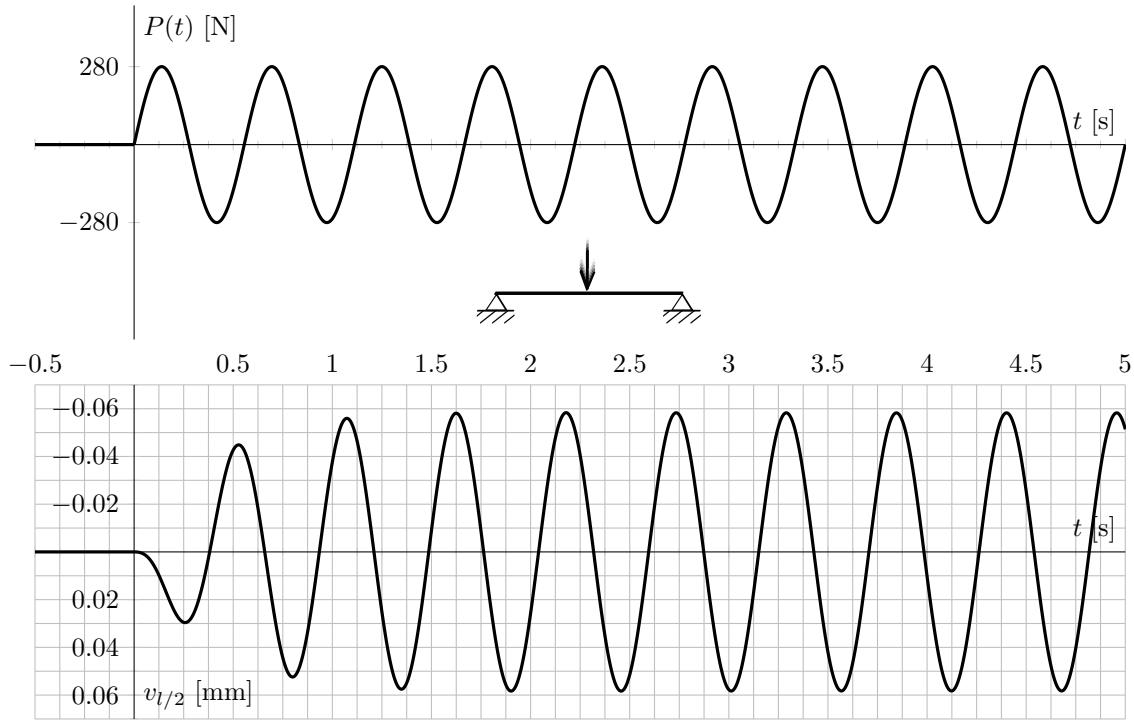

Figure 3.5: Midspan displacement under harmonic load concentrated at the midspan. $P(t) = P_D \sin(2\pi f_\mu t)$, $P_D = 280\,\mathrm{N}$, $f_\mu = 1.8\,\mathrm{Hz}$

Harmonic concentrated load, moving at $c = 1.62\,\mathrm{m/s} \ll c_{cr}$

The prescribed velocity must be referred to a perfect pedestrian which is walking with a pacing frequency equal to $1.8\,\mathrm{Hz}$ and a step length equal to $90\,\mathrm{cm}$. The load is moving and its amplitude varies following the harmonic law. Since its speed is quite lower than the critical speed we're expecting a displacement similar to that of figure 3.5, but modulated by the modal shape. Also we should find at half way a very similar magnitude.

The result, reported in figure 3.6, correctly presents these elements. The vibration of the structure ends with the exit of the load from the beam (some seconds later, actually, because of the inertia) after the crossing period $T = 30.86\,\mathrm{s}$.

In simulation 3.7 it is added to the load a constant component $P_S = 700\,\mathrm{N}$. The displacement trace is now representative that one of a synthetic pedestrian having mass $70\,\mathrm{kg}$.

Distributed constant load

We're calling it distributed for simplicity, but the loading case actually consists of a line of concentrated loads. In the simulation of figure 3.8 the load is applied in the initial instant and left still. Obviously nothing different from the test reported in figure 3.1 is expected, the only thing, the magnitude of the displacement must be greater. One finds that the modal coordinate in static conditions is:

$$y_j(t=\infty) = \frac{4ql^4}{\pi^5 EI}\frac{1}{j^5}$$

thus, the midspan displacement is:

$$v_{l/2,t=\infty} = \frac{4ql^4}{\pi^5 EI}\sum_{j=1}^{10}\frac{\sin\frac{j\pi}{2}}{j^5} = \frac{4ql^4}{\pi^5 EI}\left(1 - \frac{1}{3^5} + \frac{1}{5^5} - \frac{1}{7^5} + \frac{1}{9^5}\right) = 0.937\,\mathrm{mm} \tag{3.6}$$

which in turn tends to the exact value by Euler-Bernoulli:

$$v_{l/2} = \frac{5}{384}\frac{ql^4}{EI} = 0.937\,\mathrm{mm} \tag{3.7}$$

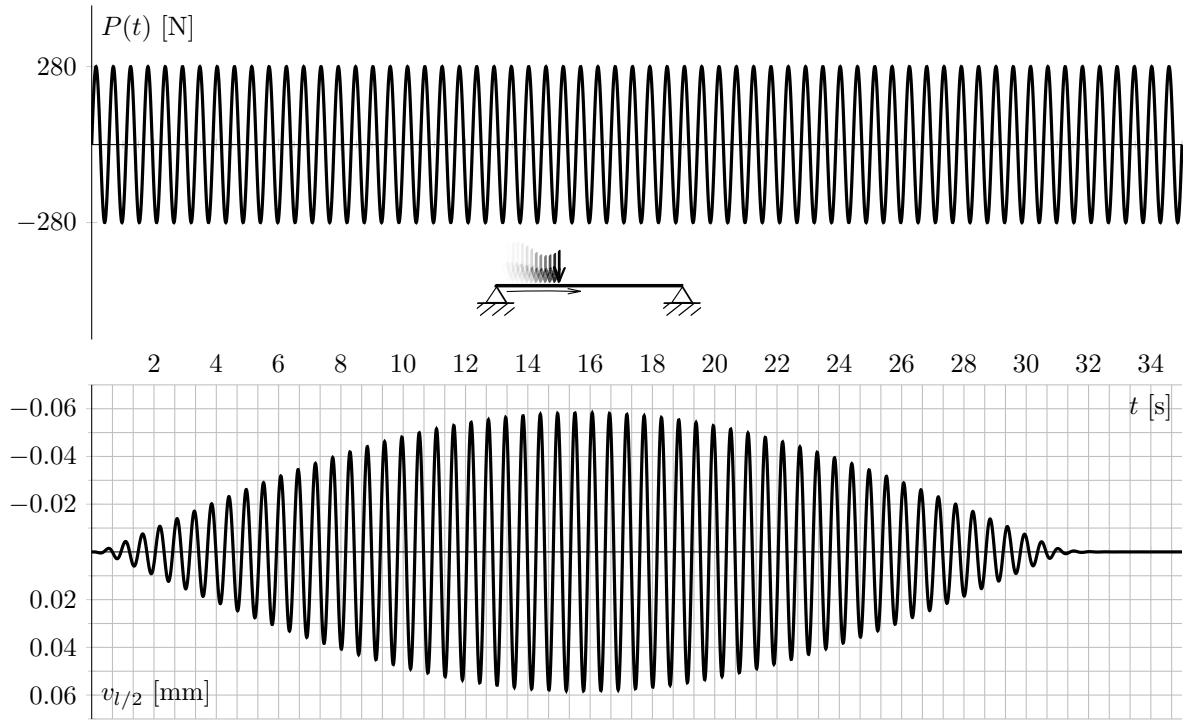

Figure 3.6: Midspan displacement under concentrated harmonic load, moving at $c = 1.62\,\mathrm{m/s}$. Crossing begins at time $t = 0$. $P(t) = P_D \sin(2\pi f_\mu t)$, $P_D = 280\,\mathrm{N}$, $f_\mu = 1.8\,\mathrm{Hz}$

with an absolute error 4.12×10^{-6}.

Distributed constant load in motion

The test 3.8 shall be used in order to simulate a crowd crossing the footbridge. The simulation is carried out with a sample of $2N$ forces, representing the walking pedestrians, which are equally spaced along twice the beam length, so that we can observe a transitional stage from $t = 0$ to $t = T$ in which the bridge is filling up, followed by a stationary stage from $t = T$ to $t = 2T$ where the brisge contains N forces in motion, and after that a last transitional phase in which the bridge is emptying out from $t = 2T$ to $t = 3T$.

During the first period the displacement is supposed to increase from 0 to $0.937\,\mathrm{mm}$, which corresponds to the maximum static displacement $v_{\max}$ already found that we would get if the load is not moving. Then it's expected to remain more or less constant (very small oscillations can occur because the first punctual load in the line goes down before than a new one comes up, and this repeat continually). Finally, it gradually goes to 0.

We are interested in studying the second period, by virtue of its stationary in time. Some useful quantities like the variance and the effective value of the response, both in terms of displacements and accelerations, shall be computed in the following chapters.

Distributed load with constant and harmonic component in motion

As concerns this case, what has been observed for the distributed constant load in motion and for the concentrated harmonic load also applies to it. In figure 3.10 three simulations with different structural frequencies are performed. The distributed load consists in a string of concentrated loads, each one having oscillation frequency set to $f_\mu = 1.8\,\mathrm{Hz}$. The magnitude of the dynamic component is $280\,\mathrm{N}$ and the static one is $700\,\mathrm{N}$. They are in phase and thus the overall distribution load is $q = 350\,\mathrm{N/m} + 140\,\mathrm{N/m}\sin(2\pi f_\mu t)$.

For the three cases a predicted theoretical displacement can be computed (note that if f_{str} changes, the modulus of inertia I changes as well). The obtained values are reported in

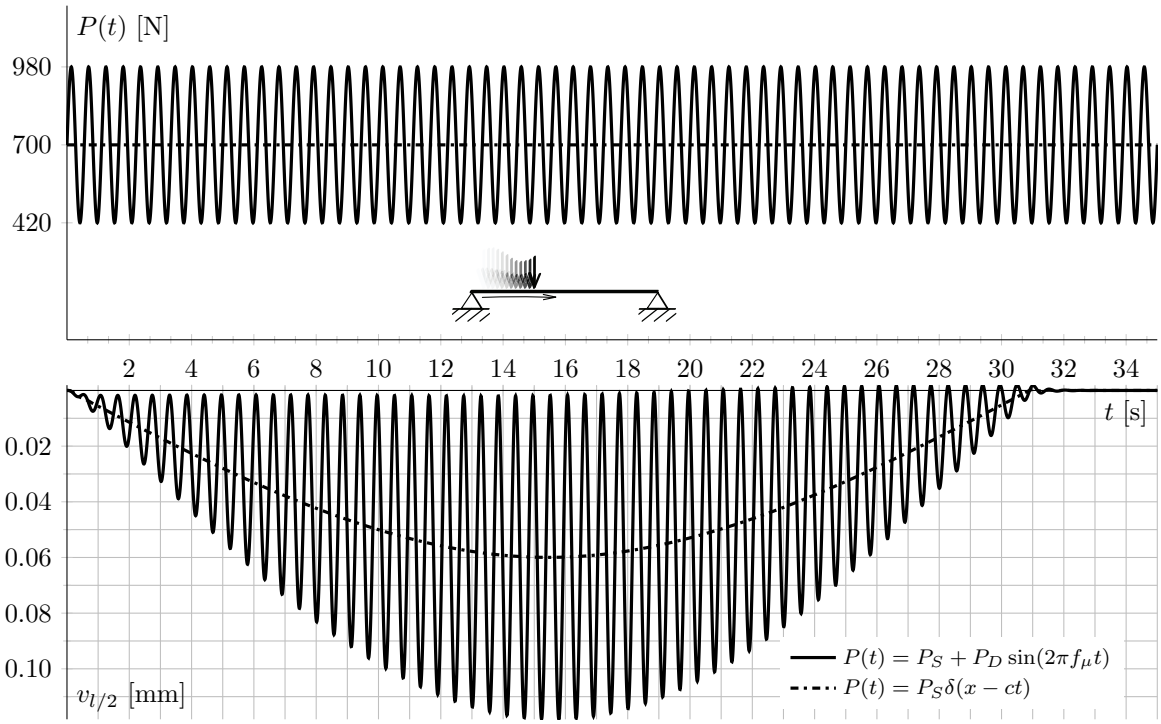

Figure 3.7: Midspan displacement under harmonic concentrated load, moving at $c = 1.62\,\mathrm{m/s}$. Crossing starts at time $t = 0$. $P(t) = P_S + P_D \sin(2\pi f_\mu t)$, $P_S = 700\,\mathrm{N}$, $P_D = 280\,\mathrm{N}$, $f_\mu = 1.8\,\mathrm{Hz}$

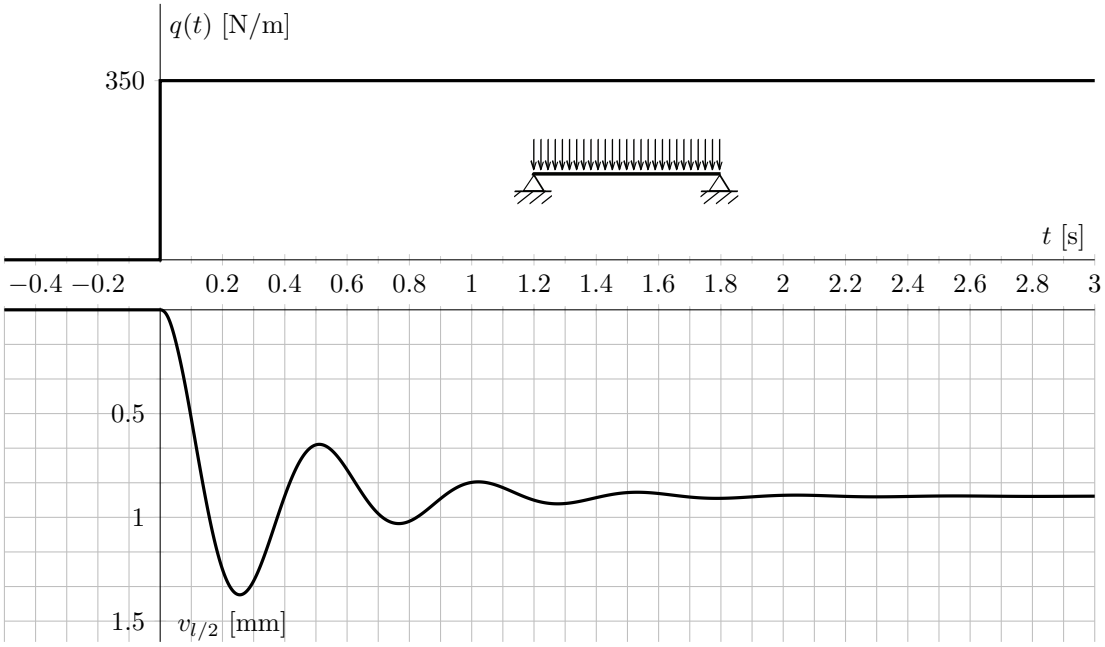

Figure 3.8: Midspan displacement under distributed static load applied at time $t = 0$.

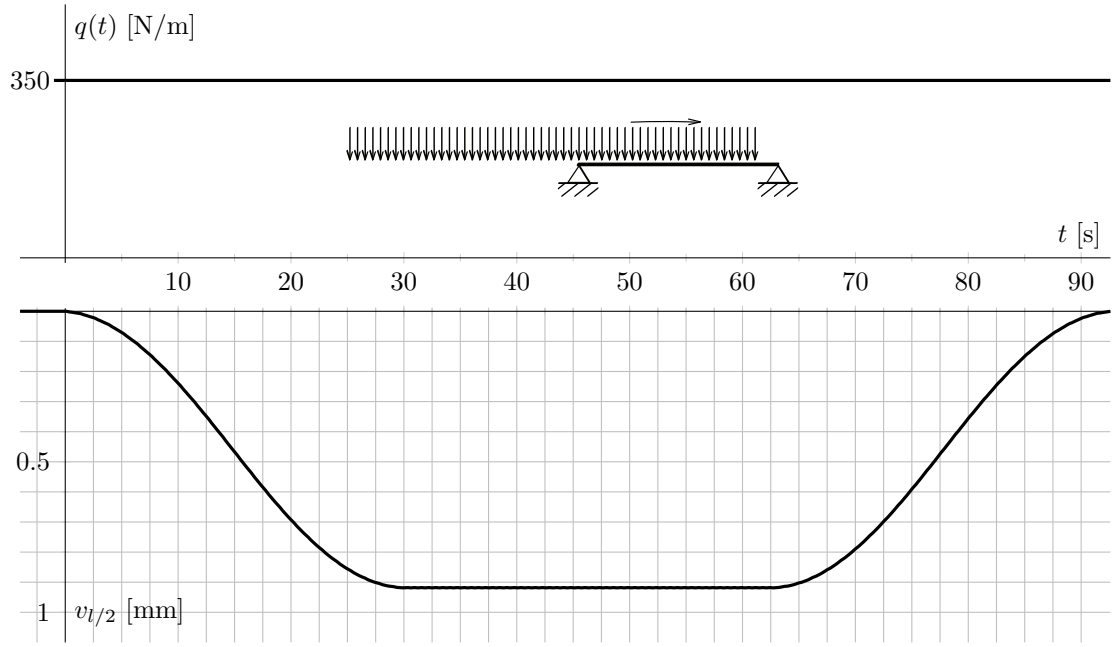

Figure 3.9: Midspan displacement due to distributed constant load, transiting at speed $1.62\,\mathrm{m/s}$. Crossing period equal to $T = 30.86\,\mathrm{s}$.

f_{str}	β	Amplification factor $N(\beta)$	v_S	Theoretical v_D	Output v_D	Error
0.5	3.6	0.083	5.749	0.477	0.504	5.5%
1	1.8	0.425	1.437	0.610	0.618	1.1%
2	0.9	2.456	0.359	0.883	0.887	0.4%

Table 3.2

table 3.2. The static displacement v_S refers to the displacement due to a constant distributed load $q = 140\,\mathrm{N/m}$, hence the dynamic displacement v_D, which is given by the static displacement times the amplification factor $N(\beta)$ (figure 3.11), stands for the magnitude of the oscillation one can see in figure 3.10 in the stationary phase.

Number of harmonics

Figure 3.12 shows the convergence of the midspan displacement computed by means of the eigenfunctions decomposition. The values refers to the midspan displacement under concentrated load described at page 23, and in particular to the series equation 3.1. One can find that the method benefits from a quick convergence through the axact value, which is $\frac{1}{48}\frac{Pl^3}{EI}$,and that is marked by the dotted line in the graph. The even terms of the series are not taken into account because they does add a null contribute to the sum. By virtue of the small error registered, we can arrest the computation even to the first term, without incurring in lack of accuracy.

The computed values for the converging maximum displacement are given in table 3.3.

Discretization

A not negligible fact is regarding the discretization limits to be set in the program. They concern the space discretization and the time discretization. The space discretization means the number of elements the beam is split into of the abscissa vector. This basically doesn't affect the measurement at the midspan, since it counts only in the recomposition of the

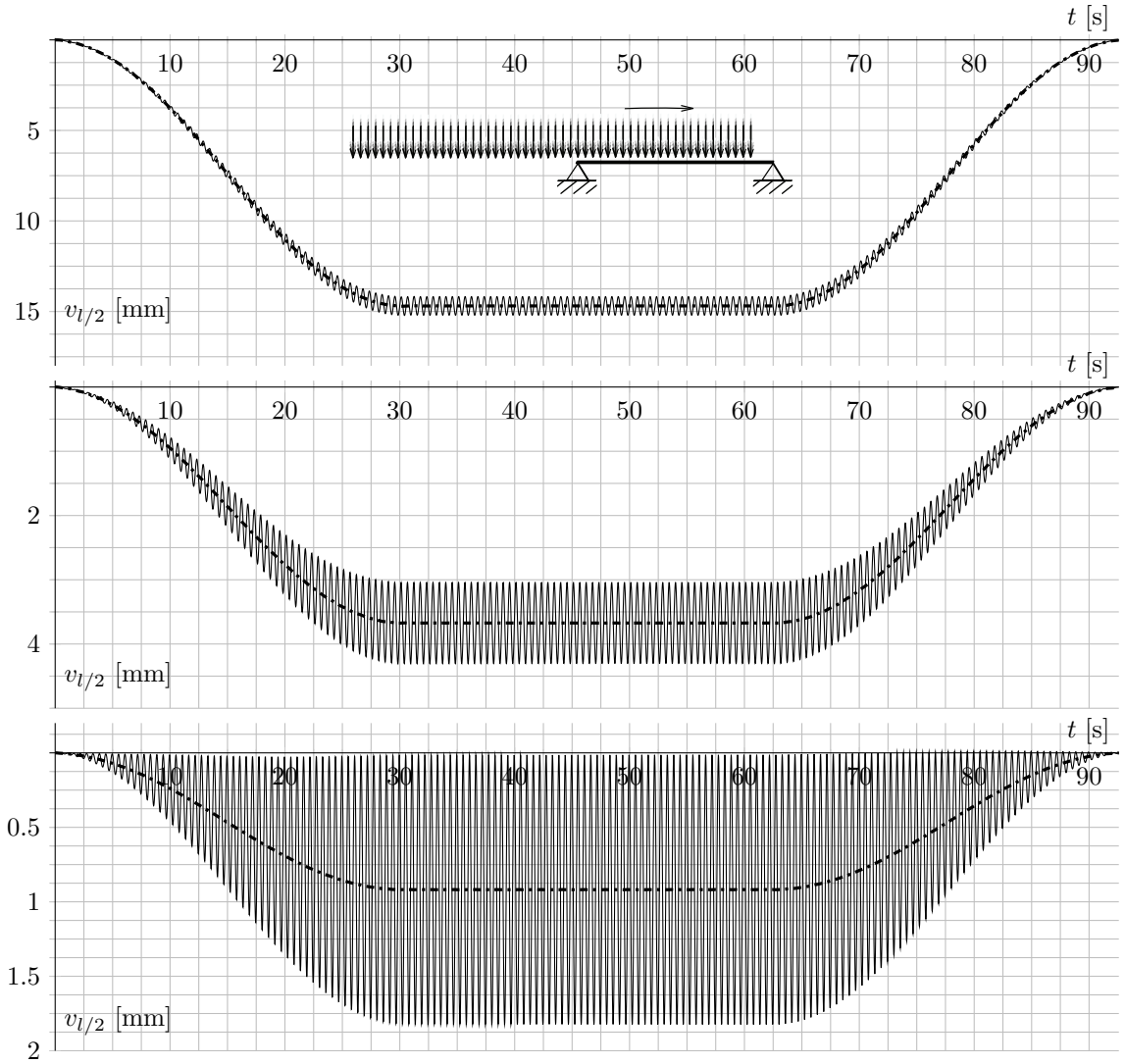

Figure 3.10

solution. But it is guaranteed only as long as a node coincides with it or is very close. The same applies if an other point is used as a sample.

A different consideration concerns the time discretization. Since it ultimately determines the accuracy in the time history of the modal coordinates, it plays a crucial role. Figure 3.13 illustrates how the midpan displacement tie history is affected by the time discretization, passing from a time-step equal to $\Delta = 0.1\,\mathrm{s}$ to $\Delta = 0.001\,\mathrm{s}$. There is a great gain in terms of accuracy passing from $\Delta = 0.1\,\mathrm{s}$ to $\Delta = 0.01\,\mathrm{s}$ whereas we get only a marginal profit passing from $\Delta = 0.01\,\mathrm{s}$ to $\Delta = 0.001\,\mathrm{s}$. By virtue of this evidence, the discretization step adopted for following developments is $\Delta = 0.01\,\mathrm{s}$.

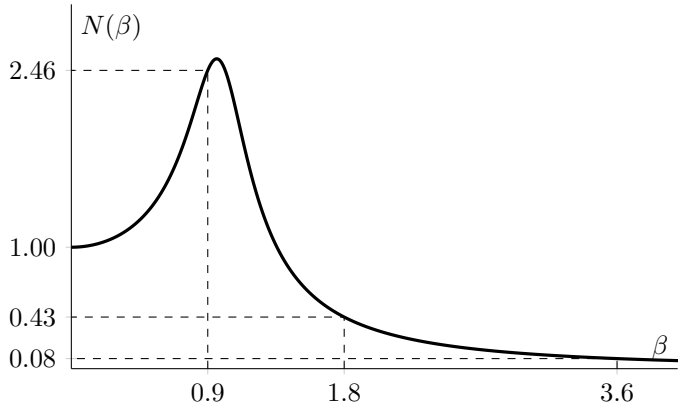

Figure 3.11: Amplification factor for $\xi = 0.2$

Number of harmonics	$v_{S,t=\infty}$
1	0.059 104
3	0.059 833
5	0.059 928
7	0.059 952
9	0.059 961
Exact value	0.059 971 55...

Table 3.3

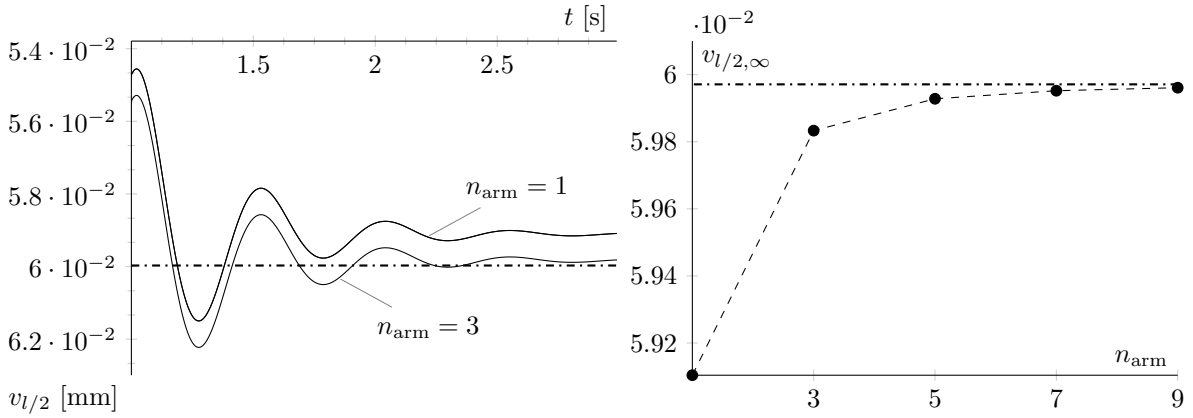

Figure 3.12: Convergence to the exact value of the midspan displacement by increasing the number of harmonics.

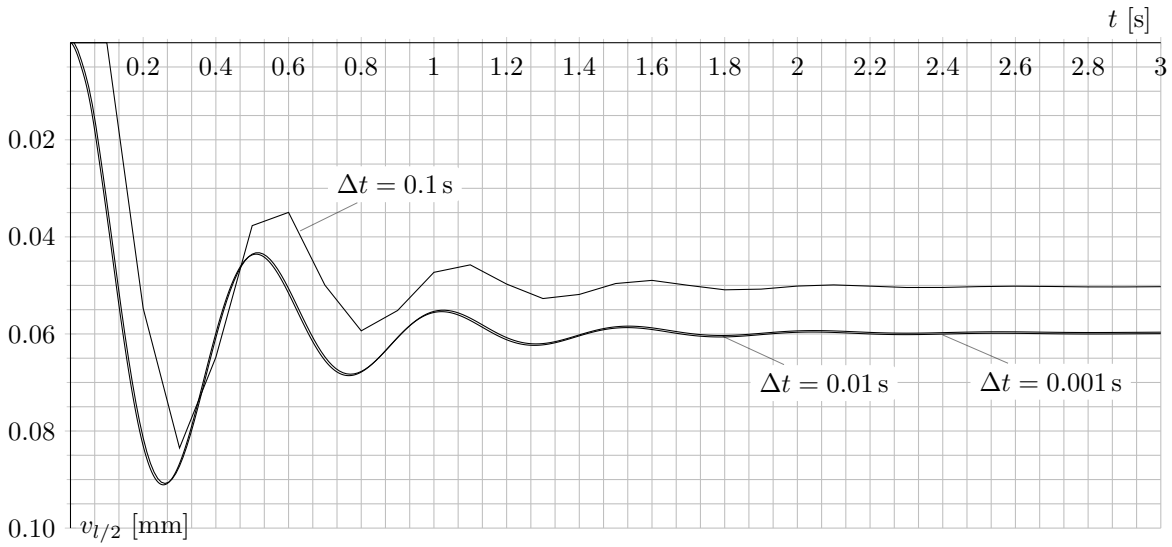

Figure 3.13: Midspan displacement time history with different time-step discretizations.

Chapter 4

Acceleration response — varying pedestrian phase and frequency

In this chapter the two random variables of the model are introduced: the pedestrian phase and pacing frequency. Subsequently a formula for the computation of the RMS of the response in terms of displacement and acceleration is proposed.

The adopted approach falls within the random vibration theory, which allows to represent the loading and the response in the frequency domain through their Power Spectral Density (PSD). The formulation is then accompanied and supported by MATLAB simulations.

4.1 Random variables introduction

The dynamic system to be examined consists in a simply supported beam, as seen in previous chapter, that represents the static scheme of a footbridge, with a continuous file of pedestrian passing on it. The pedestrian are uniformly spaced so that when the beam is entirely covered the total number is 25.

The force exercised by each pedestrian, the Ground Reaction Force, is now rewritten from equation 2.1 with a little change in notation:

$$F_{\text{ped}} = W + \sum_{i}^{n_{\text{arm}}} W \cdot \text{DLF}_i \sin\left(2\pi i f_{\text{ped}} t + \phi_i\right) \tag{4.1}$$

From now on, W shall be set to $700\,\text{N}$, DLF to 0.4, and it is taken into account the 1^{st} harmonic only.

4.1.1 Phases distribution

With regard to the phases ϕ no information are known, that is to say they are supposed to be randomly distributed, and in a spread crowd there are no reasons for them to be somehow correlated. In this respect, we've been led to set the phases probability distribution as a uniform distribution.

In order to be able to modulate the overall distribution, we're introducing the parameter α. It meaures the width of the band where the phases are spread out. Figure 4.1 clarifies its meaning. If $\alpha = 2\pi$ the phases are uniformly distributed between 0 and 2π, if $\alpha = 0$ all the phases are equal to 0. The smaller is the parameter α the closer are the phases each other.

$$p(\phi) = \frac{1}{\alpha}\text{rect}\left(\frac{\phi}{\alpha} - \frac{1}{2}\right) \tag{4.2}$$

This parameter was initially introduced by Capsoni [9] and adopted by Mariani & Mandelli [23].

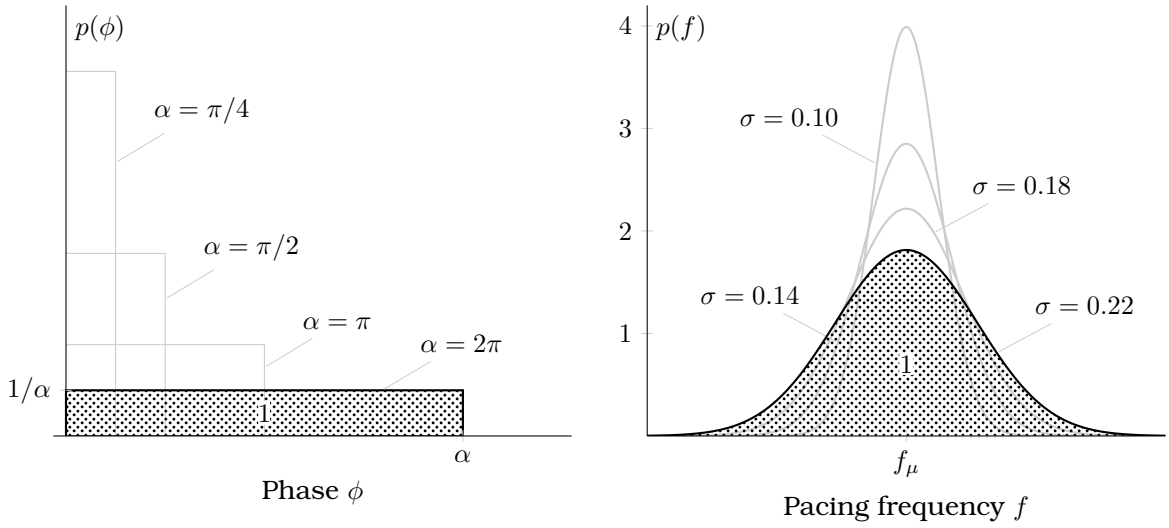

Figure 4.1: Probability density distribution of loads phases and frequencies

4.1.2 Pacing frequency distribution

For the pacing frequency a normal distribution is assumed, according to the literature (see section 2.4). Among the many values for the mean pacing frequency proposed by the researchers, it is chosen $f_\mu = 1.8\,\mathrm{Hz}$, [1] for its simplicity.

It is known that the variance of the walking frequency has a high level of randomness, so this one will be our random variable. Although we know it normally stands between $0.1 \div 0.2$ the wider interval $0 \div 1$ is going to be studied.

The normal distribution is described by:

$$p\left(f_{\mathrm{ped}}\right) = \frac{1}{\sigma}\,\varphi\left(\frac{f_{\mathrm{ped}} - f_\mu}{\sigma}\right) \tag{4.3}$$

where $\varphi(x)$ is the standard normal distribution. In extended form:

$$p\left(f_{\mathrm{ped}}\right) = \frac{1}{\sigma\sqrt{2\pi}} e^{-\frac{\left(f_{\mathrm{ped}} - f_\mu\right)^2}{2\sigma^2}} \tag{4.4}$$

Figure 4.1 shows the probability density function of the pacing frequency as it has just been defined.

In figure 4.2 and 4.3 are provided some simulation made with the MATLAB program with varying α and σ. One can see the principal difference in how these two parameter of randomness affect the time histories. A greater scattering in the phases of the pedestrian produces a smaller response, which however keeps a certain regularity in time.

The major scattering in the walking frequencies leads to a substantially different result, the output is much more irregular, and even if very small values are reached in some time instants, biggest ones are reach in others, so that cannot be concluded that the effective value of the response is smaller. It could be bigger, as it is demonstrated in section 4.3.

4.2 Stochastic load model

Random vibration theory provides us the useful formula in terms of ASD (Auto Spectral Density):

$$S_y(f) = H^*(f)H(f)S_x(f) = |H(f)|^2 S_x(f) \tag{4.5}$$

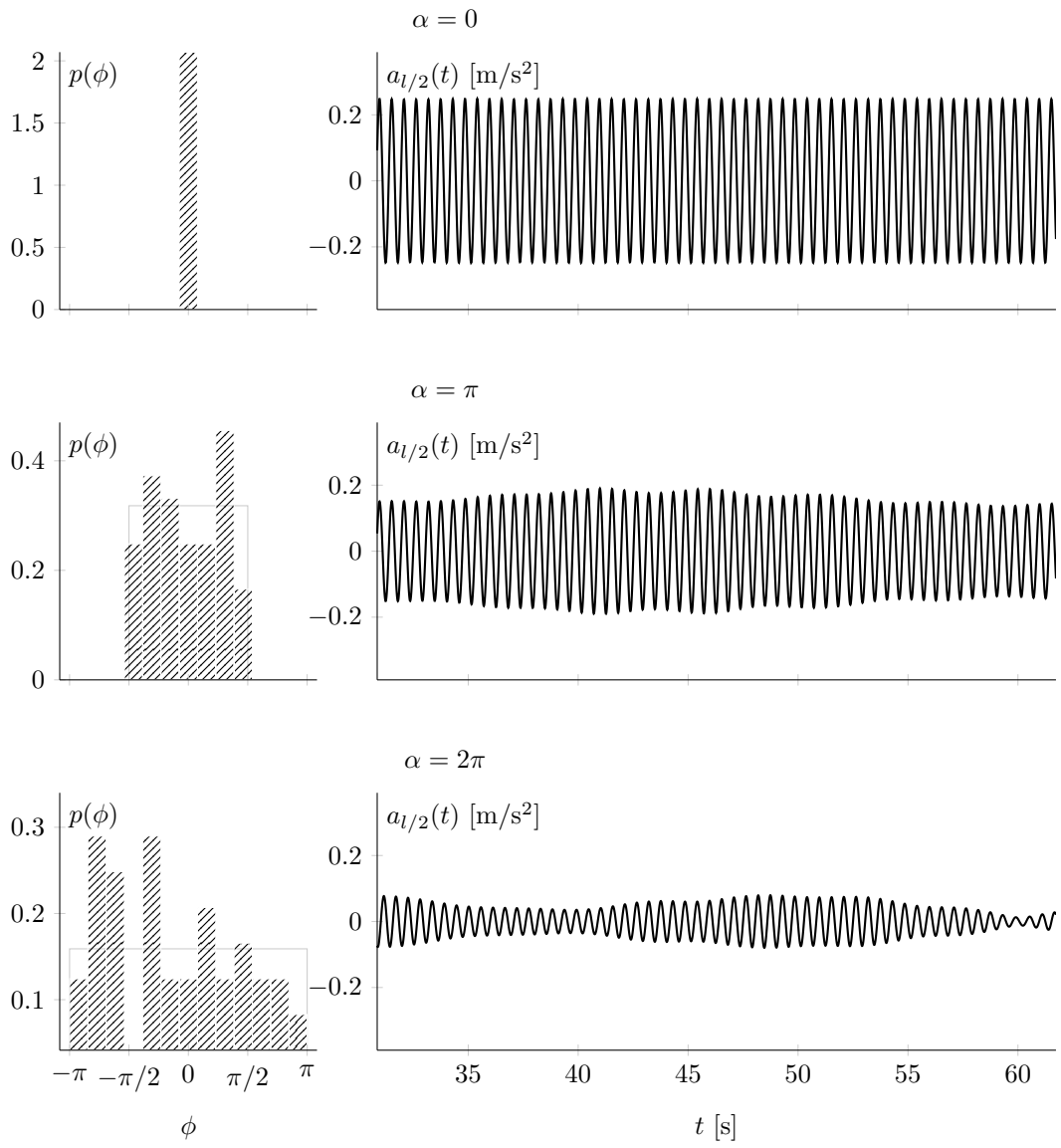

Figure 4.2: Three generated time histories with zero, π, and 2π width of the phase band.

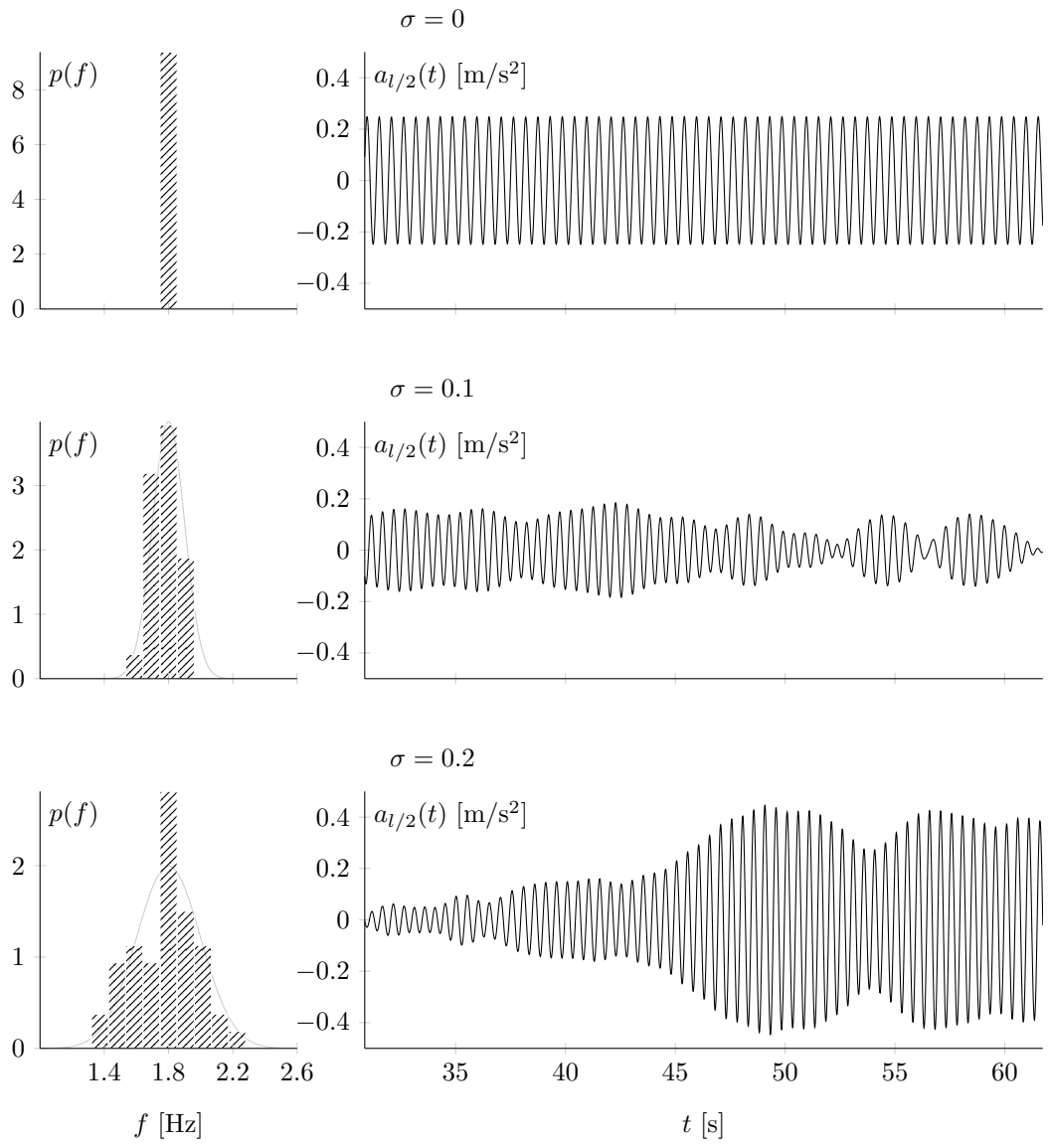

Figure 4.3: Three generated time histories with zero, small and great frequency variance.

that expresses the ASD of the response of a generic single-degree of freedom system excited by a single force. What is also called single input-single output system. The Frequency Response Function is:

$$H(f) = \frac{1}{k}\frac{1}{1-\beta^2+2i\xi\beta}$$

while its modulus is:

$$|H(f)| = \frac{1}{k^2}\frac{1}{\sqrt{(1-\beta^2)^2+4\xi^2\beta^2}}$$

with the usual meaning of the variable $\beta = \dfrac{f}{f_n}$. f is the frequency of the excitation force and f_n the natural frequency of the system. It should more correctly be indicated in respect of the modal number f_j, but in this context only the first harmonic is used, so the term f_n, standing for f_1, is sufficient.

Adapted for this case the relation links the input ASD of a force and the output of a displacement:

$$S_v(f) = |H(f)|^2 S_F(f) \tag{4.6}$$

In the case of 2 input forces the relation changes form:

$$S_v = H_1^* H_1 S_{F_1} + H_1^* H_2 S_{F_1F_2} + H_2^* H_1 S_{F_2F_1} + H_2^* H_2 S_{F_2}$$

having used S_{F_1} and S_{F_2} as the ASD of the two random forces and $S_{F_1F_2}$ for the cross spectral density. The notation also implies that $S_{F_1F_1} = S_{F_1}$.

Extending it to any multi-input system, in a compact way it becomes:

$$S_v = \sum_{r=1}^{N}\sum_{s=1}^{N} H_r^* H_s S_{F_rF_s}$$

which is, — in the Newland words — *the central result of random vibration theory, and its simplicity justify our faith in the Fourier transform and frequency response approach.* Nethertheless its application is restricted to single dof systems.

For a continuous system which can be described by means of eigenfunctions, the 4.6 becomes:

$$S_v(z, z_1, f) = |H(z, z_1, f)|^2 S_F(f)$$

where:

$$H(z, z_1, f) = |H(f)|\psi(z)\psi(z_1)$$

$$|H(z, z_1, f)| = \left\{ \left[\sum_{j}^{n_{\text{arm}}} \psi_j(z)\psi_j(z_1)H(f, f_j)\cos\phi_j\right]^2 + \left[\sum_{j}^{n_{\text{arm}}} \psi_j(z)\psi_j(z_1)H(f, f_j)\sin\phi_j\right]^2 \right\}^{0.5}$$

with $\psi_j(z)$ the j-th modal shape. $H(z, z_1, f)$ is here describing the frequency output in an arbitrary abscissa when the structure is excited by a random force in z_1. So that is the case of single outputs.

More extensively it reads:

$$S_v(z, z_1, f) = |H(z, z_1, f)|^2 S_F(f) = \psi_1(z)^2\psi_1(z_1)^2|H(f)|^2 S_F(f)$$

For multi-input — single-output case (2 forces) the formulation is the following:

$$S_v(z, z_1, z_2, f) = |H_1|^2 S_{F_1} + |H_2|^2 S_{F_2} + 2|H_1||H_2|\left\{S^C_{F_1F_2}\cos(\zeta_1-\zeta_2) + S^Q_{F_1F_2}\sin(\zeta_1-\zeta_2)\right\}$$

where $S^C_{F_1F_2}$ and $S^Q_{F_1F_2}$ are the cross spectral density in phase and in quadrature. With the following phase shift:

$$\zeta_i = \arctan\left(\frac{2\xi_i\beta_i}{1-\beta_i^2}\right)$$

It is the case that every force exercised by the pedestrian has the same ASD, so we can simplify $S_{F_1} = S_{F_2} = S_F$ and collect out of the parentesis:

$$S_v(z, z_1, z_2, f) = S_F\left\{|H_1|^2 + |H_2|^2 + 2|H_1||H_2|\left\{\frac{S^C_{F_1F_2}\cos(\zeta_1-\zeta_2) + S^Q_{F_1F_2}\sin(\zeta_1-\zeta_2)}{S_F}\right\}\right\}$$

It is now introduced the *coherence* function as:

$$\text{Coh}(f) = \frac{|S_{F_1F_2}|^2}{S_{F_1}S_{F_2}}$$

It mainly gives a measure of how much the forces are correlated each other. It assume the value 0 when the correlation is totally absent, and 1 when it is maximal.

One has:

$$S_v = S_F\left(|H_1|^2 + |H_2|^2 + 2|H_1||H_2|\sqrt{\text{Coh}}\right)$$

and then extending to the general multi-input case:

$$S_v = S_F\left(\sum_r^N |H_r|^2\left(1-\sqrt{\text{Coh}}\right) + \sum_r^N\sum_s^N |H_r||H_s|\sqrt{\text{Coh}}\right)$$

we substitute the frequency response function taking just the first harmonic:

$$S_v = S_F\left(\sum_r^N \psi_1(z)^2\psi_1(z_r)^2|H|^2\left(1-\sqrt{\text{Coh}}\right) + \sum_r^N\sum_s^N\big(\psi_1(z)\psi_1(z_r)\big)\big(\psi_1(z)\psi_1(z_s)\big)|H|^2\sqrt{\text{Coh}}\right)$$

and collecting:

$$S_v = |H|^2\psi_1(z)^2\left\{\sum_r^N \psi_1(z_r)^2\left(1-\sqrt{\text{Coh}}\right) + \sum_r^N\sum_s^N \psi_1(z_r)\psi_1(z_s)\sqrt{\text{Coh}}\right\}S_F \tag{4.7}$$

If the loads are full correlated, $S_{F_1F_2} = S_F$ and $\text{Coh} = 1$, so that it becomes:

$$S_v = |H|^2\psi_1(z)^2\left\{\sum_r^N\sum_s^N \psi_1(z_r)\psi_1(z_s)\right\}S_F$$

In the loads are fully correlated, $S_{F_1F_2} = 0$ then $\text{Coh} = 0$ and it becomes:

$$S_v = |H|^2\psi_1(z)^2\left\{\sum_r^N \psi_1(z_r)^2\right\}S_F$$

One can see that, if we have two full correlated loads acting in the same place, and with the same phase, then $\psi(z_1) = \psi(z_2)$ and the response is four times the corresponding counterpart for a single load. But if they have opposite phase, it is $\psi(z_1) = -\psi(z_2)$ and the effect cancel. On the other side, if they are not correlated at all, the response is doubled, but independently on the phases.

The first modal shape corresponds to

$$\psi_1 = \sin\frac{\pi x}{l}$$

from their integral definition the following relations can be expressed:

$$\lim_{n\to\infty}\sum_{i=1}^{N}\sin\frac{\pi x_i}{l}^2 = \lim_{n\to\infty}\frac{n}{2}$$
$$\lim_{n\to\infty}\sum_{i=1}^{N}\sin\frac{\pi x_i}{l} = \lim_{n\to\infty}\frac{2n}{\pi}$$
$$\lim_{n\to\infty}\sum_{i=1}^{N}\sum_{j=1}^{N}\sin\frac{\pi x_i}{l}\sin\frac{\pi x_j}{l} = \lim_{n\to\infty}\frac{4n^2}{\pi^2}$$

In such a way that they can be substituted in eq.4.7 provided that the number of pedestrians N, is sufficiently high. We got:

$$S_v = |H|^2\psi^2\left\{\frac{N}{2}(1-\sqrt{\mathrm{Coh}}) + \left(\frac{2N}{\pi}\right)^2\sqrt{\mathrm{Coh}}\right\}S_F$$

Which ultimately represents how the response changes in relation to the crowd correlation. This is a form similar to the one that can be read in [9] by Capsoni, where the coherence $\sqrt{\mathrm{Coh}}$ is expressed by a *synchronization parameter* s.

Looking for a simpler form, one can take the coherence-affected term into the ASD of the distributed load; finding the same compact form of the single-input — single-output system:

$$S_v(f) = |H(f)|^2 S_F(f)$$

with the following load spectral density:

$$S_F = \frac{F^2 p(f)}{2}\cdot\begin{cases}\frac{N}{2} & \text{fully uncorrelated}\\ \left(\frac{2N}{\pi}\right)^2 & \text{fully correlated}\end{cases} \tag{4.8}$$

About the acceleration response, it can be derived knowing that:

$$S_{\ddot{v}} = \omega^4 S_v$$

Indicated with $S_{\ddot{v}} = S_a$, it is

$$S_a = \omega^4|H|^2 S_F$$

and then:

$$|H_a| = \omega^4|H| = \frac{1}{m}\frac{\beta^2}{\sqrt{(1-\beta^2)^2 + 4\xi^2\beta^2}}$$

$$S_a(f) = |H_a(f)|^2 S_F(f)$$

The variance of the acceleration response is given by:

$$\mathrm{E}[a^2] = \int_0^\infty |H_a|^2 S_F \mathrm{d}f = \int_0^\infty \frac{1}{m^2}\frac{\beta^4}{(1-\beta^2)^2 + 4\xi^2\beta^2}\frac{F^2 p(f)}{2}\eta\ \mathrm{d}f$$

where η was used to indicate the coefficient that multiplies the ASD in eq.4.8.
The effective value is just the square root of the variance:

$$a_{\mathrm{RMS}} = \sqrt{\int_0^\infty |H_a|^2 S_F\ \mathrm{d}f} = \sqrt{\int_0^\infty \frac{1}{m^2}\frac{\beta^4}{(1-\beta^2)^2 + 4\xi^2\beta^2}\frac{F^2 p(f)}{2}\eta\ \mathrm{d}f} \tag{4.9}$$

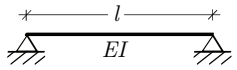

	Text notation	Code notation	Value
Length	l	`l`	$50\,\mathrm{m}$
Elastic modulus	E	`E`	$200\,000\,\mathrm{N/mm^2}$
Linear mass	γ	`gamma`	$3000\,\mathrm{kg/m}$
Sectional moment of inertia[a]	I	`I`	$1.5198\,\mathrm{cm^4}$
Natural frequency	f_{str}	`fstr`	$2\,\mathrm{Hz}$
Circular frequency	ω_{str}	`omega_j(1)`	$12.6\,\mathrm{rad/s}$
Viscous damping factor	ξ	`csi`	0.004
Number of considered harmonics	n_{arm}	`n_armoniche`	1
Time discretisation step	Δt	`step_temp`	$0.01\,\mathrm{s}$

Table 4.1: Base model

[a]The moment of inertia is derived from 1.10 in order to have the natural frequency equal to $2\,\mathrm{Hz}$

4.3 Simulations with variable parameters α and σ

The data used in the following simulation are reported in table 4.1. From now on

The pedestrian load, as previously anticipated, is modelled by a file of harmonic force with randomness coefficients α and σ. The number of pedestrian implemented in the program is $N = 50$, uniformly spaced between $z = 0$ and $z = -2l$. In such a way they start walking, with a speed given by

$$c = f_\mu \lambda$$
$$c = 1.8\,\mathrm{Hz} \times 0.9\,\mathrm{m} = 1.62\,\mathrm{m/s}$$

and after a period T which is $T = l/c = 50\,\mathrm{m}/1.62\,\mathrm{m/s} = 30.86\,\mathrm{s}$, the footbridge bears 25 pedestrian from one edge to the other.

Then a second period T occurs, in which the number of pedestrian simultaneously walking on the footbridge remains 25 (to be precise it is 25 for just an instant, and in the rest of time it is 24, cause the first pedestrian is just gone off and the 25^{th} is yet to go on).

At last, a third period of time T occurs in which the footbridge is emptying. We're referring our computations on the central period, when the response can be considered as a random stationary process.

Clearly the reference remains the midspan. Figure 4.4 contains a typical simulation with quite a good intrinsic randomness ($\alpha = 2\pi$, $\sigma = 0.1$). It is shown the displacement time history and the corresponding acceleration between the first pedestrian entrance and the last exit.

One can see that the acceleration response is not influenced by the static load of the pedestrian, which instead produces a overall lowering in displacement history. That defines the acceleration response as a zero mean value process, and consequently its variance is equal to the mean square.

Now the parameters σ and α are investigated. In the following figures are presented the effective value of the acceleration response, taken in the stationary range, with varying one between σ and α with respect to the other.

Each plot reports 20 simulations groups, in transparency, each one containing 100 effective simulations which represent each point in the plot, between 0 and 2π for α and 0 and 0.2 for σ. The mean of the 20 groups is reported in thick line over them.

We can observe that if the frequencies are all concentrated upon a same value, and one increase the scattering in phases, the effective response decrease in quite a regular manner. The same does not happen if the frequency are in some way scattered, where instead the response appears not to be dependent on α.

In other words the phases shift in the crowd seems to mostly affect the response if the crowd is already correlated in frequency.

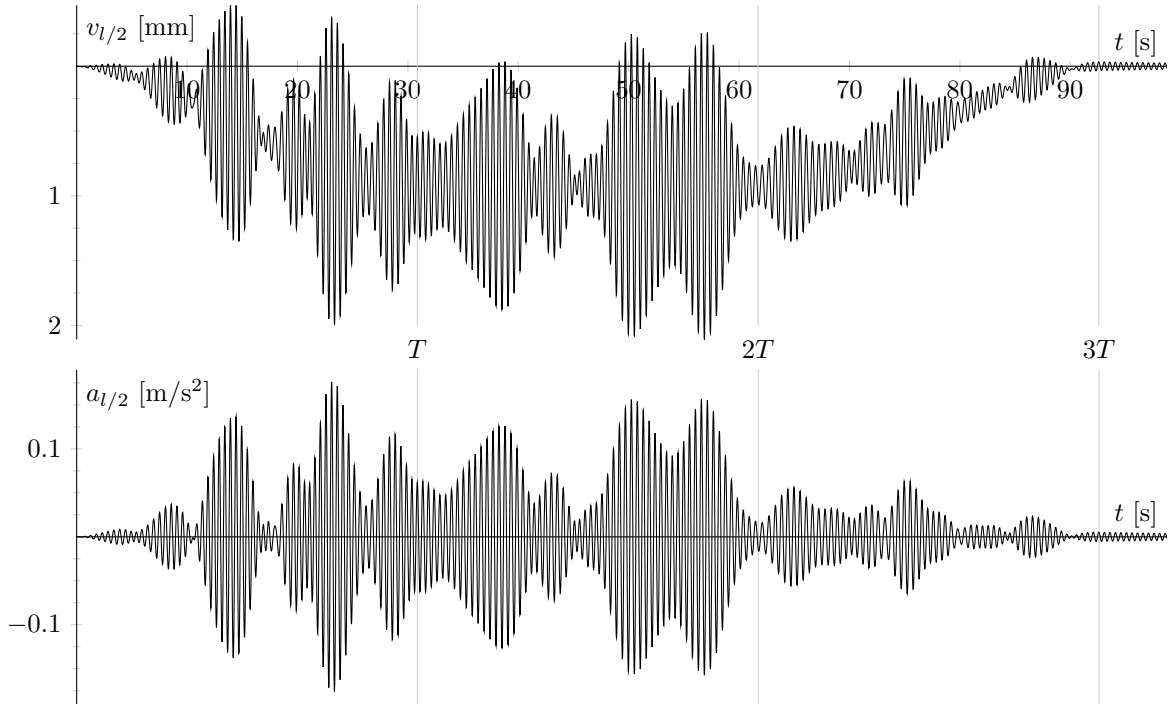

Figure 4.4: $\xi = 0.4\%$, $f_{\text{str}} = 2\,\text{Hz}$, $f_\mu = 1.8\,\text{Hz}$, $\beta = 0.9$, $\sigma = 0.1$, $\alpha = 2\pi$ 1 sola armonica, Δ t=0.01s

For uncorrelated

In figure 4.6 α is taken as a constant and σ is left varying. What stands out is the mainly identical shape of the mean curve, for any σ but near 0, where the response has a local peak and matches with the local value of figure 4.5 left, for $\alpha = 0$.

So, there is the evidence of a local behaviour near $\sigma = 0$ which is activated *only* if the phases are correlated. This occurs for a very narrow range of standard deviation, namely $0 \div 0.01$, which are quite far from the usual frequency rate distribution for real pedestrian.

In figure 4.7 is plotted the analytical curve, given by equation 4.9 and computed by MATLAB, using $\eta = \frac{N}{2}$ for anywhere but for $\sigma = 0$ where the coefficient $\eta = \left(\frac{2N}{\pi}\right)^2$ is used (left).

A good matching with the simulations is observed, even more accurate for small standard deviations. The punctual value for null variance is correctly estimated. Only a few concern can be expressed on the remaining part of the curve where the gap appears to be more consistent.

This accordance with the analytic formula in the form with $\eta = \frac{N}{2}$ seems to tell us that the pedestrian loads have to be considered inherently uncorrelated with reference to the frequencies even if their standard deviation is small.

In the following plots the surface $a_{\text{RMS}}(\sigma, \alpha)$ is represented by mean of MATLAB simulations. The domain is 20 points along α axis, and 100 points along σ axis. For each point in the domain a total of 100 simulation have been performed, whose mean is the final value plotted.

Against the lateral face of the graph is plotted the analytical function given by eq. 4.9.

From the three graphs 4.8, 4.9, 4.10 some observations follow:

- The effective response does not depend on the parameter α, which is to say the inherent phase shift in the crowd, if the pacing frequencies are even very low spread out.
- If all the pedestrian have the same frequency, there is a singularity behaviour and the response is highly dependent on the phases shift.

A relevant aspect of the $a_{\text{RMS}}(\sigma)$ trend is the local peak that occurs in expanding the frequency variance. Such a behaviour can generate some doubts, since one is likely to expect a monotonous trend. In fact, the variance of the frequency distribution is linearly increasing and it is in some sense more intuitive consider the response proportionally decreasing with this variance. That would be true only if the mean pacing frequency coincides with the natural

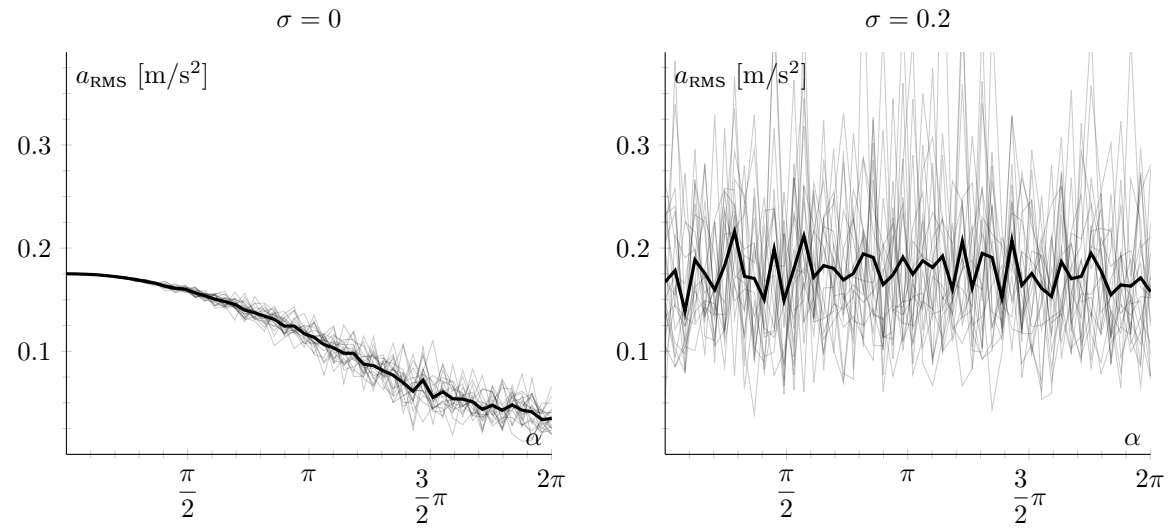

Figure 4.5: 20 simulations groups with varying α, with frequencies concentrated on $f_{ped_i} = f_\mu = 1.8\,\mathrm{Hz}$ on the left, and spared frequencies on the right.

frequency, but generally it is not. An easy representation of how this mechanism works is sketched in figure 4.11.

4.4 Loads correlation

The latest conclusion, the fact that the phase synchronisation doesn't affect the response when the frequencies are — even the slightest — distributed, deserves some more deepenings.

Let us take as a reference just two pedestrian forces $P_1(t)$ and $P_2(t)$. These are two possible realizations of the random process in time $P(t)$, which is:

$$P(t) = F\ \sin\left(2\pi f t + \phi\right) \tag{4.10}$$

The frequency f and the phase ϕ are random variables characterised by the parameters already introduced: α and σ[1] respectively.

Thus, $P_1(t)$ and $P_2(t)$ are time-dependent random variables, which are by definition, *independent* each other, because the occurrence of one does not affect the probability of occurrence of the other.

We are interested in studying the sum of them, as the simplest case of mutual action of two forces. In this regard the variance of the sum of the two forces is:

$$\begin{aligned}\sigma^2_{P_1+P_2} &= \mathbb{E}\left[\left((P_1+P_2) - \mathbb{E}\left[P_1+P_2\right]\right)^2\right] \\ &= \mathbb{E}\left[P_1^2\right] - \mathbb{E}\left[P_1\right]^2 + \mathbb{E}\left[P_2^2\right] - \mathbb{E}\left[P_2\right]^2 + 2\mathbb{E}\left[P_1P_2\right] - 2\mathbb{E}\left[P_1\right]\mathbb{E}\left[P_2\right] \\ &= \sigma^2_{P_1} + \sigma^2_{P_2} + 2\sigma_{P_1P_2}\end{aligned} \tag{4.11}$$

Where has been made use of the fundamental relations:

$$\begin{aligned}\sigma^2_{P_1} &= \mathbb{E}\left[P_1^2\right] - \mathbb{E}\left[P_1\right]^2 \\ \sigma^2_{P_2} &= \mathbb{E}\left[P_2^2\right] - \mathbb{E}\left[P_2\right]^2 \\ \sigma_{P_1P_2} &= \mathbb{E}\left[P_1P_2\right] - \mathbb{E}\left[P_1\right]\mathbb{E}\left[P_2\right]\end{aligned}$$

[1] Not to be confused with the root square of the variance. Here σ stands for the standard deviation of the probability density distribution of the frequency (eq. 4.4). The variance $\sigma^2_{P_j}$, or its root σ_{P_j}, are always indicated with the subscript of the relating variable, or with the notation $\mathrm{Var}\left[\cdot\right]$

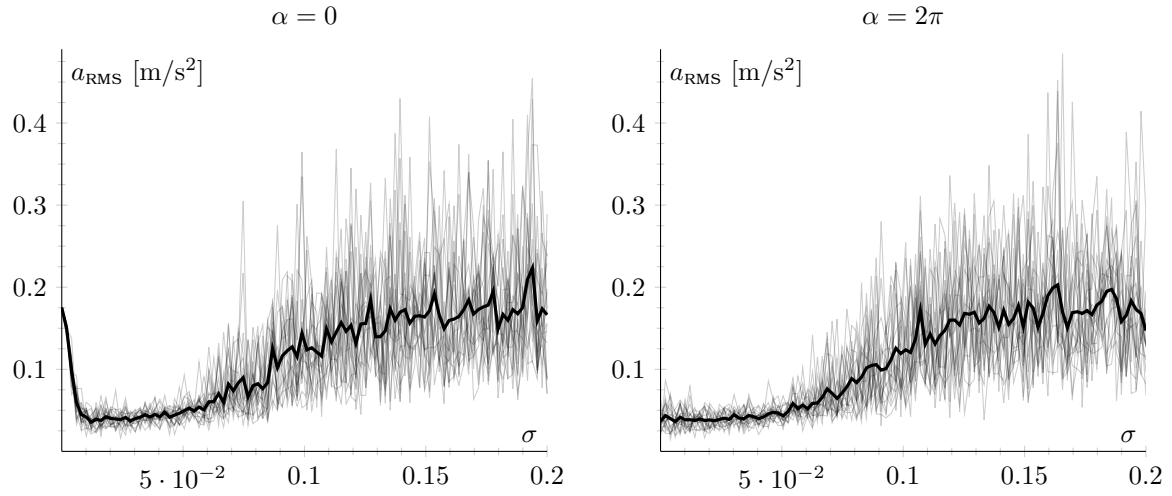

Figure 4.6: 20 simulations groups with varying σ. All of them having the same phase (left) or completely random distributed phases (right).

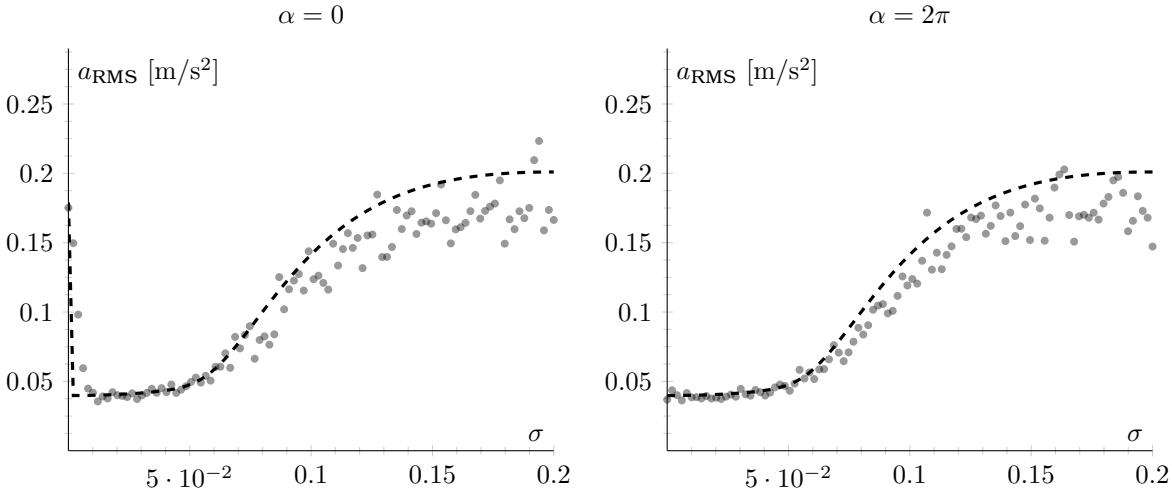

Figure 4.7: Confrontation of the simulations output (scatter) with the analytic function (dashed, continuous) provided by eq. 4.9

Identifying with $\sigma^2_{P_1}$ and $\sigma^2_{P_2}$ the variances of $P_1(t)$ and $P_2(t)$, and with $\sigma_{P_1P_2}$ their covariance.

Before proceeding, the nature of the *expected value operator* $\mathbb{E}[\cdot]$ has to be specified. A first way the expected value operator can be conceived, is as a time-average operator:

$$\mathbb{E}[X(t)] = \frac{1}{T}\int_0^T X_j(t)\ dt$$

in this case we're studying the randomness of the variable with respect to the time.

A second way is to consider all the possible realizations of the process for a given time instant t_k, and take the average. As a matter of fact, in doing so we are considering a new random variable X_{t_k} that represents all the values $X(t)$ can assume when computed in t_k. This provides us the probabilistic properties of the process for any instant. The formal way to express it, is by integrating all the values x that the variable can assume, multiplied by their relevant probability p_X:

$$\mathbb{E}[X_{t_k}] = \int_{-\infty}^{+\infty} x\ p_X dx$$

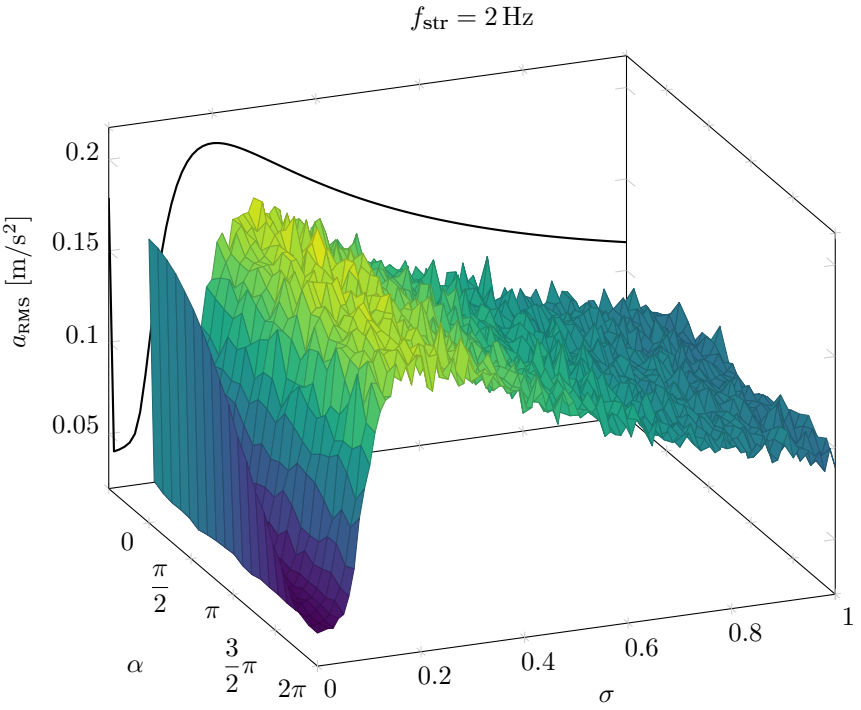

Figure 4.8: $a_{\text{RMS}}(\sigma, \alpha)$ surface for structure frequency $f_{\text{str}} = 1.8\,\text{Hz}$.

If $\mathbb{E}[X_{t_k}]$, which we're going to call *punctual-average*, is constant in time, the process is stationary in wide sense. Furthermore, if $\mathbb{E}[X_{t_k}] = \mathbb{E}[X(t)]$ for each t, the process is *ergodic*.

Now, in the computation of eq. 4.11 the time-average definition is assumed. Since $P(t)$ is a zero-mean process in time, whichever $P_j(t)$ realization we take, the terms $\mathbb{E}[P_1]^2$ and $\mathbb{E}[P_2]^2$ are both null.

Otherwise $\mathbb{E}\left[P_1^2\right]$ and $\mathbb{E}\left[P_2^2\right]$, which are the mean square of the two variables and in this case also correspond to the variances $\sigma^2_{P_1}$ and $\sigma^2_{P_2}$, can be computed as follow:

$$\begin{aligned}\mathbb{E}\left[P_j^2\right] = \sigma_P^2 &= F^2 \frac{1}{T}\int_0^T \sin^2(2\pi f t + \phi)dt \\ &= \frac{1}{T}\frac{F^2}{2\pi f}\left[-\frac{1}{2}\sin(2\pi f t + \phi)\cos(2\pi f t + \phi) + \frac{1}{2}(2\pi f t + \phi)\right]_0^T \\ &= \frac{F^2}{2}\end{aligned}$$

This is a well-known value and it is the same no matter which value f and ϕ assume, and thus is the same for any $P_j(t)$. But that is true when computed within the proper T: the exact period of the function. What if we remove this limitation?

Let us take the only frequency as random, and a fixed phase $\phi = 0$. By means of an high number of simulation using MATLAB one can find that the punctual-average $\mathbb{E}\left[P_{t_k}^2\right]$ moving in time, oscillates between $-F$ and F for a certain time range, whose length increases the higher is the frequencies randomness, depending on the parameter σ. In other words, the process exhibits a non-stationary behaviour in the initial stage, and after that it becomes stationary, since its punctual-average and its time-average coincide. We conclude that the process $P(t)$ can be regarded as stationary, given the frequency as the only random variable, if the reference period is sufficiently long.

About the phase randomness, it is described by the parameter α in such a way that $\phi \sim \text{U}[(-\alpha/2, +\alpha/2)]$. With the same numerical procedure, one finds that the punctual-average of $P(t)$ with the only randomness given by the phase shift, that is to say given by α, is never constant, but is actually cyclostationary. That occurs for every α but 2π, when instead $\mathbb{E}[P_{t_k}]$

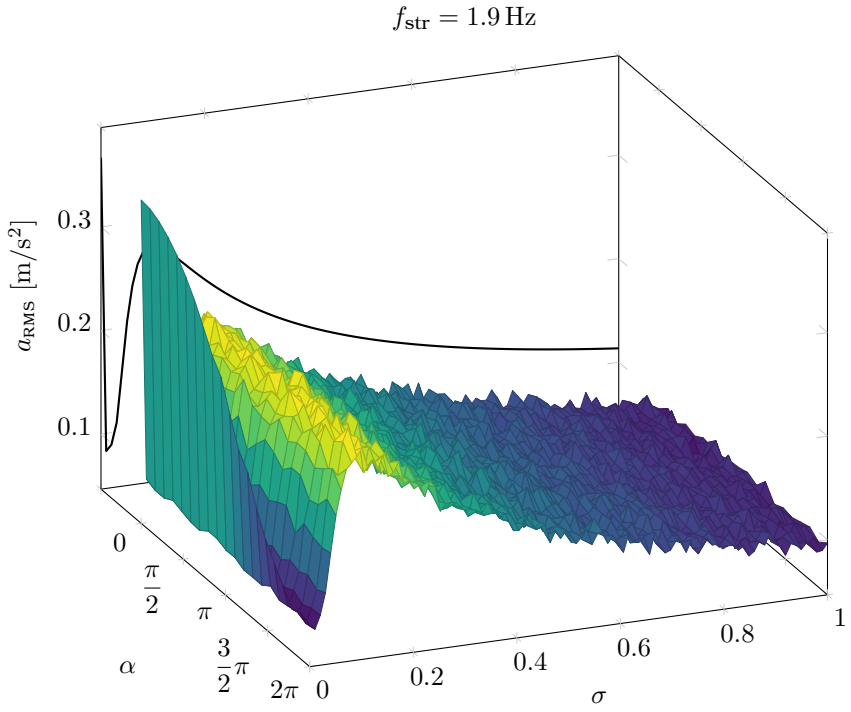

Figure 4.9: $a_{\text{RMS}}(\sigma, \alpha)$ surface for structure frequency $f_{\text{str}} = 1.9\,\text{Hz}$.

is constant and equal to 0. However, it is found that the time-average is always the same, whatever the α.

As a conclusion, the process $P(t)$ cannot be said stationary in wide sense. But, if the observation period is sufficiently long, it can be treated like it is stationary. This is relevant because it means that the probabilistic properties of the process seen in equations 4.11, are time-independent.

Against this background, the variance of the sum of the two forces can be rewritten:

$$\begin{aligned} \sigma^2_{P_1+P_2} &= \mathbb{E}\left[P_1^2\right] + \mathbb{E}\left[P_2^2\right] + \mathbb{E}\left[P_1 P_2\right] \\ &= \sigma^2_{P_1} + \sigma^2_{P_2} + 2\sigma_{P_1 P_2} \\ &= 2\sigma^2_P \left(1 + \frac{\sigma_{P_1 P_2}}{\sigma^2_P}\right) \\ &= 2\sigma^2_P \left(1 + \rho_{P_1 P_2}\right) \end{aligned} \tag{4.12}$$

where has been collected σ^2_P since has been proved that $\sigma^2_{P_1} = \sigma^2_{P_2} = \sigma^2_P = \frac{F^2}{2}$, and it is introduced the *correlation coefficient*:

$$\rho_{P_1 P_2} = \frac{\sigma_{P_1 P_2}}{\sigma^2_P}$$

It stands between $-1 < \rho_{P_1 P_2} < 1$ and expresses the grade of correlation between the two forces. It is 0 if they are uncorrelated, 1 if they are perfectly correlated, and -1 if they are inversely correlated.

The equation 4.12 makes it clear how the correlation between two random variable affects their sum. If they are uncorrelated, the variance of the sum is equal to the sum of the variances of the two variable separately. If they are perfectly correlated instead, the variance of the sum is equal to the double of the sum of their variances.

As stated before, the forces which share the probabilistic properties with $P(t)$ are independent, and consequently they are uncorrelated. Two uncorrelated variables has zero covariance: $\sigma_{P_1 P_2} = 0$, that means $\mathbb{E}\left[P_1 P_2\right] = \mathbb{E}\left[P_1\right]\mathbb{E}\left[P_2\right]$. In our case the second term in null,

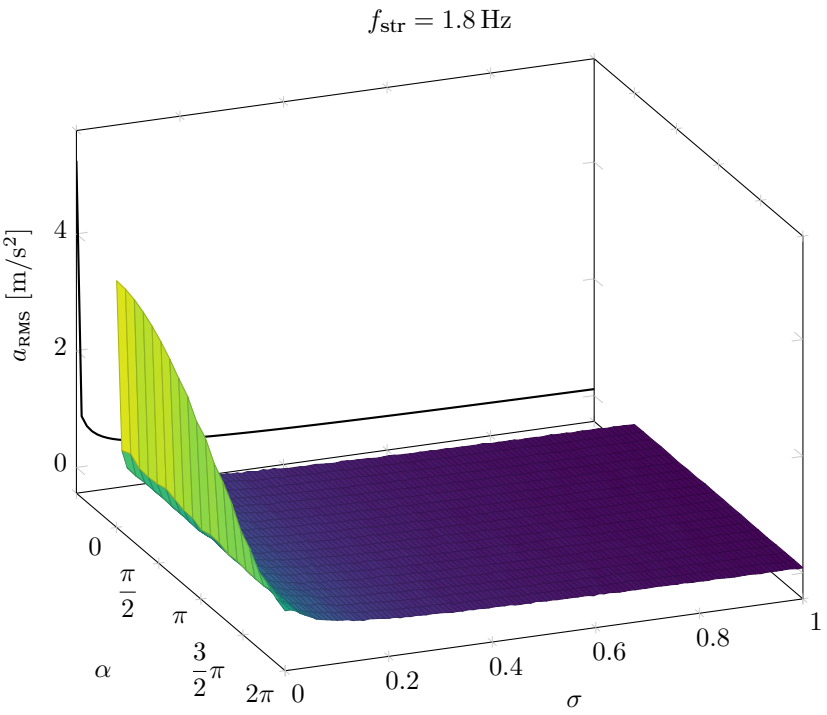

Figure 4.10: $a_{\text{RMS}}(\sigma, \alpha)$ surface for structure frequency $f_{\text{str}} = 2\,\text{Hz}$.

and we get $\mathbb{E}[P_1 P_2] = 0$. That allows us to write the correlation coefficient in the simple form:

$$\rho_{P_1 P_2} = \lim_{T\to\infty} \frac{2}{T} \int_0^T \sin(2\pi f t + \phi) \sin(2\pi f t + \phi)\ \mathrm{d}t \tag{4.13}$$

where the limit form is introduced in order to approach the computation in a numerical way.

Until now has been stated that the two variable $P_1(t)$ and $P_2(t)$ are by definition uncorrelated. This statement ends to be true in two cases. First, when the frequency and the phases probability distribution converge towards a Dirac delta function, that is to say: they have the same frequency and the same phase. Obviously, in such a limit case, the two variables lose their randomness, and become deterministic functions of time. Having the same value in every moment, their correlation coefficient must be 1 and the variance of their sum is $4\sigma_P^2$. Second, when the frequency probability distribution is a Dirac delta function, and the phases probability distribution is uniformly distributed in the band $[-\alpha/2, +\alpha/2]$, with $0 \leq \alpha \leq 2\pi$.

The correlation coefficient can be computed by exploiting equation 4.13, through an high number of simulation in MATLAB. What comes out is shown in figure 4.13 depending on the probability band-width α.

The plot shows that the correlation coefficient of the two forces goes from 1 for $\alpha = 0$ (perfectly correlated) to 0 for $\alpha = 2\pi$ (uncorrelated) in a continuous and almost sinusoidal shape.

Figure 4.14 insted shows the correlation coefficient when σ varies from 0 to 1. The phases are both taken null ($\alpha = 0$), so that in $\sigma = 0$ we find again the full correlation $\rho_{P_1 P_2} = 1$. Then, from that point on, the correlation coefficient quickly converge to 0.

Both the plot include 1000 computed points, each of which is averaged upon a sample space of 100 random simulations.

4.4.1 Further evidences: frequency gap

It is interesting to observe the sudden decrease of the correlation in figure 4.14. This correspond to a sudden decrease of the variance of the sum of the two forces, from $4\sigma_P^2 = 2F^2$ to $2\sigma_P^2 = F^2$. This drift apparently happens when a tiny scattering in the frequencies takes place. The

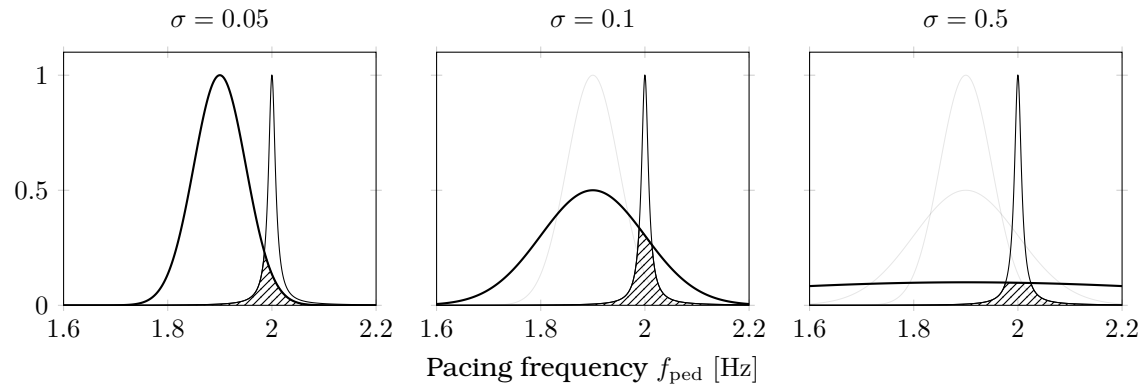

Figure 4.11: Explanation of the local peak in the response. In the spreading of the pedestrian walking frequencies their probability function overlaps the frequency response function, and the resulting crossed area — which is proportional to the RMS response — firstly increases, and then decreases. Notice that the FRF is very narrow, mainly because of the low damping factor. Both the FRF(f) and the pdf(f) were normalised in order to be well visible.

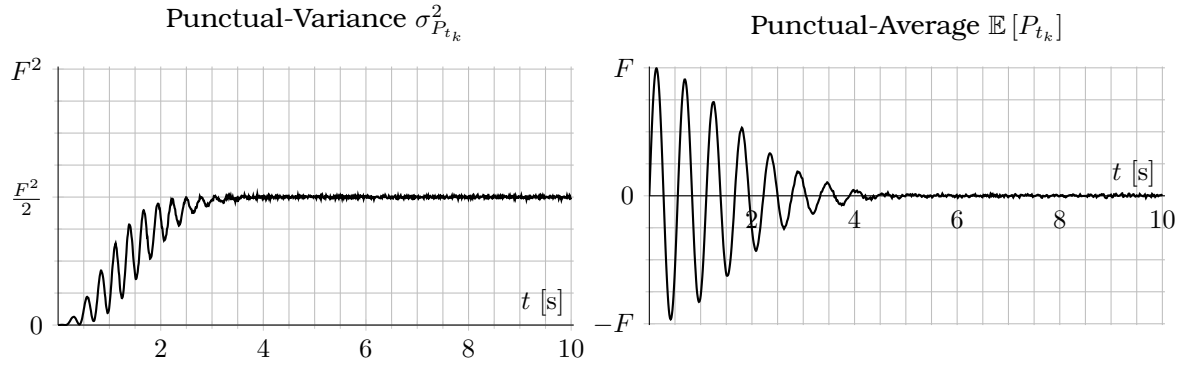

Figure 4.12: Punctual statistic properties of the random process $P(t) = F\sin(2\pi ft)$ with $f_\sigma = 0.1$. Each plot is computed upon a sample space of ten thousand random simulations.

question is: a so small scattering in frequencies justifies such a breakdown? If we take two forces with a frequency shift Δf:

$$P_1(t) = \sin(2\pi 1.8\,\text{Hz}\ t)$$
$$P_2(t) = \sin\big(2\pi(1.8\,\text{Hz} + \Delta f)t\big)$$

and sum them up, we obtain what is depicted in figure 4.15. Even if the difference in the frequencies is small, the resultant wave is rather far from the two generating, and the beats phenomenon is clearly visible. If the difference is larger then the sum wave is even more different from the original, and its shape less regular. This graphically helps to understand how the frequency difference interferes with the effective value of the resultant wave, indeed the third wave has local peaks generally closer to the zero, and this means a lower variance and a lower effective value.

Then, the example is proposed with the frequency gap Δf changing in continuous manner (figure 4.16). For every point in the plot the effective value RMS$(P_1(t) + P_2(t))$ is computed over a period of time equal to T.

One can see that increasing the period T the function better approximate the values for small Δf. That because the smaller Δf is, the greatest is the time which some consistent difference in the two waves appear after, or, in other terms, the lower is the frequency of the beats, and a higher period of computation is required to include these lower frequencies into the computation.

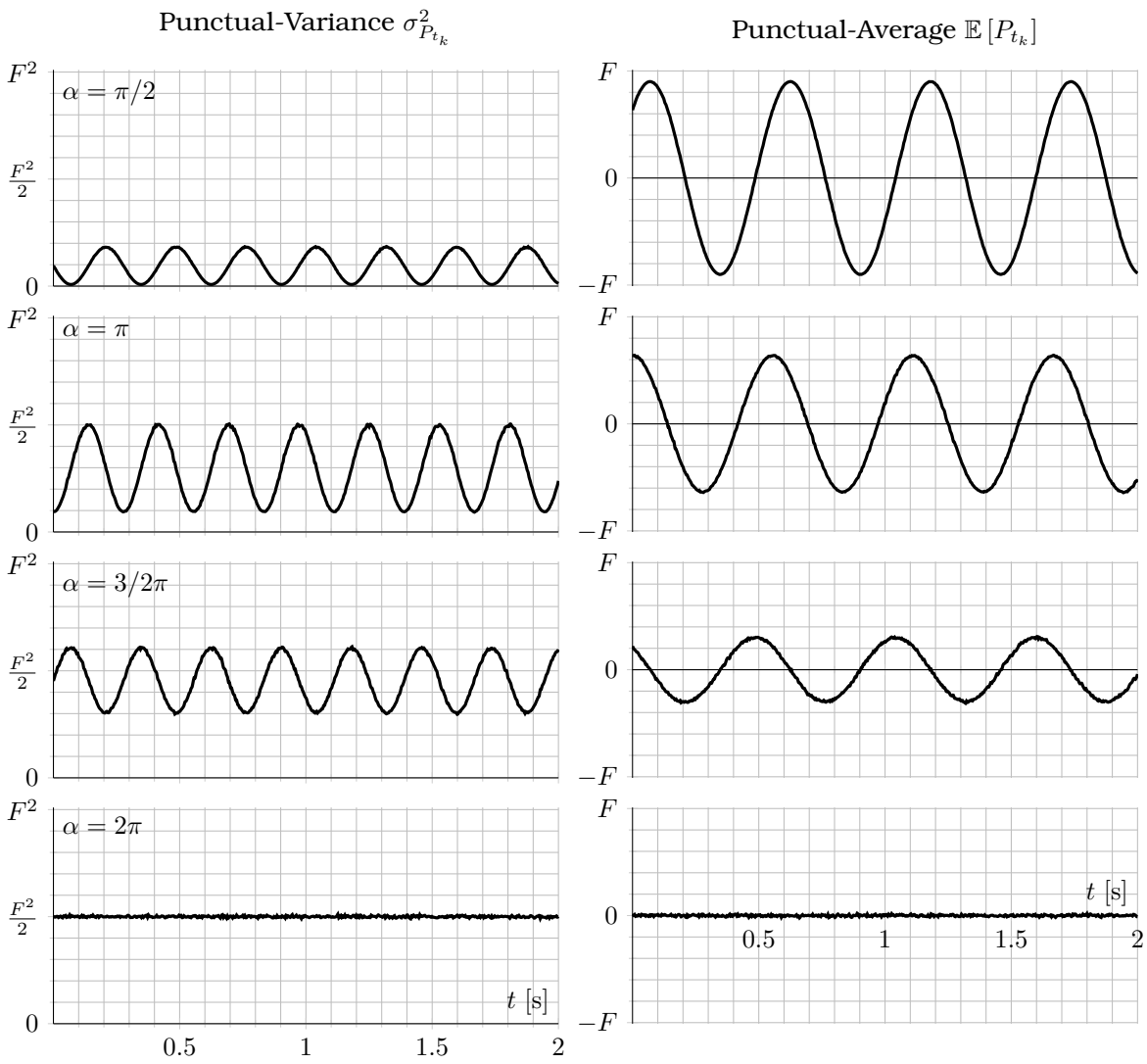

It can be reasonably stated that the function tends to the limit situation: $\sqrt{2}$ when $\Delta f = 0$ and 0 elsewhere. Extending this result to the correlation coefficient:

$$\rho_{P_1 P_2} = \begin{cases} 1 & f_1 = f_2 \\ 0 & f_1 \neq f_2 \end{cases}$$

That, it should be recalled, is valid for a sufficiently long period.

Everything that has been said about the two forces $P_1(t)$, $P_2(t)$, clearly also applies to the case of several forces. The variance formulation can be extended to a summation where the correlation coefficients of every pair of forces appear. Under the assumption that each variable $P_j(t)$ got the same statistical properties, $\sigma^2_{P_j}$ and $\rho_{P_i P_j}$ is always the same. One can collect them all, obtaining:

$$\text{Var}\left[\sum_j^N P_j(t)\right] = N\ \sigma_P^2\big[1 + (N-1)\rho\big] \tag{4.14}$$

hence:

$$\text{Var}\left[\sum_j^N P_j(t)\right] = \begin{cases} N\sigma_P^2 = N\ \dfrac{F^2}{2} & \text{full correlated} \\ N^2\sigma_P^2 = N^2\ \dfrac{F^2}{2} & \text{uncorrelated} \end{cases}$$

See section 4.2 for response spectrum formulation.

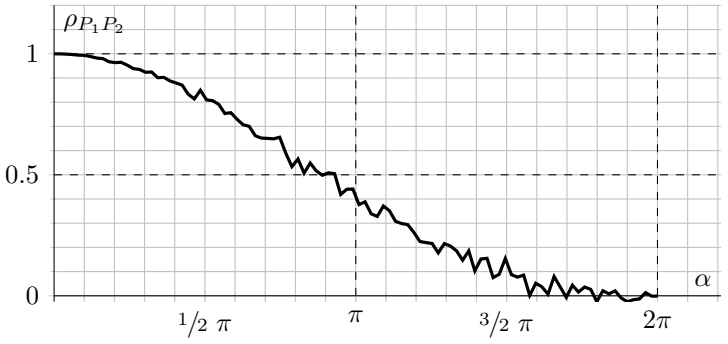

Figure 4.13

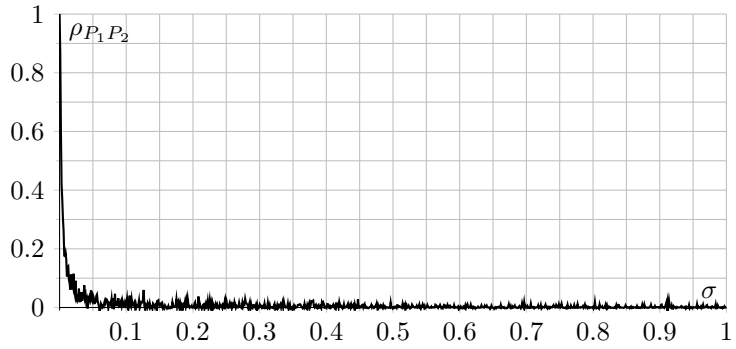

Figure 4.14

4.4.2 Deterministic frequencies and random phases

Figure 4.18 shows results from a simulation test with five forces fixed in space, each one oscillating at a given frequency. The scatter plot shows the effective acceleration response in midspan, computed over a period of $100\,\mathrm{s}$, in ten thousand simulation with changing the parameter α. This means that the amplitude of the relative phase shift between the forces, representing pedestrian, increases from 0 to 2π.

As the mean line (thick, black) shows, the effective acceleration is not significantly affected by this parameter change. Only, a greater α determines a greater variability of the result.

This further validates the thesis that, if the frequencies are scattered, any change in the phases shifts doesn't affect the response. We could say because the forces are already uncorrelated and cannot be more uncorrelated.

As a conclusion we can assume that the correlation coefficient varies as it is sketched in figure 4.17.

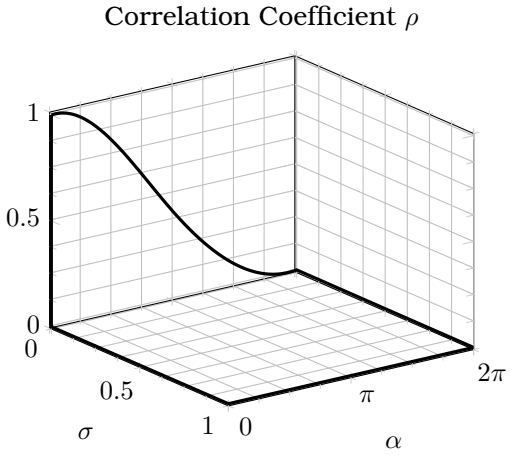

Figure 4.17

4.4.3 Disturbed load model

In some sense the obtained distribution of ρ sounds unintuitive because of its discontinuity. Also, one is led to believe that the full correlated state is never achieved in reality, because it requires that the forces have exactly the same frequency. In the case of the pedestrians,

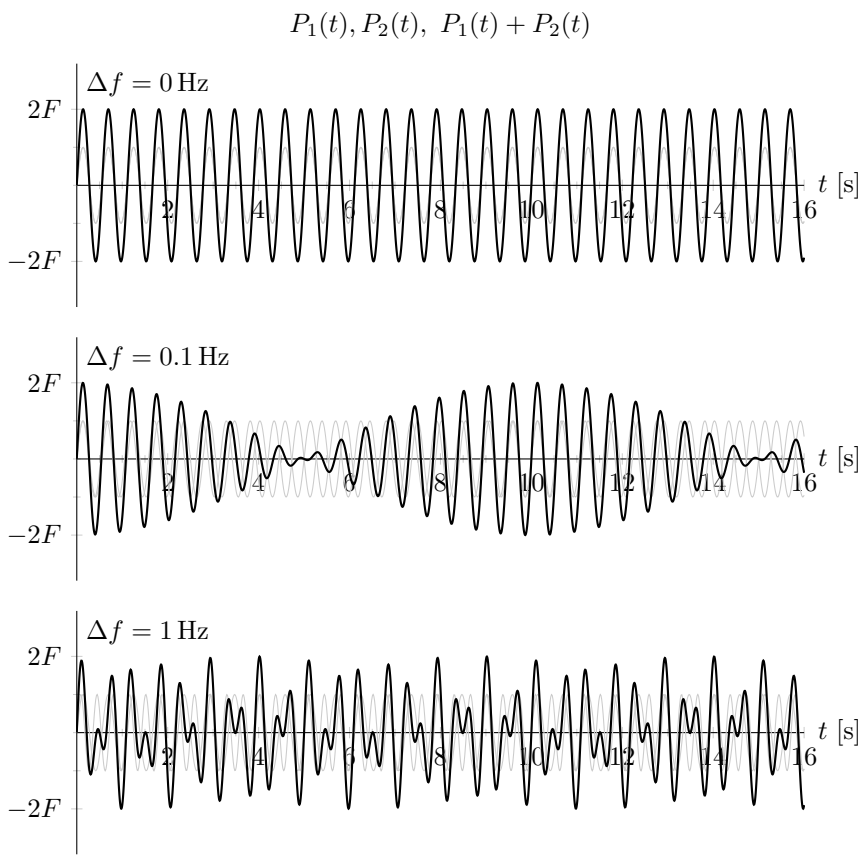

Figure 4.15: Sum of two sinusoidal signal with differing frequencies.

this means that they must walk perfectly synchronized, in such a way that the frequency distribution has zero deviation $\sigma = 0$ and this is quite unrealistic.

An attempt to explain how the full correlation can be physically achieved is to change the starting model which sees the pedestrian as perfect sinusoidal forces. Instead, we can introduce a disturb in the perfect wave, for instance by adding a random quantity to the phase:

$$P(t) = F \sin(2\pi f t + \mathrm{D}(t))$$

the added disturb $\mathrm{D}(t)$ is generated in such a way it is sufficiently regular, better say *smooth*, cause otherwise the force would result excessively noisy and unnatural. One generated sample is reported in figure 4.19 (continuous line), with respect to the original wave (dashed).

The property of this derived function is that it maintains the original frequency globally, while locally it presents slight deviations. We expect that the frequency, computed as the number of crossings the time axis in an observation period, tends to the frequency f as the period increases

Then, if we sum up two signals of this type and compute its variance, we find $\sigma^2 \approx 1.7 \div 1.8 F^2$, which is more than the uncorrelated value ($F^2/2 + F^2/2 = F^2$) but less then the correlated one ($2F^2$). The value of the response depends in this case by the amplitude of the disturb, which in the previous case has a maximum value of 0.8, and is normally distributed.

4.5 Simulations with variable natural frequency f_{str}

What it follows is to study how the natural frequency of the structure affects the response. Once demonstrated the reliability of the analytical model in predicting the response, we put the simulations aside for a while. The analytical model gives us the curves with varying f_{str}

reported in figure 4.20. We're referring to the $\alpha = 0$ case, so the curves present a very narrow, local peak in $\sigma = 0$.

What stands out is that the peak that for $f_{str} = 2\,\mathrm{Hz}$ occurs around $\sigma = 0.2$ moves closer and closer to $\sigma = 0$ with f_{str} going to the mean pacing frequency f_μ. That corresponds to the resonance.

In this range the peak is increasing as well. For great standard deviation, instead, the response is almost unaffected by the structure frequency.

What has been stated is nothing more than the proof of the resonance in frequency domain.

What shown in figure 4.20 is then confirmed with simulations. In figure 4.22 the surface $a_{RMS}(\sigma, f_{str})$ is plotted across a domain of 20×100, where each point corresponds to the mean of 100 simulations. The simulations are taken in the case of $\alpha = 0$, this explain the singularity in $\sigma = 0$.

The same surface is then obtained by the analytical expression. The result is plotted in figure 4.23. This case the surface refers to $\alpha = 2\pi$

$$\text{RMS}\big[P_1(t)+P_2(t)\big] \quad \left(=\sqrt{\mathbb{E}\left[\big(P_1(t)+P_2(t)\big)^2\right]}\right)$$

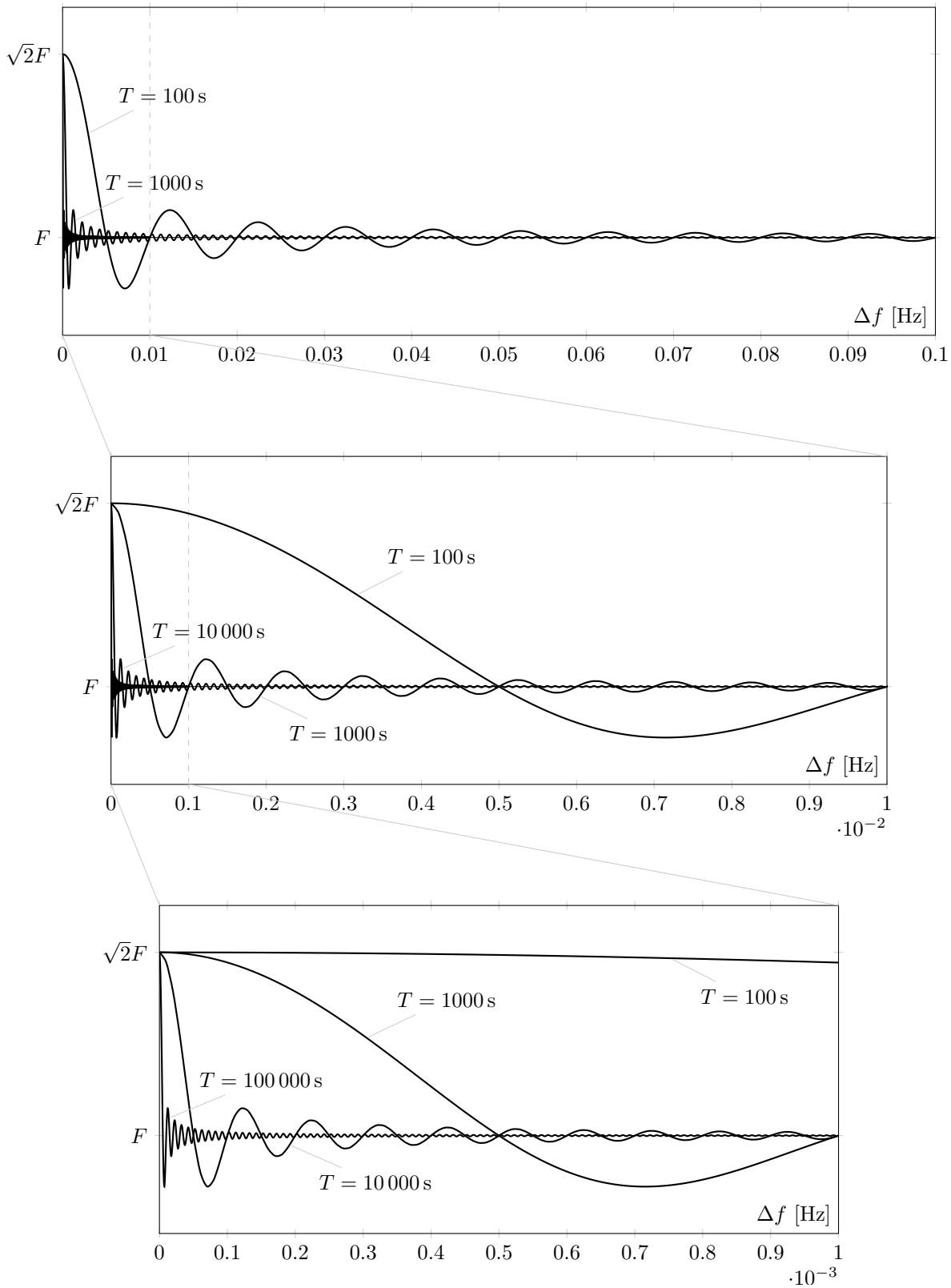

Figure 4.16: Effective value of the sum of two sinusoidal signal with respect to the difference between their frequencies. For each value Δf on the abscissa, the rms value is computed upon an observation time T.

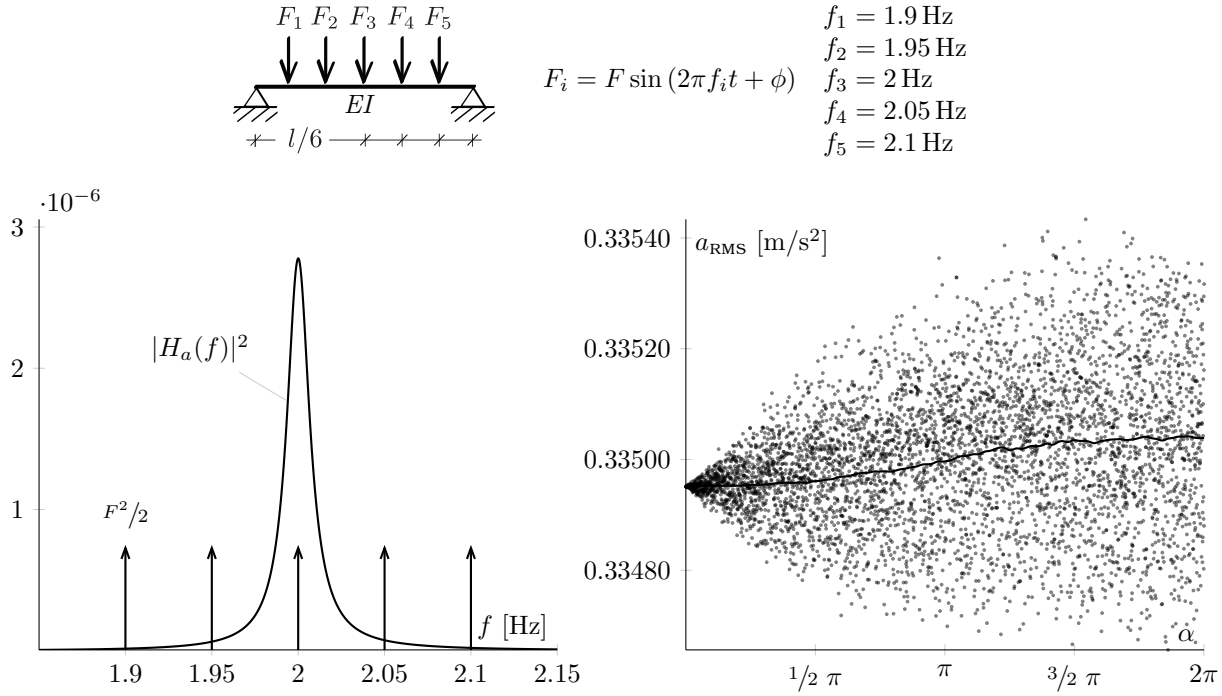

Figure 4.18: Left: Power Spectral Density representation of five forces with fixed frequencies and variable phases (not in scale), and square modulus of Frequency Response Function for the acceleration in midspan. Right: Effective value of the acceleration response, depending from the phase randomness parameter α

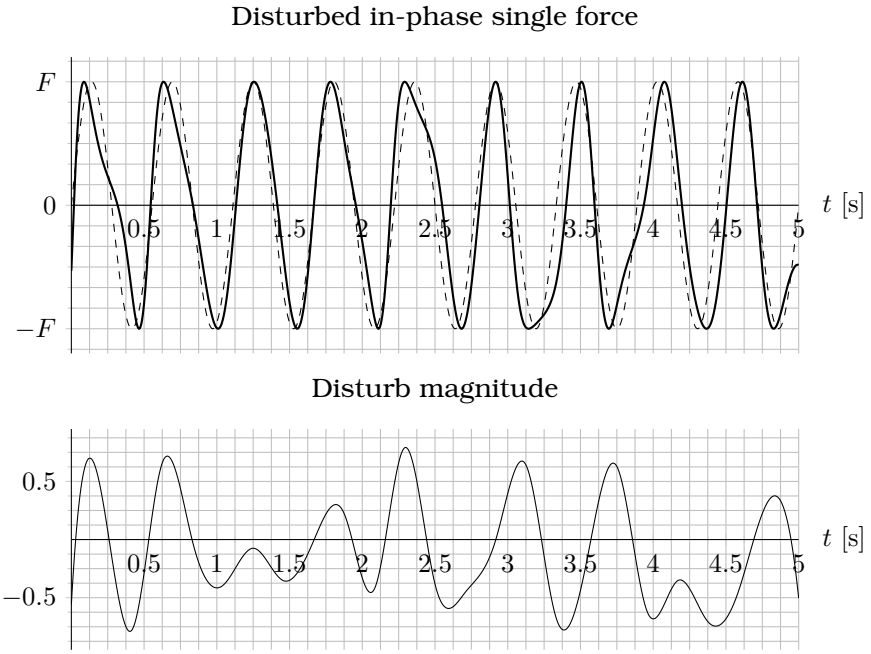

Figure 4.19: Perfect, synthetic signal (dashed), against more realistic signal obtained by adding random in-phase disturb (continuous).

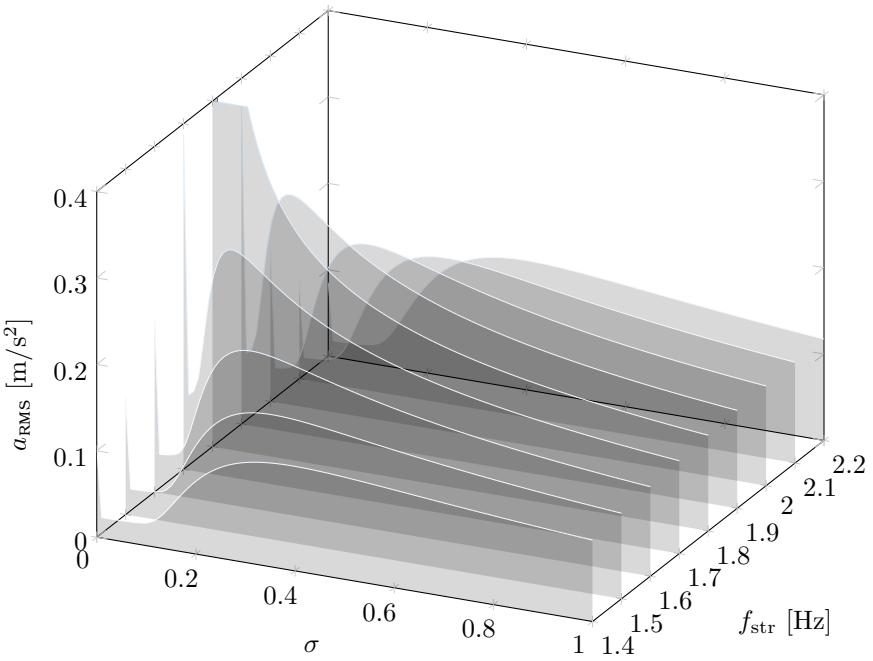

Figure 4.20: Function $a_{\mathrm{RMS}}(\alpha, \sigma)$ for different values of the natural frequency of the footbridge ($f_{\mathrm{str}} = \{1.4, 1.5, ...2.2\}$). Notice that the resonant curve ($f_{\mathrm{str}} = 1.8\,\mathrm{Hz}$) has been cut since his maximum was an order of magnitude grater.

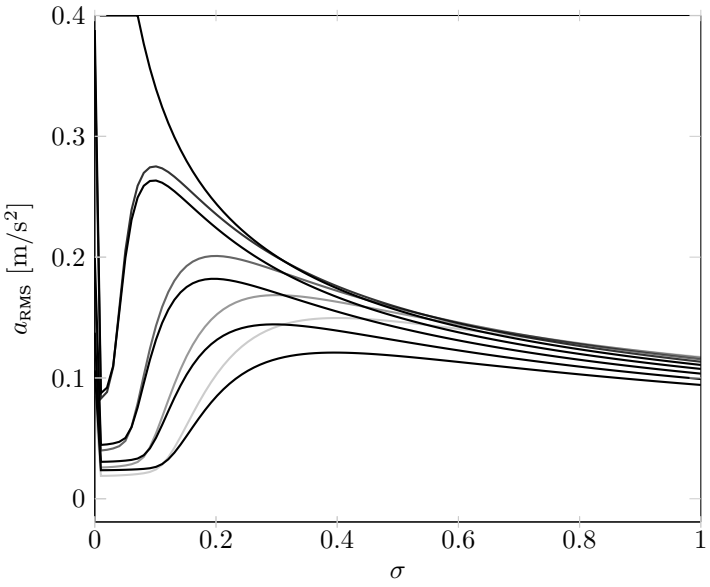

Figure 4.21: Relation $a_{\mathrm{RMS}}(\sigma)$ with different structure frequencies like figure 4.20 viewed by the side

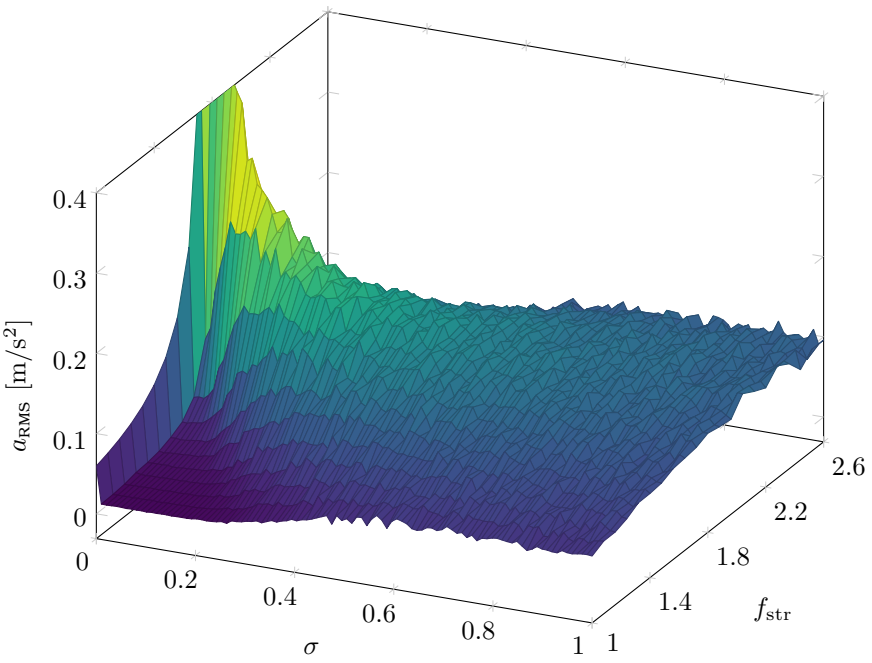

Figure 4.22: $a_{\mathrm{RMS}}(\sigma, f_{\mathrm{str}})$ surface for $\alpha = 0$.

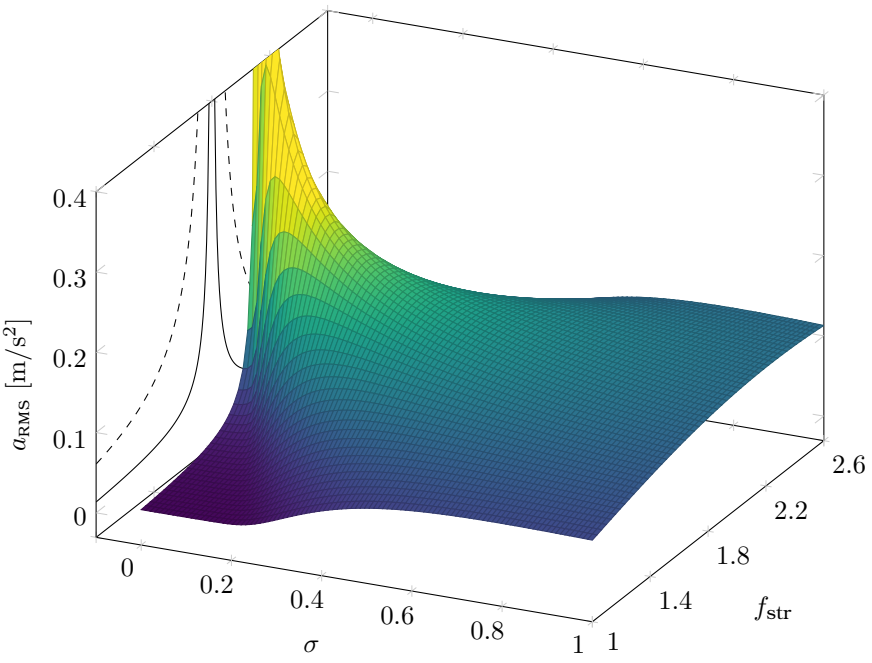

Figure 4.23: $a_{\mathrm{RMS}}(\sigma, \alpha)$ surface for $\alpha = 2\pi$. On the edge the $a_{\mathrm{RMS}}(f_{\mathrm{str}})$ relation for $\alpha = 2\pi$ (continuous line) and $\alpha = 0$ (dashed line)

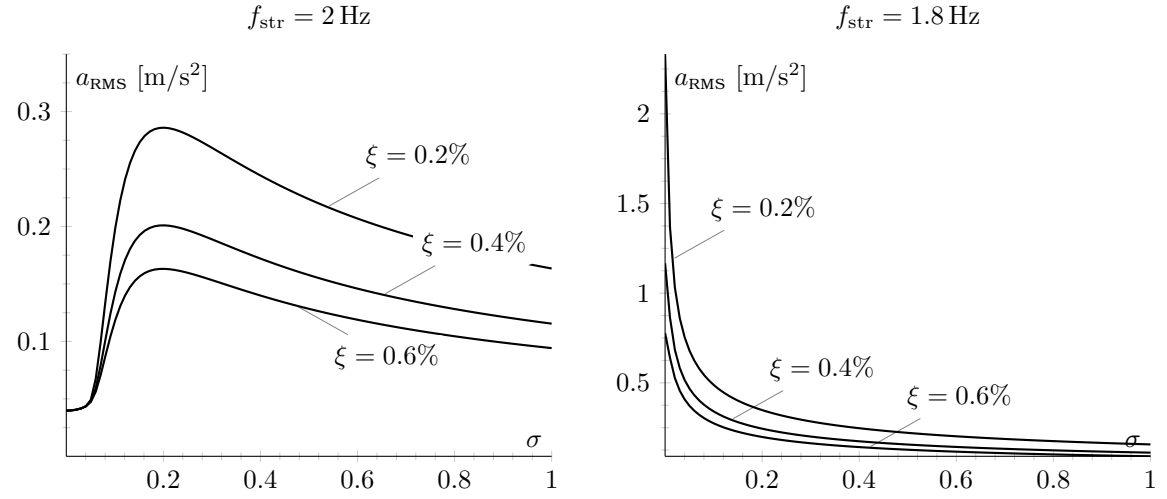

Figure 4.24: $a_{\mathrm{RMS}}(\sigma)$ relation for high, medium and low damping factor ξ (from the lower curve: $\xi = 0.006$, $\xi = 0.004$, $\xi = 0.002$) for $f_{\mathrm{str}} = 2\,\mathrm{Hz}$ left, and for resonance conditions $f_{\mathrm{str}} = 1.8\,\mathrm{Hz}$ right.

Chapter 5

Acceleration Response — varying pedestrian density

5.1 Introduction of the density-dependent parameters

As seen in section 2.5 the pedestrian walking is highly affected by the density of the crowd. Many studies, in that sense, had tried to define the $\mathrm{speed}\,(\mathrm{density})$ and $\mathrm{frequency}(\mathrm{speed})$ relationships.

The density factor is going now to be added to the model, in order to provide a more realistic and complete response. The analytic formula 4.9 gives us the effective acceleration response knowing the pacing frequency probability distribution, which is, from now on, a function of the density.

Apparently, no $\mathrm{frequency}(\mathrm{density})$ laws are available in the literature, as also its PDF function. So, these relations are going to be derived from the ones which are known, by their linear mathematic relations.

5.1.1 Walking speed

As the $\mathrm{speed}(\mathrm{density})$ relation, the *Nelson formula* is chosen:

$$c = k\,(1 - an) \tag{5.1}$$

We are referring to the mean speed $c = c_\mu$ as usual, k is a terrain dependent constant, $k = 1.4$ (for corridor, doorways, and ramps) and $a = 0.266$ (for the floor movement).

This law was developed by Nelson and MacLennan [26] in a context of emergency evacuations movement. They calculated a *region of interest* within the crowd densities of 0.54 and $3.8\,\mathrm{ped}/\mathrm{m}^2$ where an individual could maintain a relatively free movement of his choice. Instead, at the density of $3.8\,\mathrm{ped}/\mathrm{m}^2$ or above, they experienced that serious congestion and little or even no movement may happens.

Within the two limits the equation 5.1 represents the speed flows. It is rather convenient because of its linearity, and because it goes to zero for a precise value of density — that we are calling the stagnation density: $n_{\mathrm{stagn}} = 3.76\,\mathrm{ped}/\mathrm{m}^2$ — allowing us to take into account a limited range of density.

Please note that we are extending the linear relation also to the densities lower than the studied range, for simplicity. One could also take the speed constant below the lower threshold.

Other laws, like the one proposed by Kladek [34] (see fig.2.7), have exponential or polynomial forms, but even if they better approximate the empirical data, such a complexity appears unjustified for our purposes.

Figure 5.1 exposes the Nelson formula (thick line) with respect to a large amount of other analogous formulas, already shown in figure 2.7e and 2.7c.

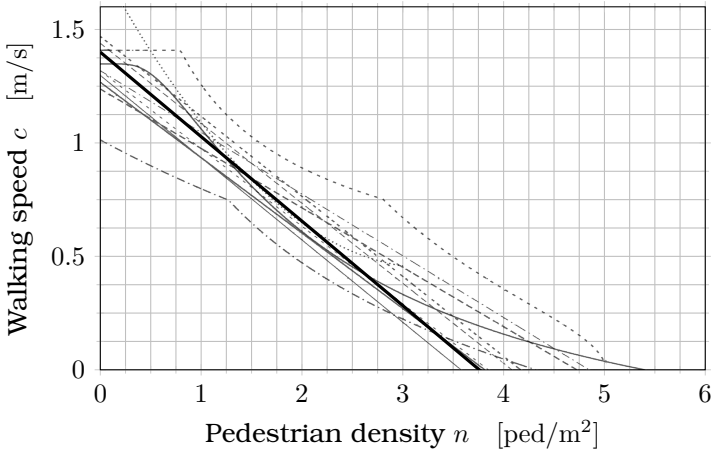

Figure 5.1: The relationship between crowd densities and velocities. Various authors (gray) versus the linear Nelson [26] law (black)

5.1.2 Step length and pacing frequency

Despite the ample dataset regarding walking speed, much less is usable about step length and pacing frequency, with a substantial lack of empirical laws. Here we propose a simple law based on few clear evidences.

The basic relation linking step length λ, walking velocity c and frequency f_{ped} is $c = \lambda \cdot f_{\text{ped}}$, hence, introducing the pedestrian density:

$$f_{\text{ped}}(n) = \frac{c(n)}{\lambda\left(c(n)\right)} \tag{5.2}$$

Where appear the already known $c(n)$ law and an empirical $\lambda(c)$ relation in order to find $f_{\text{ped}}(n)$.

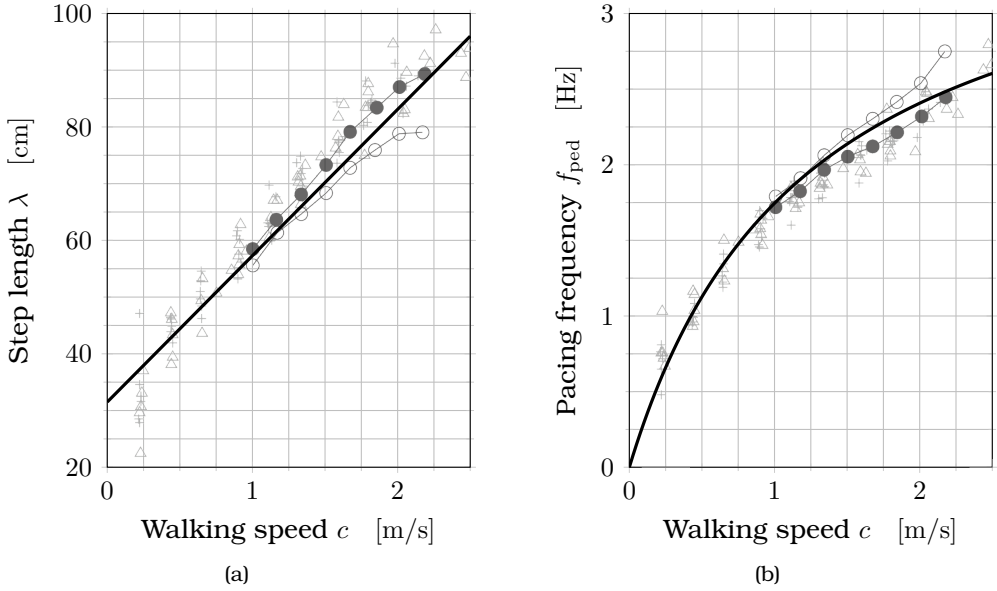

Figure 5.2: Step length and pacing frequency as function of the walking speed. Measurements from Betram & Ruina 2001 [5] and Yamasaki et al. 1991 (gray) and adopted function (black). The dataset is imported from Ingólfsson [20]

The steplength(walkingspeed) proposed equation is a linear function based on the data from

Betram & Ruina 2001 [5] and Yamasaki et al. 1991, both reported in figure 5.2. The measurements fit well with a linear interpolation; moreover, no other laws seem suitable in describing such a physical phenomenon. It is reasonable as well to assume that the step length doesn't become null for zero walking speed, cause the dimension of the foot itself constitutes a minimum threshold.

The found equation read:

$$\lambda = 31.5 + 25.8\ c \quad (\mathrm{cm}) \tag{5.3}$$

from which we have that the minimum length is set to $\lambda_{\min} = 31.5\,\mathrm{cm}$ for c that tends to zero, and the maximum one $\lambda_{\max} = 96\,\mathrm{cm}$ for $c = 2.5\,\mathrm{m/s}$.

We formulate now the relation between frequency and speed, according to:

$$f(c) = \frac{c}{\lambda(c)}$$

and by including eq. 5.1 and 5.3 we find:

$$f(c) = \frac{c}{0.315 + 0.258\ c} \tag{5.4}$$

that is plotted in figure 5.2b.

Finally, with a further substitution into eq. 5.2 the searched relation is obtained:

$$f(n) = \frac{1 - 0.266\ n}{0.483 - 0.0686\ n} \tag{5.5}$$

Its plot is drawn in figure 5.3. One other attempting curve was provided by Ricciardelli [32] and is reported in the figure as well. The latter is defined for the only range $0.2 \div 1.5\ \mathrm{ped/m^2}$, and its second order expression:

$$f(n) = 0.79\left(0.13\ n^2 - 0.82\ n + 1.80\right) + 0.79$$

give reasons to think that has been obtained by a data interpolation, and no by a physical consideration.

The further curve, obtained by substituting the Kladek expression for pedestrian speed into the 5.2, well fits to the one proposed here, but for higher density assumes an asymptotic-like behaviour. The curves that present this tendency are supposed to be derived in practical contexts where really high density can be reached, like the emergency crowd movements. That is not the case of pedestrian footbridges. All of these issues make us to consider the proposed curve a good choice.

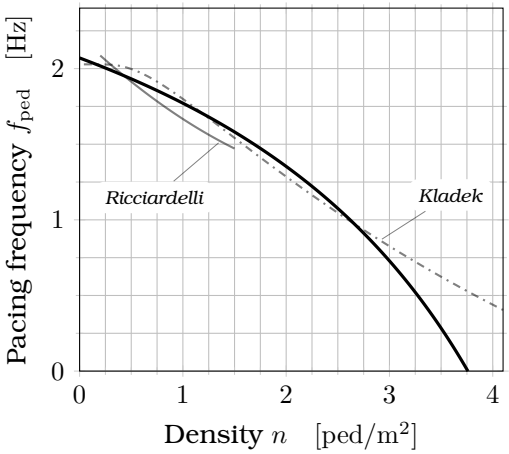

Figure 5.3: Adopted $f_{\mathrm{ped}}(n)$ function (black) together with the one proposed by Ricciardelli [32] within the range $0.2\,\mathrm{ped/m^2} \div 1.5\,\mathrm{ped/m^2}$, and the one that would be obtained with the same passages (eq. 5.2) but starting from the Kladek formula for the velocity [34] (gray).

5.1.3 Standard deviation of the frequencies

So far the expression of the pacing frequency has been achieved. But, as for the pedestrian speed, it stands for the *mean* pacing frequency, and some variance is supposed to be affecting the value. The literature hardly takes that into account with respect to the density, limiting to measure such parameter for the free walking. Instead, it is precisely this parameter the main attendant in quantifying the synchronisation among the pedestrian.

Here an exponential law is submitted, which properly fits the one that Ricciardelli [32] gave together with the previous expression. This reads:

$$\sigma(n) = 0.08\left(0.13\ n^2 - 0.82\ n + 1.80\right) - 0.03$$

and the fitting curve is:

$$\sigma(n) = 0.1088\ e^{-0.613\ n} \tag{5.6}$$

Its plot is drawn in figure 5.4. It comes out a value of $\sigma = 0.1088\,\mathrm{Hz}$ for the free walk ($n = 0$), which is something less than the mean standard deviation $f_\sigma \simeq 0.146$ among the authors of table 2.4.

Figure 5.5 illustrates the Probability Density Function of the pacing frequency with respect to the density, taking into account the mean value from eq. 5.5 and the standard deviation from eq. 5.6.

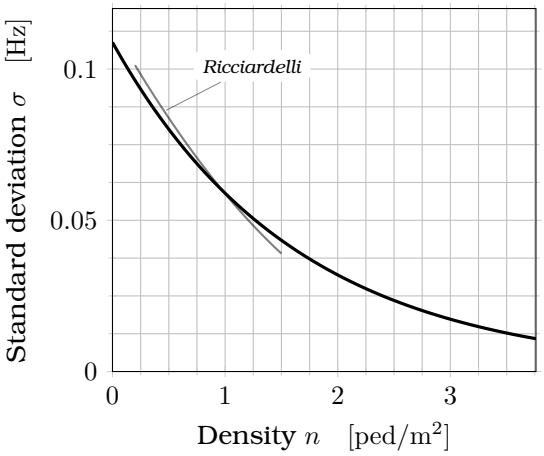

Figure 5.4: Variation of the standard deviation of the pacing frequency with respect to the crowd density. Adopted exponential law (thick) and polynomial law proposed by Ricciardelli [32] within the range $0.2\,\mathrm{ped/m^2} \div 1.5\,\mathrm{ped/m^2}$

5.1.4 Dynamic Loading Factor

As summarised in section 2.2, the Dynamic Loading Factor increases with the walking frequency. Among the relations proposed, the Kerr's [21] includes an upper and a lower limitation, and its polynomial shape make possible to readily identify a starting and a final stationary value. That is the expression chosen in this handling. It is drawn in figure 5.6 in comparison with the linear law by Bachmann & Ammann [3].

In figure 5.7 the three varying parameter of the model are comprehensively collected.

5.2 Acceleration Root Mean Square response

The effective value of the acceleration is given by eq. 4.9, where the density-dependent parameters are now included. A useful visualisation is presented in figure 5.8.

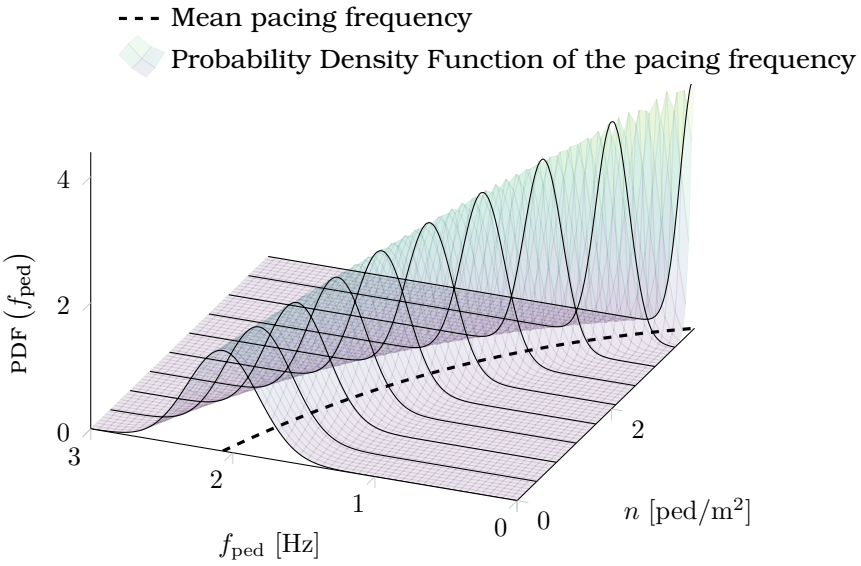

Figure 5.5: Probability density function of the pacing frequency plotted in a tridimensional visualization.

The tridimensional plot make easy to visualise how the response changes with both the density and the structural frequency.

The first significant point is that a resonance condition is achieved for every structural frequency less than $f_{\text{ped,free}} \simeq 2\,\text{Hz}$. The difference among them is the density state in which the resonance takes place: lower frequencies are excited by higher densities.

The second point is the existence of a local maximum in the response, which is set in this case around $f_{\text{str}} \simeq 1.6\,\text{Hz}$, $n \simeq 1.2\,\text{ped/m}^2$. That makes possible to draw an envelope curve, as illustrated in figure 5.8b, where for every crowd density, the worst condition, that is to say the maximum response, is detected.

5.3 Simplified approach

5.3.1 Dallard's formulation

A simpler form of the acceleration RMS can be provided. Dallard et al. in [11] assume:

$$\mathrm{E}\left[a^2\right] \approx \omega_n^4 \mathrm{E}\left[v^2\right] \approx \frac{\pi N}{16\xi} f_n p(f_n) \left(\frac{F}{m}\right)^2 \tag{5.7}$$

The reason behind such an approximation is that the peak of the Frequency Response Function $H(f)$ is supposed to be really marked, that is to say the response in f_n is *dominant*. In this case the forcing spectrum S_X can be treated like a white noise in the strict around of f_n, hence:

$$\mathrm{E}\left[v^2\right] = \int_0^\infty S_F(f)|H(f)|\,\mathrm{d}f \approx S_F(f_n)\frac{\pi f_n}{4\xi k^2}$$

Further, for the same reason, the variance of the acceleration response can be compute as follows:

$$\mathrm{E}\left[a^2\right] = (2\pi f)^4 \mathrm{E}\left[v^2\right] \approx (2\pi f_n)^4 \cdot S_F(f_n)\frac{\pi f_n}{4\xi k^2}$$

and recalling the basic relation 1.10 we find the expression 5.7 with the modal mass m in place of k. A graphic demonstration is provided in figure 4.11, where one can find a confirm of the dominance of the FRF $|H(f)|$.

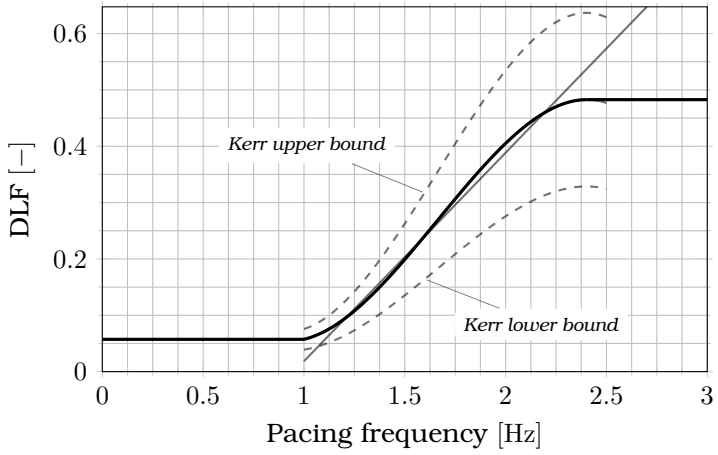

Figure 5.6: Adopted DLF law for the model, which is the curve proposed by Kerr [21] (black). Linear law proposed by Bachmann & Hammann [3] (gray).

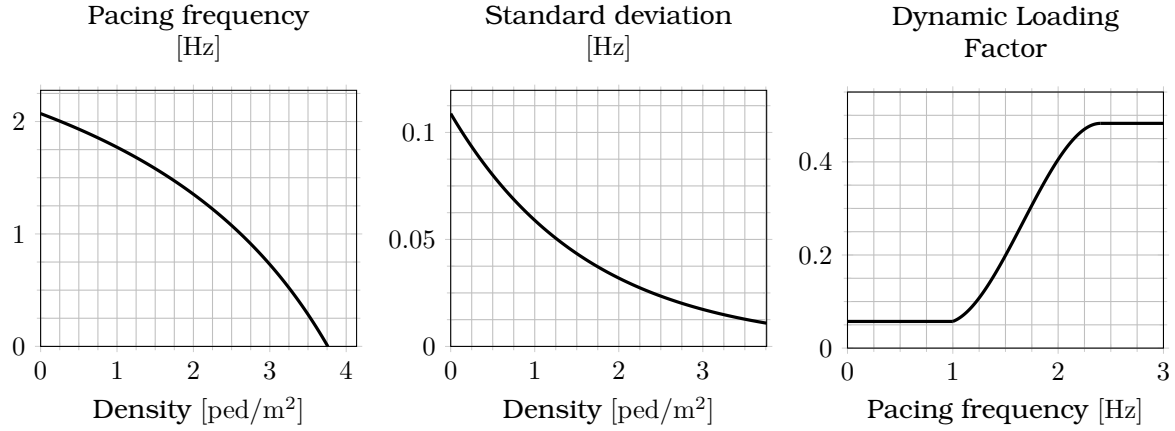

Figure 5.7: Summary of the three parameters affected by the varying density which are implemented in the model.

5.3.2 Acceleration Root Mean Square

The effective value of the acceleration is the square root of 5.7:

$$a_{\mathrm{RMS}} = \frac{F}{4m}\sqrt{\frac{\pi}{\xi} N f_n \; p(f_n)} \tag{5.8}$$

As stated in the previous section the approximated formula is the more accurate, the more dominant is the frequency response function with respect to the spectrum of the walking force. This is true when ξ is small and σ is high, that is to say that their ratio is sufficiently small: $\sigma/\xi \to 0$.

Figure 5.9 illustrates the sensibility with respect to these two parameters in the reliable of the formula.

One can notice how the smaller damping factor plays a primary role in the validation of the formula, that provide a very good approximation for $\xi = 0.004$ which is the usual order of magnitude.

In view of these considerations the envelope of a_{RMS} is proposed again in figure 5.10, now obtained by the approximated formula 5.8.

Finally, in figure 5.11 the actual and the approximated envelope derived so far are compared. Their similarity justify the use of the approximated formula, which we are referring to from

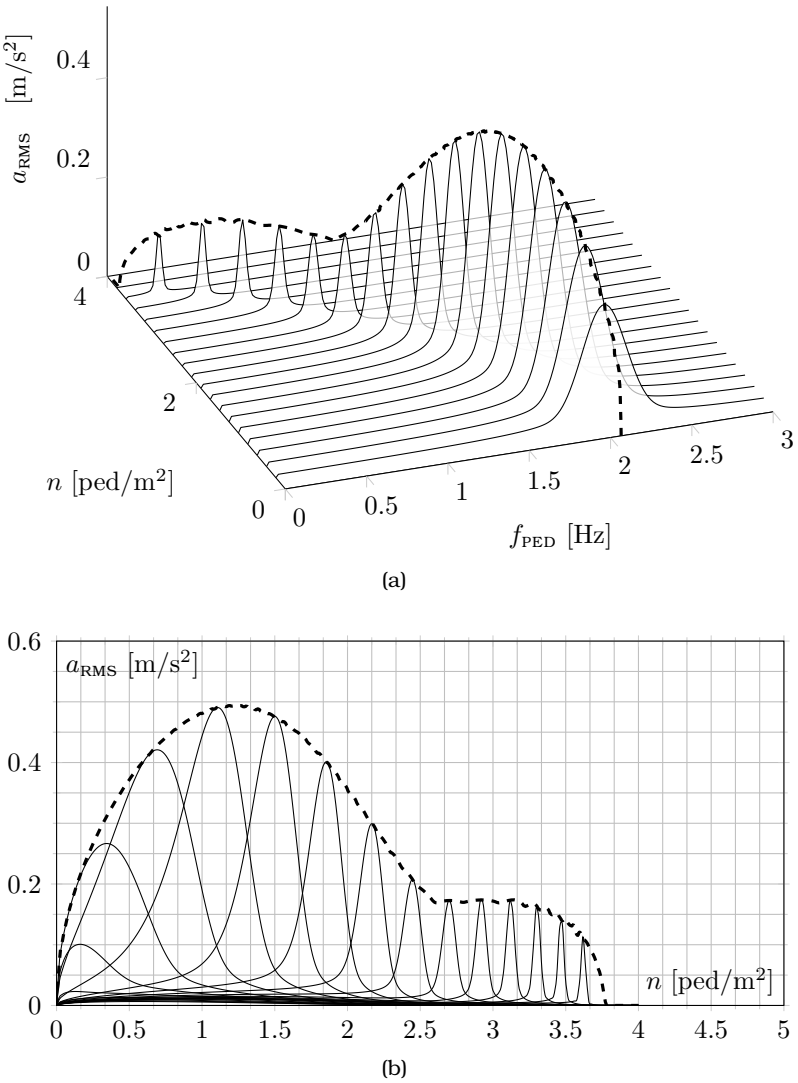

Figure 5.8: RMS acceleration response as a function of both the structure frequency and the density (a) and maximum envelope with respect to the density (b).

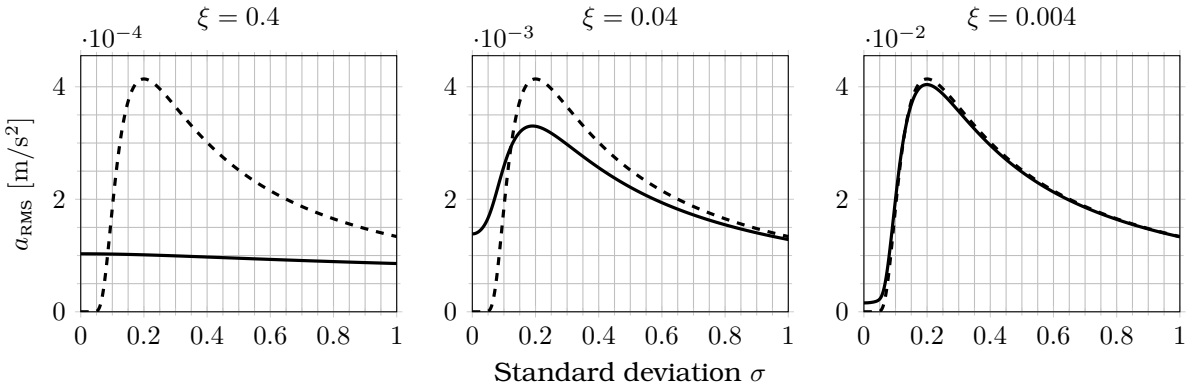

Figure 5.9: How the Dallard's formula (dashed) approximates the actual response (continuous), for different damping factors and different σ.

now on.

5.3.3 Peak acceleration

In order to align the formulation to the standards, the peak value of the acceleration has to be quantified.

From 5.8, given that $a_{\mathrm{peak}} = g_p \; a_{\mathrm{RMS}}$ we get that

$$a_{\mathrm{peak}} = g_p \frac{F}{4m} \sqrt{\frac{\pi}{\xi} N f_n \; p(f_n)} \tag{5.9}$$

That is subjected to the *peak factor* determination.

Figures from 5.12a to 5.12c shown simulations similar to the ones reported in Fig.4.6, for which also the peak value is computed.

We can assume on good basis the peak factor to be 2.5. (notice that in $\sigma = 0$ the peak factor correspond instead to $\sqrt{2}$, which the factor for sinusoidal signal, as here for fully correlated forces is.)

Finally the envelope 5.13 is produced by the analytic approximated formula. One can observe that each response curve with its proper natural frequency finds its peak for a density corresponding more or less to the density for which the crowd has that mean pacing frequency.

Looking to each plots separately one can states that for this range of footbridges frequencies, increasing the density of the crowd, the response increases too. That because of the slowing down of the pacing frequency, which ends up in crossing the structure frequency. Also, there is a certain density which maximise the response.

The overall envelope shows that a global maximum exists and, for the given properties, is reached for structure with frequency approximately equal to $1.25\,\mathrm{Hz}$, at a rate of $a_{\mathrm{peak}} \approx 1.3\,\mathrm{m/s^2}$.

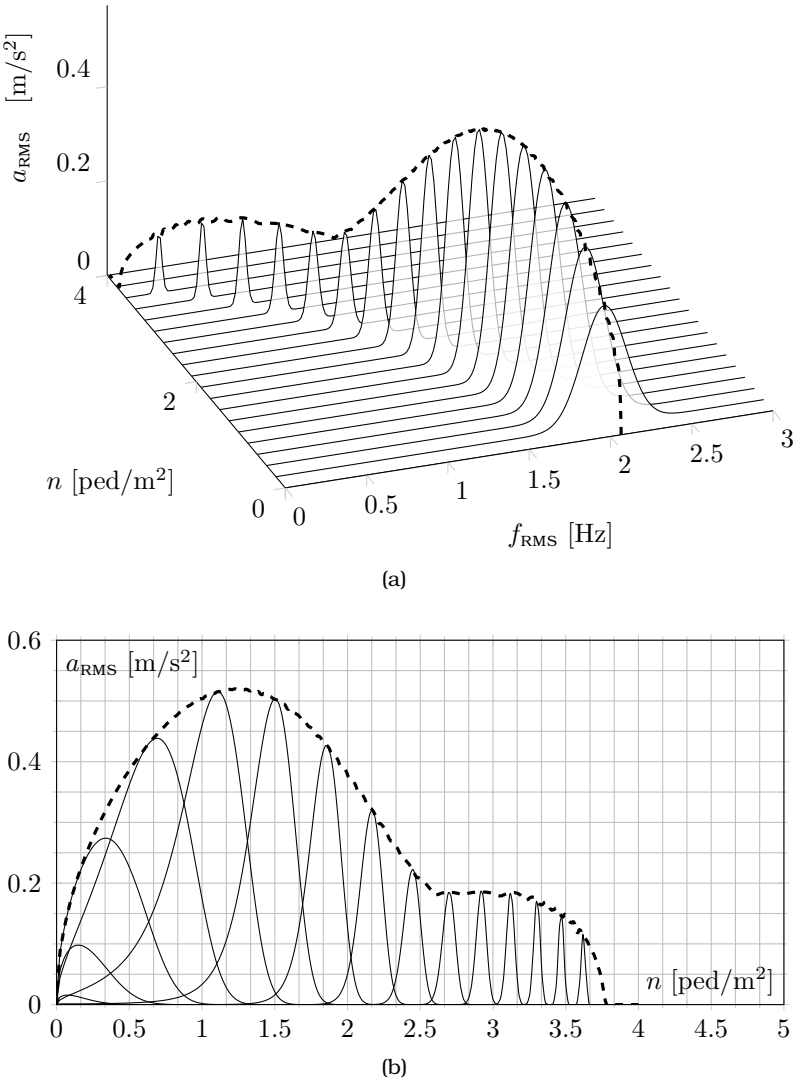

Figure 5.10: RMS acceleration response as a function of both the structure frequency and the density (a) and maximum envelope with respect to the density (b), both given through the simplified formulation.

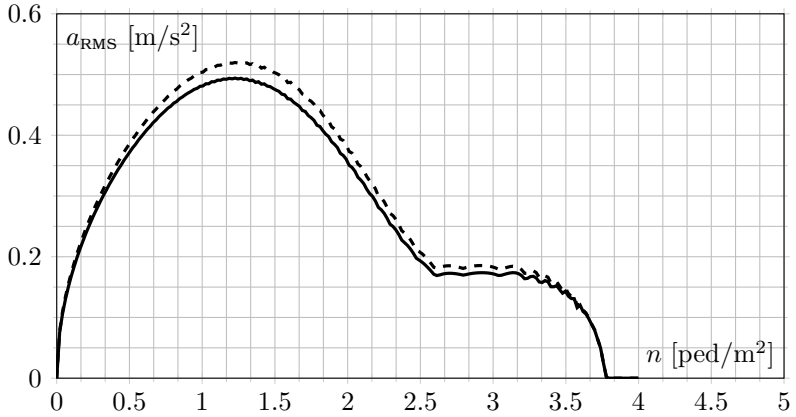

Figure 5.11: Comparison between the *exact* acceleration RMS response (continuous), and the *approximated* acceleration RMS response (dashed) by means of 5.8

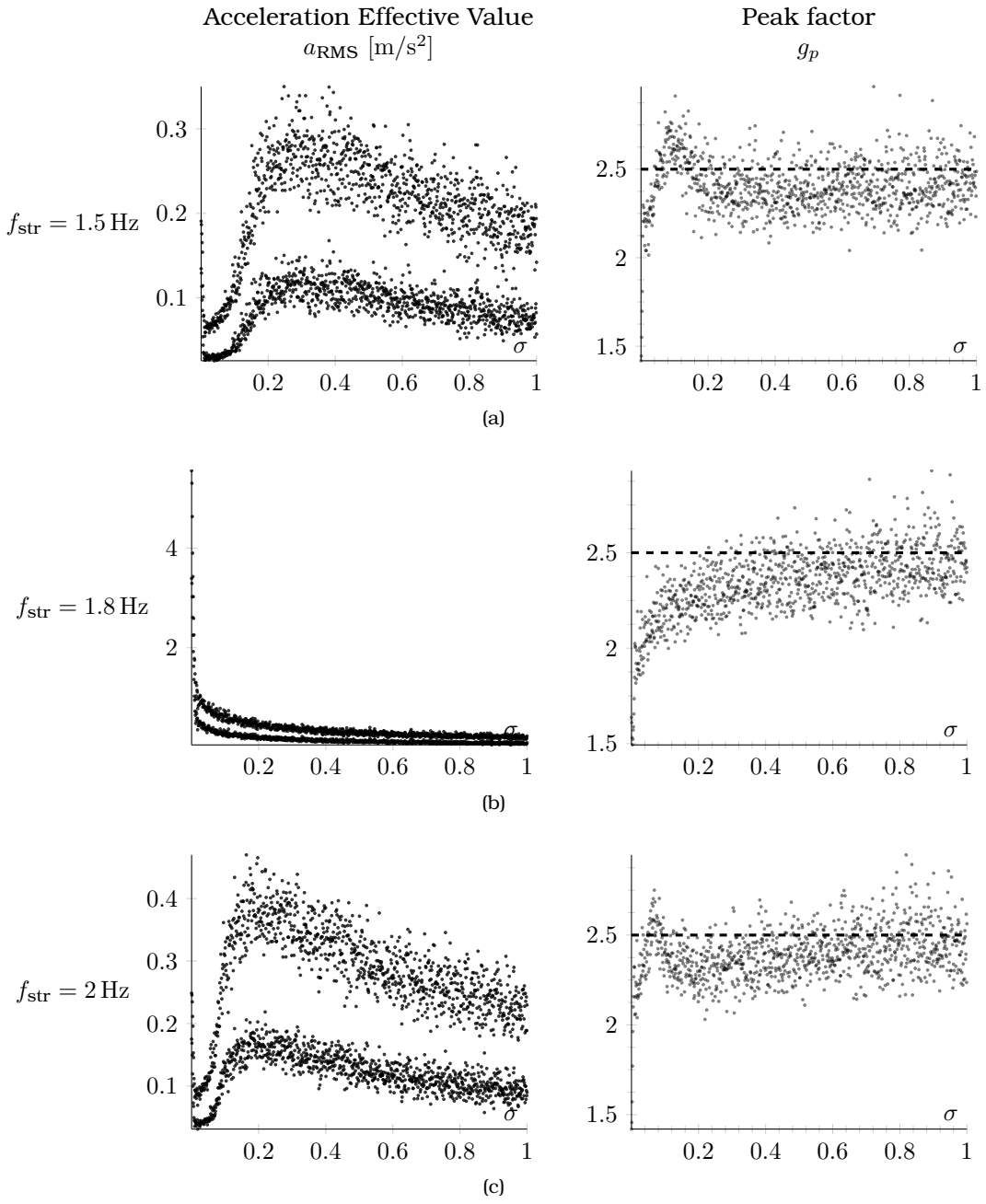

Figure 5.12: Simulated $a_{\mathrm{RMS}}(\sigma)$ (lower) and $a_{\mathrm{Peak}}(\sigma)$ (upper), and their ratio (right). Every point is the 100 simulations mean.

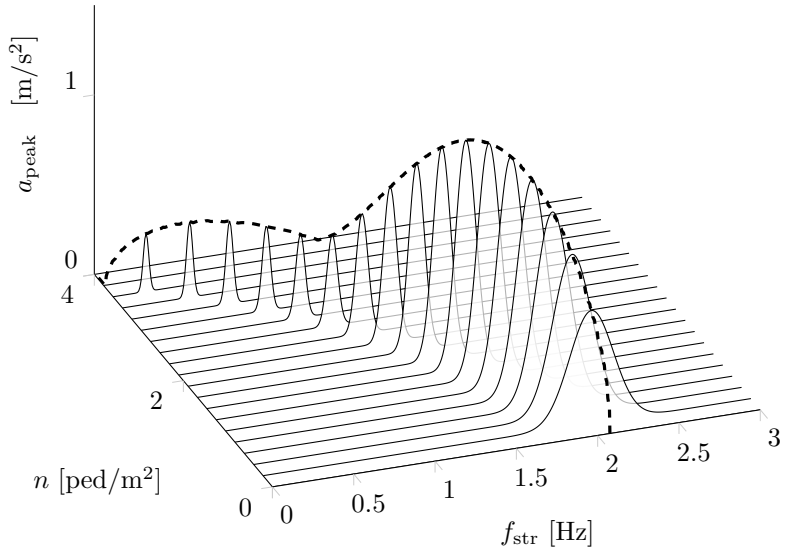

(a)

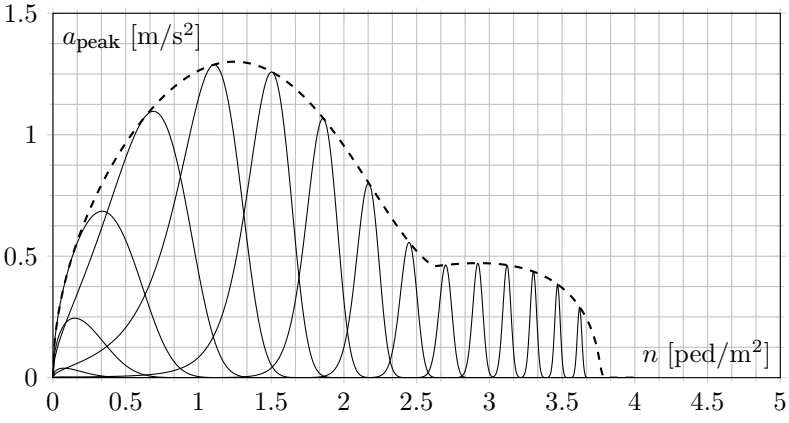

(b)

Figure 5.13: Peak acceleration response as a function of both the structure frequency and the density (a) and maximum envelope with respect to the density (b)

Chapter 6

Comparison with standards and guidelines

6.1 Guidelines overview

The early standards prescribed that natural frequencies close to the first and second walking harmonics, and to the jogging frequency, should be avoided. BS5400 of the British Standards Institution (BSI 1978), for instance, prescribes that dynamic analyses should be carried out if the *lateral* fundamental frequency is less than $1.5\,\mathrm{Hz}$. SIA 1989 and FIB 2010 both suggest to avoid vertical natural frequencies in the range of $1.6 \div 2.4\,\mathrm{Hz}$ (first walking harmonic), in the range of $3.5 \div 4.5\,\mathrm{Hz}$ (second walking harmonic), and in the range of $2.4 \div 3.5\,\mathrm{Hz}$ (running/jogging). If these requirements are not fulfilled, the acceleration response of the structure is to be checked.

With the increasing knowledge on the issue, other standards faced in the design scenario, proposing a framework to predict the acceleration response.

6.1.1 Frequency limitations

Sétra (2006) [13] defined levels of risk of vibration in both vertical and horizontal directions, depending on frequency. The maximum level of vibration risk is associated with vertical vibration frequencies in the range of $1.7 \div 2.1\,\mathrm{Hz}$ and lateral vibration frequencies in the range of $0.5 \div 1.1\,\mathrm{Hz}$; a medium level of vibration risk is associated with vertical vibration frequencies in the range of $1.0 \div 1.7\,\mathrm{Hz}$ and $2.1 \div 2.6\,\mathrm{Hz}$ and lateral vibration frequencies in the range of $0.3 \div 0.5\,\mathrm{Hz}$ and $1.1 \div 1.3\,\mathrm{Hz}$; a low level of vibration risk is associated with vertical vibration frequencies in the range of $2.5 \div 5.0\,\mathrm{Hz}$ and lateral vibration frequencies in the range of $1.3 \div 2.5\,\mathrm{Hz}$. Other vibration frequencies should not be considered a concern.

HIVOSS (Heinemeyer et al. 2009) defined the critical ranges of natural frequencies for footbridges excited by the first harmonic of the walking load as $1.25 \div 2.3\,\mathrm{Hz}$ for the vertical direction and $0.5 \div 1.2\,\mathrm{Hz}$ for the lateral direction, and by the second harmonic as $2.5 \div 4.6\,\mathrm{Hz}$ for the vertical direction.

6.1.2 Equivalent number of pedestrians and maximum acceleration

The maximum acceleration due to a single, a group, or a stream of walkers, either in the vertical or in the lateral direction, is usually given as

$$\ddot{y}_{\max} = N_{eq} \cdot \ddot{y}_{\max}(1) \cdot \Psi(f_1)$$

where $\ddot{y}_{max}$ is the maximum transient acceleration due to one walker resonant with the lowest harmonic that can be matched by the walking frequency, $\Psi(f_1)$ is a coefficient that reduces the response when the fundamental frequency of the bridge f_1 is away from the walking frequency, (for Sétra is reported in fig. 6.1), and N_{eq} is the equivalent number of

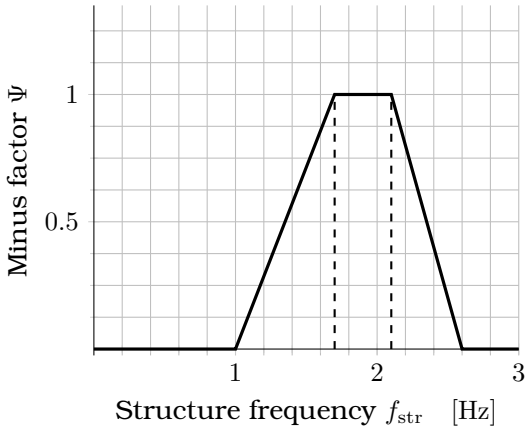

Figure 6.1: Minus factor for the first harmonic, adopted by Sétra guidelines

walkers on the bridge and accounts for the level of synchronisation. It stands for the number of pedestrians which are fully synchronised — in phase and frequency — and walking at the same frequency of the structure, that produce an acceleration response equal to the one produced by N incoherent pedestrians.

Sétra [13] guidelines use a stationary harmonic load model for the evaluation of the maximum acceleration induced by one pedestrian; the equivalent number of pedestrians is given as a function of n:

$$N_{eq} = \begin{cases} 10.8\sqrt{\xi N} & n < 1\,\mathrm{ped/m^2} \\ 1.85\sqrt{N} & n > 1\,\mathrm{ped/m^2} \end{cases} \tag{6.1}$$

This setting presents a sudden change in the response for $n = 1\,\mathrm{ped/m^2}$, which can be magnified or not by other parameters like the damping. What it is implicitly assumed by Sétra is that above the $1\,\mathrm{ped/m^2}$ threshold the pedestrians gain a full synchronisation in frequency. Such an assumption is apparently not properly justified in [13] and it possibly refers to the pedestrian-structure type of synchronisation, which is not treated here and however is not common to take place.

The linear load generated by the equivalent number of pedestrian is consequently:

$$F_{\mathrm{lin}} = \frac{280\ N_{eq}\ \Psi}{l} = \begin{cases} 280\ 10.8\sqrt{\xi N}\Psi/l & n < 1\,\mathrm{ped/m^2} \\ 280\ 1.85\sqrt{N}\Psi/l & n > 1\,\mathrm{ped/m^2} \end{cases}$$

and the produced maximum acceleration:

$$a_{\mathrm{peak}} = \frac{1}{2\xi}\frac{4F_{\mathrm{lin}}}{\pi\gamma} \tag{6.2}$$

Figure 6.2a shows the peak acceleration predicted by Sètra, for the reference case treated here, which is to say $\xi = 0.004$ and $l = 50\,\mathrm{m}$.

HIVOSS (Heinemeyer et al. 2009) adopts two approaches for the evaluation of the maximum acceleration: the stationary harmonic load model and the response spectral model. In the harmonic load model, N_{eq} and $\ddot{y}_{\max}$ coincide with those given by Sétra, but $\Psi(f_1)$ differs. The response spectral model was derived from Monte Carlo simulations based on numerical time-step simulations of various pedestrian streams on various bridges geometries (Butz 2006 [1]).

The Eurocode 5 (EC5; CEN 1995) considers both the case of a group of three synchronized walkers and that of a stream of walkers, but the former becomes relevant only for very small footbridges, with a deck smaller than $37\,\mathrm{m^2}$. Subsequently, the European Standard version, designated EN, of EC5 (CEN 2005) modifies the equations, but the case of a group of walkers remains dominant for very small footbridges, with a deck area in this case smaller than $22\,\mathrm{m^2}$.

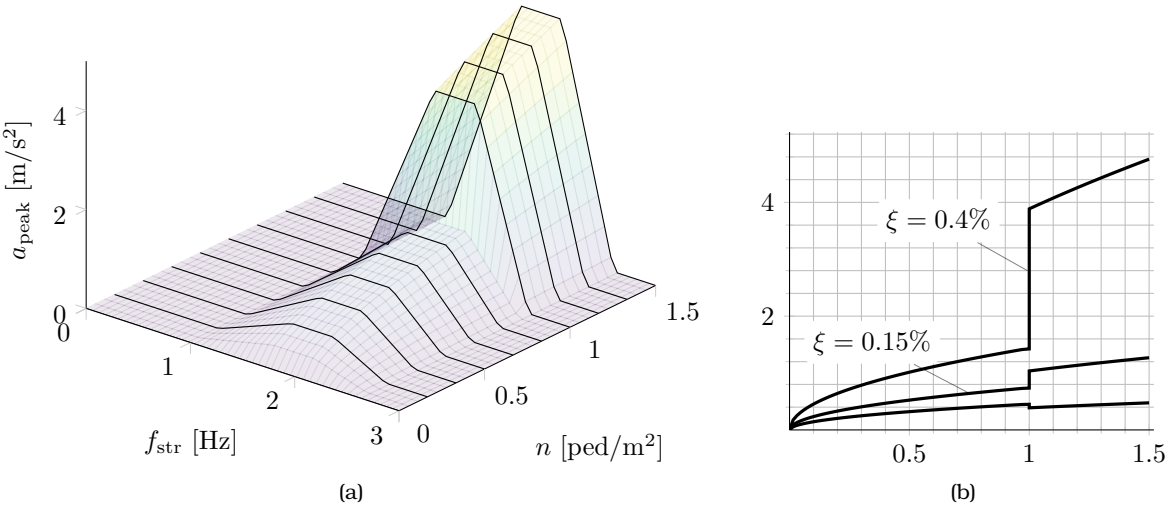

Figure 6.2: Sétra peak acceleration as a function of the crowd density and the structural frequency (a), and its maximum envelope for different damping factors (b). The used factors are proposed by Christoph Heinemeyer 2009 (HIVOSS) as building typology reference in design stage. From the lower to the higher curve: $\xi = 0.04$ (-), $\xi = 0.015$ (timber), $\xi = 0.004$ (steel avarage).

6.2 Peak acceleration comparison

Taking as a reference the Sétra guidelines, an analogous expression for the equivalent number of pedestrians is now derived. In the following table the formal steps are listed, in order to obtain the maximum acceleration due to an uncorrelated pedestrian crowd (to the left) and the corresponding maximum acceleration due to a fully synchronised pedestrian crowd (to the right) which is constituted by definition by N_{eq} pedestrians.

The used approach is the simplified one, seen in section 5.3.

Uncorrelated	Correlated
$\mathrm{E}\left[a^2\right] = \int_0^\infty \lvert H_a(f)\rvert^2 \, S_F(f) \, \mathrm{d}f$	$\mathbf{E}\left[a^2\right] = \int_0^\infty \lvert H_a(f)_{\beta=1}\rvert^2 \, S_F(f) \, \mathrm{d}f$[1]
$S_F = \frac{F^2 p(f)}{2} \cdot \frac{N}{2}$	$S_F = \frac{F^2 p(f)}{2} \cdot \left(\frac{2N_{eq}}{\pi}\right)^2$
$p\left(f\right) = \frac{1}{\sigma\sqrt{2\pi}} e^{-\frac{(f-f_\mu)^2}{2\sigma^2}}$	$p(f) = \delta(f - f_{\text{str}})$
$a_{\text{RMS}} \approx \frac{F}{4m}\sqrt{\frac{\pi}{\xi} N f_n \, p(f_n)}$	$a_{\text{RMS}} = \frac{F}{\sqrt{2}\pi m \xi} N_{eq}$
$a_{\text{peak}} = 2.5 \, a_{\text{RMS}}$	$a_{\text{peak}} = \sqrt{2} \, a_{\text{RMS}}$
$a_{\text{peak}} = 2.5 \frac{F}{4m}\sqrt{\frac{\pi}{\xi} N f_n \, p(f_n)}$	$a_{\text{peak}} = \frac{F}{\pi m \xi} N_{eq}$
$\lvert H_a(\beta)\rvert = \frac{1}{m} \frac{\beta^2}{\sqrt{(1-\beta^2)^2 + 4\xi^2\beta^2}}$	$\lvert H_a(\beta = 1)\rvert = \frac{1}{m}\frac{1}{2\xi}$

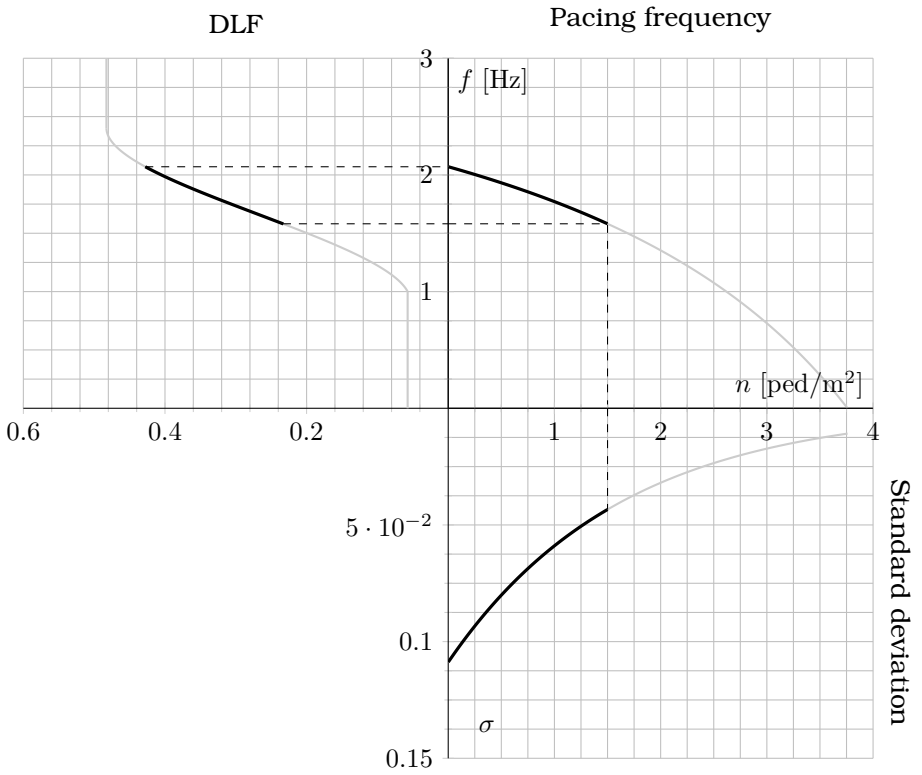

Figure 6.3: Governing functions as previously introduced (fig. 5.7), here the restricted domain $0 \div 1.5\,\mathrm{ped/m^2}$ as in guidelines, is highlighted.

Then asking the peak acceleration in both the cases to be the same, it is found the number of equivalent pedestrians:

$$N_{eq} = 3.48\sqrt{\xi f_n p(f_n) N}$$

where, by adopting the same formulation of the guidelines, $f_n p(f_n)$ assumes the role of $\Psi(f_1)$, if normalised to the range $0 \div 1$:

$$\Psi(f) = \frac{f_n p(f_n)}{\max\left(f_n p(f_n)\right)}$$

Finally the formula directly comparable with Sètra must be written:

$$N_{eq} = 3.48\sqrt{N\xi} \cdot \max\left(f_n p(f_n)\right)$$

That shows a divergence, mainly related to the value of $f_n p(f_n)$.

While this study covered a density range of $0 \div 4\,\mathrm{ped/m^2}$, Sétra, HIVOSS and the majority of the guidelines only take into account the range $0 \div 1.5\,\mathrm{ped/m^2}$. Some studies reported that above $1.5\,\mathrm{ped/m^2}$ the crowd flux lost its continuity and becomes a start-and-stop movement. That could explain such choice in taking it as an upper limit.

If the handling is restricted to the $0 \div 1.5\,\mathrm{ped/m^2}$ domain only a small section of the adopted governing functions (fig. 5.7) has to be considered. This subdomain is plotted in figure 6.3.

Figure 6.4 shows the comparison between the Sétra peak acceleration envelope — which is simply taken at $f_{\mathrm{str}} = 1.8\,\mathrm{Hz}$ or generally at a frequency belonging to the peak of the minus factor function — and the envelope derived from the discussed framework, and already introduced in figure 5.13.

A substantial divergence characterises the section above the $1\,\mathrm{ped/m^2}$. The reasons why Sétra exhibits such a high curve are already treated. The model here developed doesn't take into account any pedestrian-structure synchronisation so that its envelope doesn't present

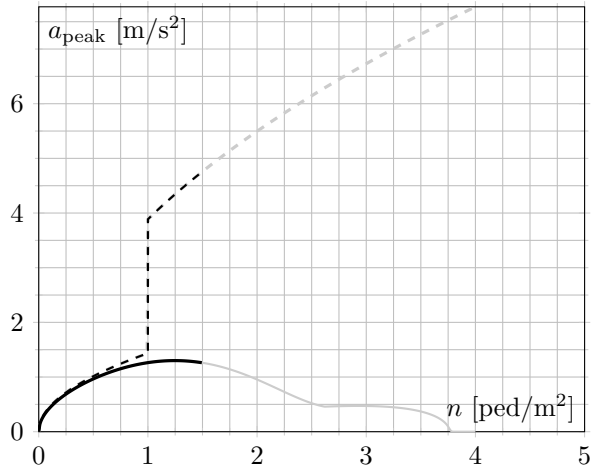

Figure 6.4: Envelope of the predicted peak acceleration by Sétra (dashed) and by the present formulation (conntinouos), with highlighted the range usually covered by the guidelines.

a sudden peak or something similar. One can find the usefulness of the treated model in describing what happens in high density conditions like those, in absence of any interaction with the structure that could perturb the natural walking condition, only affected by the density of the crowd.

Chapter 7

Concluding remarks

7.1 Conclusions

This work initially intended to study the synchronisation of the pedestrians in high density condition in order to develop a comprehensive formulation of how such a phenomenon affect the serviceability in footbridges. The idea was to express that level of synchronisation by means of a parameter that quantify the average phase shifts among the pedestrians. That is the aim of the parameter α. By analytical random simulations the limitations of such a choice have become clear, since α appears to be relevant only in synchronous conditions, that is to say all pedestrians at the same frequency.

Then the work focused on the variance of the frequencies of the pedestrians, examining how this affects the response. Quite an interesting result is that the maximum response does not occur in coincidence with the perfectly synchronous condition (assuming phase-uncorrelated pedestrians, otherwise it does).

In support of these results an analytical formulation has been provided, on the basis of the random vibration theory. The formulation closely predicts the numerical results.

On these analytical basis, the density variable has been introduced by means of the known relations available in the literature. The final result is a model that aims to predict the peak acceleration of a footbridge comparable to a simple supported beam, under the action of uniform pedestrian stream, with assigned density and frequencies distribution.

In comparison to the current normative scenario this model includes in a continuous way the density variable and, more important, how pedestrians-induced actions are affected by it. This tool may be deployed to better investigate how structures that are characterised by lower natural frequencies do behave under dense crowd action.

For regular density states instead, the model pretty well confirms the Sétra formulation. The fundamental law, that is: the acceleration is proportional to the square of the number of pedestrian, is confirmed on both theoretical and numerical basis. This makes seem weaker standards like EN EC5 or FIB that consist in linear rules, based on empirical measurements.

It should be noted that the Sétra, together with the HIVOSS guidelines, are the only ones that presents the particular distinction after $n = 1$, that so roughly runs counter to the prediction of the presented model. It is due, as already stated, to the assumption of perfect synchronisation that would somehow take place at this level of density. Some criticisms can be addressed to it, knowing that apparently no studies corroborate this fact and no easily accessible data are available about the response of simply supported-like footbridges subjected to highly dense ($n > 1$) crowd loading. Some measurements are available but at lower level of density. For instance see [28], [21], [14]. Those references are agree in stating that the guidelines provide a generally conservative prediction (in some cases out of all proportion), and among them the Sètra are often indicated as the more reliable. (Even if, like Eriksson [14] observed, the error in predictions never drops below 25%).

7.2 Further developments

- Some aspects of this model easily lend themselves to be improved. The first concerns the number of harmonics. In the model, only the 1^{st} harmonic is taken into account, while the current standards, like Sétra and HIVOSS, also include the second. It is known that above the second harmonic of the walking force a very little dynamic effect is detected; for instance Schultze goes from $\text{DLF}_1 = 0.37$ for the 1^{st} harmonic, to $\text{DLF}_5 = 0.04$ for the 4^{th}. But until the 2^{nd} one some noticeable effects are measured. For instance Eriksson [14], in a jumping test on a multi-span bridge in Mariestad, experienced an higher response when the jumping frequency was the half of the natural frequency. He concludes: *This should be something to consider in the design phase, if the bridge has a natural frequency of approximately 4 Hz, a forcing frequency of half the natural frequency may give excessive accelerations.*

  The affect of higher harmonics should be taken into account not only with regards to the pedestrian force but also referring to the structure. This issue affects the more deformable structures, which are characterised by low natural frequencies, or in the more frequent case the multi-span bridges, where many modes can interact also because their closeness, and then generate an unpredicted high response.

- Secondly, the hypothesis of simple supported beam can be removed. That implies a review of the first part and the MATLAB script, but fundamentally it changes the expressions for the natural frequency, which in case of fixed edges increases.

- Some research can concern the time-dependent parameters, those parameters that varies with the number of pedestrians getting across the footbridge. Has been documented how the damping factor is affected by that.

  Furthermore, the mass of the bridge has to be taken into account, since it increases with every pedestrian more on the bridge. The expected result is that both damping and mass contribute in decreasing the response. Sétra guidelines already include the mass factor in predicting the acceleration. From the examples provided by the Sétra itself [13] a percentage close to the 10% in terms of acceleration response is expected to vary because of the added mass.

Appendix A

MATLAB script

```
%PARAMETRI TRAVE
E=200000; % Modulo di elasticià N/mm^2
gamma=3; % Massa lineare kg/mm
l=50000; % Lunghezza mm
%fstr=pi*sqrt(5*400*5/384/4/mu/l*1000);  % Frequenza per avere freccia con
   5kN/m = 1/400 L
fstr=2; % Frequenza propria della struttura (primo modo) in Hz
I=4*fstr^2*l^4*gamma/pi^2/E/1000 % Momento d'inerzia mm^4
m=gamma*l/2; % Massa modale kg
k=omega_j.^2*gamma*l./2/1000 % Rigidezza modale N/mm^2

omega_j=sqrt(1000*E*I/gamma)*(j*pi/l).^2; % Vettore pulsazioni
f_j=omega_j/(2*pi); % Vettore frequenze modali 1/s
csi=0.0048; % Fattore di smorzamento viscoso
omega_b=csi.*omega_j;
omega_D=omega_j*sqrt(1-csi^2);
```

```
%DOMINIO DI DEFINIZIONE DEL PROBLEMA
tempo_tot=10; % Tempo totale di simulazione. s
%tempo_tot=3*T;
step_temp=0.01; % Delta temporale. s
t=[0:step_temp:tempo_tot]; % Vettore tempo discretizzato

step_x=100; % Delta spaziale. mm
x=[0:step_x:l]; % Vettore trave discretizzata nello spazio
```

```
%FORZA COMPONENTE COSTANTE +COMPONENTE ARMONICA IN MOVIMENTO A VELOCITA' c
% (con fstep=0 si ricade nel caso di forza costante a velocitï¿½ c)
N=25; % Numero di carichi
DLF=0.4; % Fattore dinamico
S=700;   D=DLF*S;    % N
fstep=2;  %Hz (passi/secondo)
c=fstep*0.9*1000;  % Velocitï¿½ pedoni mm/s
T=l/c; % Periodo di percorrenza della trave s

c_cr=pi/l*sqrt(1000*E*I/gamma);  % Velocitï¿½ critica
Alpha=c/c_cr;
beta=fstep/fstr;
FattAmpl=1/sqrt((1-beta^2)^2+4*csi^2*beta^2); %Fattore di amplificazione
   del carico armonico - utile per verificare
```

```
%Inizializza la struttura che contiene le informazioni del carico n-esimo:
Q(1,N)=struct('S',[],'D',[],'c',[],'Omega',[],'Phi',[],'x_0',[],'t_ingr'
    ,[],'t_uscita',[],'posizione',[],'ampiezza',[],'f',[]);

%Compilazione della struttura
%COMPONENTE STATICA
[Q.S]=deal(S); % Tutte le forze uguali
%static_forces={1 2 3 }; % Forze inserite una ad una..esempio con tre forze
%[Q.S]=static_forces{:};

%COMPONENTE DINAMICA
[Q.D]=deal(D); % Tutte le forze uguali
%dynamic_forces={1 2 3 }; % Forze inserite una ad una..esempio con tre
    forze
%[Q.D]=dynamic_forces{:};

%VELOCITA'
[Q.c]=deal(c); % Uguale per tutti i carichi

%PUNTI DI PARTENZA DEI CARICHI
%starting_points={l/4 3/4*l}; % Punti di partenza dichiarati uno ad uno
starting_points=num2cell(linspace(0,l,N));    % Punti di ingresso
    equispaziati
%starting_points=num2cell(2*l*rand(1,N)-2*l);    % Punti di ingresso casuali

[Q.x_0]=starting_points{:}; % Inserimento nella struttura

%OMEGA (PULSAZIONI dei carichi)
%rng default    %Seme delle variabili random, usare lo stesso per ottenere
    le stesse variabili
%rng(1)
sqm=0; %scarto quadratico medio delle frequenze.(sigma)
frequences=num2cell(fstep+sqm*randn(1,N));
pulsazioni=num2cell(2*pi*[frequences{:}]);
[Q.Omega]=pulsazioni{:}; % Inserimento nella struttura

%FASI
alpha=0;   %ampiezza di banda delle fasi da 0 a 2pi
phases=num2cell(alpha*rand(1,N)-alpha/2);
[Q.Phi]=phases{:};


forza_generalizzata = @(n,j,t,S,D,Omega,Phi,c,t_ingr) (Q(n).S+Q(n).D*sin(
    Omega*t+Phi)).*sin(j*pi*c*(t-t_ingr)/l);

for n=1:N   %Ciclo che compila le strutture dei carichi con le variabili
    dipendenti e la matrice jxt delle forze generalizzate.
     if c~=0
     Q(n).t_ingr=-Q(n).x_0/Q(n).c;
     Q(n).t_uscita=l/Q(n).c+Q(n).t_ingr;
     Q(n).f=forza_generalizzata(n,j,t,Q(n).S,Q(n).D,Q(n).Omega,Q(n).Phi,Q(n)
         .c,Q(n).t_ingr);
     Q(n).posizione=Q(n).c*(t-Q(n).t_ingr);    Q(n).ampiezza=Q(n).S+Q(n).D*
         sin(Q(n).Omega*t+Q(n).Phi);

     [var_inutile ind_t_uscita]=min(abs(t-Q(n).t_uscita));
```

```
    [var_inutile ind_t_ingr]=min(abs(t-Q(n).t_ingr));
    Q(n).f(:,[1:ind_t_ingr,ind_t_uscita:size(Q(n).f,2)])=0;

    else
        Q(n).t_ingr=0;
        Q(n).t_uscita=tempo_tot;

        forza_generalizzata = @(j,t,S,D,Omega,Phi,x_0) (Q(n).S+Q(n).D*sin(
            Omega*t+Phi)).*sin(j*pi*x_0/l);
        Q(n).f=forza_generalizzata(j,t,Q(n).S,Q(n).D,Q(n).Omega,Q(n).Phi,Q(
            n).x_0);
        Q(n).posizione=Q(n).x_0*ones(1,size(t,2));   Q(n).ampiezza=Q(n).S+Q
            (n).D*sin(Q(n).Omega*t+Q(n).Phi);
    end

    %genera la Matrice delle forze generalizzate. Una riga per armonica.
end

%Matrice delle risposte all'impulso unitario. Una riga per armonica, cioè
    ogni riga costituisce la risposta della j-esima coordinata modale.
h=1000*2./(gamma*l*omega_D).*exp(-omega_b*t).*sin(omega_D*t);

%inizializza la matrice delle forze generalizzate totali
    f=zeros(n_armoniche,length(t));
    %Ciclo che somma assieme le forze generalizzate di tutti i carichi
for n=1:N
    f=f+Q(n).f;
end
```

```
%DUHAMEL - INTEGRAZIONE DELLA RISPOSTA
    % Inizializza la matrice v contenente la deformata nel tempo
v=zeros(length(t),length(x));
    vn=zeros(length(t),length(x));
    %
for i=1:n_armoniche
y(i,:)=conv(f(i,:),h(i,:))*step_temp;
yridotta=y(i,1:size(t,2));
vi=yridotta'*sin(i*pi*x/l);
vn=vn+vi;
waitbar(i/n_armoniche)
end
v=v+vn;


dvdt=diff(v,1,1)/step_temp; %attenzione ha un elemento in meno rispetto a v
     alla fine.
a=diff(dvdt,1,1)/step_temp; %attenzione ha due elementi in meno rispetto a
    v alla fine.
[punto_campionato_discreto,ind_punto_campionato]=min(abs((x-
    punto_campionato_val)));  %serve per trovare l'indice del valore
    corrispondente all'abbassamento in mezzeria. E' un più laborioso,
    sarebbe bastato prendere il valore a del vettore. Ma così è possibile
    cambiare il punto di cui tracciare lo spostamento con quello che si
    desidera.
v_mezz=v(:,ind_punto_campionato);
%{
```

```
a_mezz=a(:,ind_punto_campionato);
[a ind_a]=min(abs(t-50));
[b ind_b]=min(abs(t-100));
RMS=rms(a_mezz(ind_a:ind_b));
```

Appendix B

MATLAB script

```
num_sqm=10;
num_fstr=10;
asse_sqm=linspace(0,1,num_sqm);
asse_fstr=linspace(1,2.6,num_fstr);

L=50000; %mm
E=200000; %N/mm2
csi=0.004;
gamma=3; %kg/mm massa per unità di lunghezza
m=75000; %kg massa modale
W=700; %N peso singolo pedone
DLF=0.4; %coefficiente dinamico
F=W*DLF; %N
N=25; %#pedoni
q=W*DLF*N/L; %N/mm carico distribuito equipesante
fstep=1.8; %Hz frequenza media pedoni

contatore=0;
for indice_fstr=1:length(asse_fstr)
    fstr=asse_fstr(indice_fstr);

for indice_sqm=1:num_sqm
    sigma=asse_sqm(indice_sqm);

H2acc = @(freq) ((1/m^2*((freq/fstr).^4./((1-(freq/fstr).^2).^2+4*csi^2.*(
   freq/fstr).^2)))); %Come sopra ma moltiplicata per (2*pi*fstr)^4
S_F= @(freq) (N/2)*F^2/2*normpdf(freq,fstep,sigma); %Spettro della forzante
   . Il coefficiente N/2 deriva dall'assunzione che i segnali sono
   totalmente scorrelati.
%Se le frequenze fossere uguali (sigma=0) e i segnali perfettamente
   correlati (alpha=0), bisognerebbe usare (2*N/pi)^2.

if sigma==0
    RMSa_metodo_aleatorio(indice_sqm,indice_fstr)=(H2acc(fstep)*F^2/2*(2*N/
       pi)^2)^0.5;
else
    ValoreQuadraticoMedio_a=integral(@(freq) H2acc(freq).*S_F(freq),0,inf,'
       Waypoints',[fstep-5*sigma fstep+5*sigma]);
    RMSa_metodo_aleatorio(indice_sqm,indice_fstr)=ValoreQuadraticoMedio_a
       ^0.5;
end
```

```
contatore/(length(asse_fstr)*length(asse_sqm))*100
contatore=contatore+1;
end
end

figure
s=surf(asse_sqm,asse_fstr,RMSa_metodo_aleatorio')
s.EdgeColor = 'none';
```

Bibliography

[1] C. Butz et al. “Advanced load models for synchronous pedestrian excitation and optimised design guidelines for steel footbridges”. In: *Project RFS-CR-03019, Final Rep.* (2007).

[2] T.P Andriacchi, J.A Ogle, and J.O. Galante. “Walking speed as a basis for normal and abnormal gait measurements”. In: *Journal of Biomechanics* 10 (1977), pp. 261–268.

[3] H. Bachmann and W. Ammann. “Vibrations in Structures–Induced by Men and Machines”. In: *Structural Engineering Documents, International Association of Bridge and Structural Engineering* 3 (1987).

[4] H. Bachmann, A.J Pretlove, and H. Rainer. “Vibration Problems in Structures: Practical Guidelines”. In: Birkh ̈auser, Basel, 1995. Chap. G.

[5] J.E.A. Bertram and A. Ruina. “Multiple Walking Speed–frequency Relations are Predicted by Constrained Optimization”. In: *Journal of Theoretical Biology* 209.4 (2001), pp. 445–453. ISSN: 0022-5193.

[6] J. Blanchard, B.L Davies, and J.W. Smith. “Design criteria and analysis for dynamic loading of footbridges”. In: *Proceedings of the DOE and DOT TRRL Symposium on Dynamic Behaviour of Bridges*. Crowthorne, UK, May 1977, pp. 90–106.

[7] E. Bosina and U. Weidmann. “Estimating pedestrian speed using aggregated literature data”. In: *Physica A: Statistical Mechanics and its Applications* 468 (2017), pp. 1–29. ISSN: 0378-4371.

[8] J.M.W. Brownjohn, A. Pavic, and P. Omenzetter. “A spectral density approach for modelling continuous vertical forces on pedestrian structures due to walking”. In: *Canadian Journal of Civil Engineering* 31 (2004), pp. 65–77.

[9] A. Capsoni. “A simplified approach to predict vertical dynamic effects on footbridges under crowd loading”. Unpublished manuscript.

[10] W. Daamen. “Modelling passenger flows in public transport facilities”. PhD thesis. Delft University of Technology, 2004.

[11] P. Dallard et al. “London Millennium Bridge: Pedestrian-Induced Lateral Vibration”. In: *Journal of Bridge Engineering* 6.6 (2001), pp. 412–417.

[12] R.H. Scanlan E. Simiu. *Wind Effects on Structures, Fundamentals and Applications to Design*. Wiley, New York, 1996.

[13] French association of civil engineering. *Assessment of vibrational behaviour of footbridges under pedestrian loading*. Tech. rep. Serviced’études techniques des routes et autoroutes–Sétra, Oct. 2006.

[14] H.P.T Eriksson. “Vibration response of lightweight pedestrian bridges”. MA thesis. Chalmers University Of Tecnology, 2013.

[15] Z. Fang, S.M. Lo, and J.A. Lu. “On the relationship between crowd density and movement velocity”. In: *Fire Safety Journal* 38.3 (2003), pp. 271–283. ISSN: 0379-7112.

[16] Ladislav Frýba. *Vibration of Solids and Structures Under Moving Loads*. ThomasTelford, 1972.

[17] F.W Galbraith and M.V Barton. “Ground loading from footsteps”. In: *Journal of the Acoustic Society of America* 48 (1970), pp. 1288–1292.

[18] F.C. Harper, W.J. Warlow, and B.L. Clarke. “The forces applied to the floor by the foot in walking”. In: *National Building Studies* 32 (1961).

[19] Einar Thòr Ingólfsson, C.T. Georgakis, and J. Jönsson. “Pedestrian-induced lateral vibrations of footbridges: Literature review”. Unpublished manuscript. 2010.

[20] E.T. Ingólfsson. “Pedestrian-induced lateral vibrations of footbridges, experimental studies and probabilistic modelling”. PhD thesis. Department of Civil Engineering, 2011.

[21] S.V. Keer. “Human induced loading on staircases”. PhD thesis. University College London, 1998.

[22] D.R. Leonard. “Human tolerance levels for bridge vibrations”. In: *TRRL Report, Road Research Laboratory* 34 (1966).

[23] A. Mandelli and F. Mariani. “Sulla simulazione della risposta dinamica di passerelle pedonali”. MA thesis. Politecnico di Milano, 2007.

[24] A. Mårtensson and M. Nilsson. “Dynamic Analysis of Pedestrian Load Models for Footbridges. A review of current load models and guidelines”. MA thesis. Chalmers University of Technology, Göteborg, Sweden, 2014.

[25] Y. Matsumoto et al. “A study on design of pedestrian overbridges”. In: *Transactions of JSCE* (1972), pp. 50–51.

[26] H. Nelson and H. Maclennan. *Emergency movement, The SFPE handbook of fire protection engineering*. 1995.

[27] D.E. Newland. *An Introduction to Random Vibrations, Spectral & Wavelet Analysis*. Dover Publications, Inc, Mineola, New York, 1975.

[28] K. Van Nimmen et al. “Vibration serviceability of footbridges: Evaluation of the current codes of practice”. In: *Engineering Structures* 59 (2014), pp. 448–461. ISSN: 0141-0296.

[29] D. Oeding. “Verkehrsbelastung und Dimensionierung von Gehwegen und anderen Anlagen des Fußgängerverkehrs”. In: *Technische Hochschule Carolo-Wilhelmina zu Braunschweig* (1963).

[30] S.V. Ohlsson. “Floor vibration and human discomfort”. PhD thesis. Chalmers University of Technology, G ̈oteborg, Sweeden, 1982.

[31] V. Racic, A. Pavic, and J. M. W. Brownjohn. “Experimental identification and analytical modelling of human walking forces: Literature review”. In: *Journal of Sound Vibration* 326 (Sept. 2009), pp. 1–49.

[32] F. Ricciardelli and C. Demartino. “Design of footbridge against pedestrian-induced vibrations”. In: *Journal of Bridge Engineering* (2015).

[33] P. Thompson and E. Marchant. “A computer model for the evacuation of large building population”. In: *Fire Safety Journal* (1995), pp. 24–131.

[34] Weidmann Ulrich. *Transporttechnik der Fussgänger. Transporttechnische Eigenschaften des Fussgängerverkehrs, Literaturauswertung*. de. Tech. rep. 1992.

[35] F. Venuti and L. Bruno. “Crowd-structure interaction in lively footbridges under synchronous lateral excitation: A literature review”. In: *Physics of Life Reviews* 6.3 (2009), pp. 176–206. ISSN: 1571-0645.

[36] J.E. Wheeler. “Pedestrian-induced vibrations in footbridges”. In: *Proceedings of the 10th Australian Road Research Board (ARRB) Conference*. Vol. 10. Aug. 1980, pp. 21–35.

[37] P. Young. “Improved floor vibration prediction methodologies”. In: *ARUP Vibration Seminar*. Oct. 2001.

[38] S. Živanović, A. Pavic, and P. Reynolds. “Vibration serviceability of footbriges under human-induced excitation: a literature review”. In: *Journal of Sound and Vibration* 279 (2004), pp. 1–74.